Functional Studies of the Group A Rotavirus Non-Structural Protein NSP4

A thesis submitted by

Weiming Yang

For the degree of Doctor of Philosophy

Department of Biological Sciences

University of Warwick

Coventry

United Kingdom

September 2010

Table of Contents

Page Number

List of Table

Page Number

List of Figures

Page Number

Acknowledgements

I am thankful to my supervisor, Malcolm McCrae, for his valuable guidance and support throughout my academic study. It is a pleasure to thank past and present members of the rota/adenovirus lab and the virology people for their technical support and constructive criticism.

Weiming

September 2010

Dedication

To my mother and father, without their kindly support, this thesis might not have been written. They are always a source of encouragement and inspiration to me throughout my life.

To my wife, Minghui, who provides me a strong emotional support and a great happiness everyday. Her enthusiasm continuously encourages me to reach my potential.

Abbreviations

Å	Angstrom
A	Alanine
aa	Amino acid
ATP	Adenosine triphosphate
BAPTA/AM	1,2-bis (o-aminophenoxy) ethane-N,N,N',N'-tetraacetic acid /Acetoxymethyl
BHK	Baby hamster kidney
BSA	Bovine serum albumin
β-TrCP	β-transducin repeat containing protein
bp	Base pair
cm	Centimetre
cDNA	Complementary DNA
cpe	Cytopathic effect
°C	Centigrade
CHO	Chinese hamster ovary
CTL	Cytotoxic T-lymphocyte
CMV	Cytomegalovirus
$CaCl_2$	Calcium chloride
CsCl	Caesium chloride
CytoD	Cytochalasin D
cryoEM	Cryoelectron microscopy
DAPI	4', 6-diamidino-2- phenylindole

DLP	Double layer particle
DMEM	Dulbecco's modified Eagle's medium
DMSO	Dimethylsulphoxide
DNA	Deoxyribonucleic acid
dNTP	Deoxynucleotide triphosphate
ds	Double stranded
DS	Double-shelled
DTT	Dithioreitol
elF4E	Eukaryotic initiation factor 4E
ENS	Enteric Nervous System
ELISA	Enzyme linked immunosobent assay
ER	Endoplasmic reticulum
EM	Electron microscopy
EDTA	Ethylenediaminetetraacetic acid
EGTA	Ethyleneglycolbis (aminoethylether) tetra-acetic acid
ERGIC	Endoplasmic reticulum Golgi intermediate compartment
FACS	Fluorescence activated cell sorting
FCS	Fetal calf serum
FDA	Food and Drug Administration
Fig	Figure
GFP	Green fluorescent protein
GSK	GlaxoSmithKline
g	Gram
GMEM	Glasgow modified Eagle's minimal essential medium
HEK	Human embryonic kidney

Hsc70	Heat shock cognate 70
hpi	Hour post infection
Hz	Hertz
IFN	Interferon
Ig	Immunoglobulin
ISG	IFN-stimulated genes
kb	Kilobase
kDa	Kilodalton
kg	Kilogram
LB	Luria-Bertani
N	Asparagine
NaCl	Sodium chloride
NH_4Cl	Ammonium chloride
NTPase	Nucleoside triphosphatase
nm	Nanometer
m	Meter
M	Molar
MOPS	3[N-morpholino] propanesulphonic acid
$MnCl_2$	Manganese chloride
MVA	Modified vaccinia Ankara
MCFD	Multicoagulation factor deficiency protein
ml	Milliliter
mm	Millimeter
mM	Millimolar
mins	Minutes

μ	Micro
MOI	Multiplicity of infection
mRNA	Messenger RNA
NA	Neuraminidase
NO	Nitric oxide
NSP	Non-structural protein
ORF	Open reading frame
ORT	Oral rehydration therapy
OD	Optical density
PAGE	Polyacrylamide gel electrophoresis
PABP	Poly A binding protein
PBS	Phosphate buffered saline
PLC-IP3	Phospholipase C-inositol 1,4,5-triphosphate
PCA	Protein complementary assay
PCR	Polymerase chain reaction
pfu	Plaque forming units
pH	$-\log_{10}[H^+]$
RTPase	RNA triphosphatase
RPHA	Reverse passive hemagglutination assay
RNA	Ribonuleic acid
RNAi	RNA interference
$RbCl_2$	Rubidium chloride
rpm	Revolutions per minute
STAT	Signal transducer and activator of transcription
SAP	Shrimp alkaline phosphatase

SV-40	Simian virus 40
SDS	Sodium dodecyl sulphate
SRE	Sterol regulatory element
SS_{cal}	Signal sequence of calreticulin
TLP	Triple layer particle
TBE	Tris-borate EDTA
TE	Tris-EDTA
Tris	Tris[hydroxymethyl]aminomethane
U	Enzyme units
UV	Ultraviolet
UTR	Untranslated region
VP	Virus protein
YFP	Yellow fluorescent protein
WHO	World Health Organization

Declaration

All the results presented in the thesis were obtained by the author unless otherwise stated, and in no part have been previously presented in application for a degree. All the sources of information and materials are indicated in the text.

Summary

NSP4, encoded by rotavirus genome segment 10 has been shown to be a transmembrane, endoplasmic reticulum (ER) specific N-linked glycoprotein. Consistent with its localization to the ER membrane, NSP4 was first shown to have a role in the morphogenesis of the infectious virion. The protein has also been reported to have cytotoxic activity when applied extracellularly to cells. Consequently it has been earmarked as an enterotoxin being secreted from virus-infected cells to cause early cellular pathology in the gut.

The effect of expressing the NSP4 protein of group A rotaviruses in cells has been studied. It led to the rapid appearance of long cytoplasmic extrusions. Site-directed mutagenesis was used to block N-linked glycosylation at both of the known glycosylation sites near the amino terminus of NSP4. This revealed that the NSP4 induced formation of the cytoplasmic extrusions was dependent on the protein's ability to become fully glycosylated. The cytoplasmic extrusions seen in cells expressing glycosylated NSP4 were also evident in virus-infected cells.

Using real-time confocal microscopy a dynamic elongation of the cytoplasmic extrusions with a growth speed of 2 μm/min was observed in virus-infected cells. The cytoplasmic extrusions were found to contain β-tubulin and F-actin. Inhibiting their polymerization prevented the formation of the extrusions from virus-infected cells. Functional studies using Cell Tracker dyes showed that the cytoplasmic extrusions could disseminate vesicles from virus-infected cells onto the plasma membrane surface of uninfected cells. The vesicles were then found in the interior of the uninfected cells. Mono-specific antibody to NSP4 revealed the presence of the protein in the vesicles suggesting that the cytoplasmic extrusions facilitated the direct cell-cell spread of NSP4.

The effect of NSP4 expression on the microtubular network of cells was analysed. It was found that NSP4 de-polymerized the microtubular network from the centre of cells and promoted the assembly of microtubules at the periphery of the cells in a glycosylation independent manner. Similar de-polymerization and re-assembly of the microtubules was observed in the virus-infected cells. Interestingly in the presence of nocodazole, tubular structures containing tubulin and viral proteins excluding NSP4 were found in virus-infected cells.

A YFP-PCA assay was established to screen for cellular partners of NSP4. The functionality and the sensitivity of the assay were examined, but only two false positive colonies were isolated in the first screening.

In conclusion, the function of glycosylated and unglycosylated NSP4 was examined with the former possessing the ability to promote the formation of the cytoplasmic extrusions from cells and both being capable of disrupting the microtubular network indicating that two forms of NSP4 play different roles in NSP4 function. The cytoplasmic extrusions seen in our studies may be relevant to rotavirus infection and pathogenesis.

Chapter 1

Introduction

Rotaviruses are the predominant etiological agents of acute viral gastroenteritis in the young of a wide range of mammalian and avian species including human infants (Flewett, 1978; Kapikian, 2001; Pedley *et al*., 1983). As such they are globally important medical and veterinary pathogens that constitute a major cause of morbidity and mortality among the young. Therefore they assume a special importance worldwide.

The first recognition of human rotavirus was in 1973 by direct visualization using electron microscopy of patient faeces. The 70-nm viral particle identified using EM was subsequently designated rotavirus. Shortly afterwards, it became apparent that rotaviruses were an important etiologic agent of diarrhoea in infantile and young children accounting for approximately 35 to 50% of hospitalizations due to gastroenteritis during the first 2 years of life (Kapikian, 2001). Following their initial detection rotaviruses have been reported from many countries leading to their being established as a major viral etiologic agent in both the developed and developing world (Kapikian, 2001).

In 1980, following treatment of clinical isolates with trypsin, the successful cultivation of human rotaviruses in African green monkey kidney cells was reported facilitating extensive investigations at the molecular level (Wyatt *et al*., 1980). The development of monoclonal antibodies and recombinant DNA technologies during the 1980s and 1990s and the later application of GFP and RNAi based technologies, contributed to considerable understanding of the rotavirus replication cycle, their epidemiology, pathogenesis, and the nature of host resistance to rotavirus disease. The increasing concern about both the medical and social burdens of rotavirus disease lead to the development of the first rotavirus vaccine in 1998. The removal of this vaccine from the market in 1999, seemed to be a setback for efforts to control

rotaviruses (Centers for Disease Control and Prevention, 1999). However renewed efforts have been made and two new vaccines were released in 2006. Clinical trials of these vaccines carried out on a large scale in both developed and developing countries have resulted in the WHO recommending the use of a rotavirus vaccine worldwide in June 2009 (Nelson *et al*., 2009).

1.1 Rotavirus

1.1.1 Classification

Rotaviruses make up one genus within the family Reoviridae, with seven distinct virus groups having been recognized (Estes, 2001; Pedley *et al*., 1983; Pedley *et al*., 1986). Rotaviruses falling into each of the seven groups (A-G) share the same cross-reacting so-called group antigen measurable by a number of serologic tests (immunofluorescence, ELISA and immuno-electron microscopy) (Estes, 2001; Pedley *et al*., 1983; Pedley *et al*., 1986). Among these seven groups, group A rotaviruses have been recognized as the predominant etiological agents of acute viral gastroenteritis in infants and young children (Estes, 2001). Thus this thesis will focus exclusively on group A rotaviruses.

The salient characteristics of group A rotaviruses are as follows:

(1) The mature virions are approximately 100 nm in diameter and possess a triple layered icosahedral protein capsid with an outer layer, an inner layer and a core.

(2) 60 spikes protrude from surface of the outer layer of the virus particle.

(3) The viral genome is composed of 11 segments of double-stranded RNA (dsRNA) capable of genetic reassortment within isolates from each virus group.

(4) Virus particles are capable of making capped RNA transcripts using virion associated RNA-dependent RNA polymerase and RNA capping enzymes.

(5) Viral cultivation *in vitro* is facilitated by treatment of mature virus with proteolytic enzymes that enhances infectivity by cleavage of the external spike protein (VP4).

(6) Viral replication occurs in the cytoplasm of infected cells.

(7) Rotaviruses exhibit a unique morphogenic pathway.

Group A rotaviruses have been divided into a number of serotypes based on the reactivity of viruses in plaque reduction (or fluorescent foci reduction) neutralization assays using hyperimmune serum prepared in antibody negative animals. Through the use of such assays, 14 G serotypes (G for glycoprotein VP7) have been recognized to date. Among these G serotypes, G1-4 and G9 are the most common human strains world-wide (Centers for Disease Control and Prevention, 2008). Genotying of VP7 using sequence and hybridization assays has demonstrated a clear correlation with the serotypes defined by neutralization assays (Kapikian, 2001). The sero-genotypic correlation has not been as clearly defined in VP4 typing (Kapikian, 2001). Consequently VP4 typing (P) has focused on using sequence analysis and hybridization assays to establish in excess of 20 VP4 genotypes whereas only 13 VP4 serotypes have been recognized to date (Banyai *et al*., 2010; Hoshino and Kapikian, 1996; Kapikian, 2001). To integrate the VP4 serotype and genotype designation, an open Arabic number following P is used to denote serotype, with an Arabic number in brackets designating genotype. For example, the human Wa strain is designated P1A[8] (Kapikian, 2001).

1.1.2 Physicochemical Properties of the Virus Particle

Mature infectious rotavirus virions are nonenveloped icosahedral, triple-layered and about 100 nm in diameter. They resembled a wheel with short spokes and a

well-defined smooth outer rim when observed using standard negative staining by electron microscopy (Flewett *et al*., 1974) and it is from this wheel like morphology that they derive their name. The composition of virions includes VP1, VP2 and VP3 as the inner-most layer, VP6 as the mid-layer, with VP4 and VP7 forming the outermost shell which is required for virus infectivity.

Using cryo-electron microscopy (cryoEM) and improved image processing techniques the current understanding of virions has been enhanced reaching a resolution of about 9.5-Å (Fig 1.1) (Li *et al*., 2009). All three viral layers show icosahedral organization (Li *et al*., 2009). Starting from the inside of the virion, the major architecture of the inner layer surrounding the viral genome possesses 120 molecules of VP2 arranged as 60 dimers (Li *et al*., 2009). Beneath of this VP2 lattice there are 12 copies of VP1 and VP3 per virion. The intermediate shell surrounding the inner core is made up of 780 molecules of VP6 arranged as 260 trimers (Li *et al*., 2009). This VP6 shell may provide structural integrity to the rotavirus capsid by enhancing the morphologic homogeneity and long-term stability of the particle (Zeng *et al*., 1996). The outermost layer consists of 780 molecules of VP7 and 120 molecules of VP4. The VP7 interacts with the tips of the VP6 trimers to form the outer most shell. Meanwhile VP4 which forms 60 spikes protruding 120Å from the surface of the outer shell interacts with both VP6 and VP7 (Li *et al*., 2009). A distinctive feature of the viral capsids is the 132 aqueous channels that penetrate the virion to link the inner core with the outer surface. These channels are thought to import the metabolites required for RNA transcription and export the nascent RNA transcripts for subsequent viral replication (Lawton *et al*., 1997).

All three forms of the virus particle (triple-layered, double-layered and core) can be found in stool samples and tissue culture supernatants. However only triple-layered

particles are fully infectious under normal conditions (Bridger and Woode, 1976). In order to maintain the stability of the triple-layered particle calcium is necessary, apparently acting to stabilize the outer capsid glycoprotein VP7, with the crucial concentration of calcium required varying for different viral strains (Estes, 2001). Consequently the treatment of particles with calcium chelators (EDTA and EGTA) removes the outer capsid leading to a loss of virus infectivity. However the double shelled particles or DLPs produced by such treatment are capable of viral RNA transcription (Cohen *et al*., 1979; Estes *et al*., 1979). Reconstitution of TLPs from DLPs can be achieved by presenting VP4 and VP7 at the proper concentration of calcium (Chen and Ramig, 1993a). Viral cores can be produced from DLPs by treating them with chaotropic agents such as sodium thiocyanate or high concentrations of calcium chloride (Chen and Ramig, 1993b).

The three types of viral particle have distinct densities in cesium chloride (CsCl) and sedimentation values in sucrose which are as follows:

(1) TLPs have a density of 1.36g/cm^3 in CsCl and sediment at 520-530S in sucrose.

(2) DLPs have a density of 1.38g/cm^3 in CsCl and sediment at 380-400S in sucrose.

(3) Cores have a density of 1.44g/cm^3 in CsCl and sediment at 280S in sucrose.

Thus the different viral particles can be separated by density equilibrium centrifugation on CsCl gradients. Additionally agarose gel electrophoresis has been shown to allow separation of the three types of particle (Estes, 2001).

TLPs are relatively stable under normally environmental conditions. They are resistant to fluorocarbon extraction, and treatment with ether, chloroform or nonionic

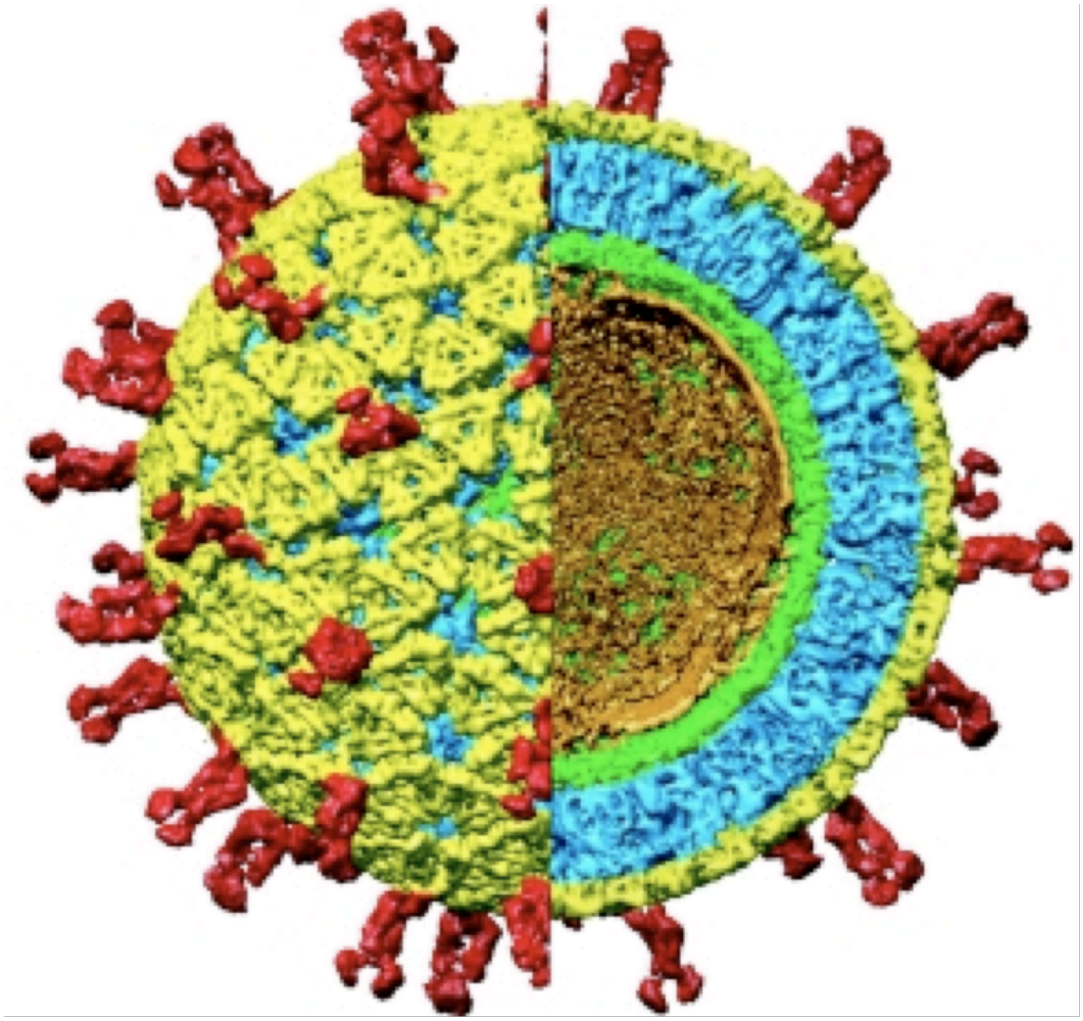

Figure 1.1: Structure of reconstruction of rotavirus particle at 9.5-Å resolution.

Picture adapted from Li *et al* (Li *et al*., 2009). From the outermost layer, VP4 spikes are in red, VP7 layer is in yellow, VP6 layer is in blue, VP2 layer is in green, the internal density (RNA and polymerase complex) is in orange.

detergents which probably reflects the lack of a lipid envelope on mature particles (Estes *et al*., 1979). Infectivity of TLPs is stable within the pH range of 3 to 9. However VP4 is selectively lost at high pH and the particle can be broken down by exposure to very low pH (Anthony *et al*., 1991; Weiss and Clark, 1985). In the presence of 1.5 mM $CaCl_2$ TLPs remain infectious for at least a month at room temperature but there is a loss of infectivity after repeated freezing and thawing

(Narang and Codd, 1983). Despite their stability, there are several potent disinfectants effective against rotaviruses including SDS, 95% ethanol, phenols, formalin and chlorine (Narang and Codd, 1983). Among these, 95% ethanol is the most potent disinfectant which works by removing the outer capsid shell (Narang and Codd, 1983).

1.1.3 Viral Genome

The viral genome is composed of 11 segments of double-stranded RNA (dsRNA). Deproteinized rotavirus dsRNAs are not infectious indicating the need for the viral RNA-dependent RNA polymerase to transcribe mRNA. The general features shared by all 11 dsRNA are as follows:

(1) The +RNA of dsRNA contains a 5' m^7G cap but lacks a 3' poly-A tail (Imai *et al*., 1983; McCrae and McCorquodale, 1983).

(2) The open reading frame of each segment is flanked by 5' and 3' untranslated regions (UTRs) that are of variable length. The open reading frame typically encodes a single protein except for gene 11 that encodes two proteins (NSP5 and NSP6) in some strains of rotavirus (Mattion *et al*., 1991; Rainsford and McCrae, 2007).

(3) All segments share very little sequence identity except for very short consensus sequences at the termini (McCrae and McCorquodale, 1983; Mitchell and Both, 1990a). The 3' consensus sequence of the plus sense RNA strand has the conserved sequence 5'-UGUGACC-3' as the minimal essential promoter for dsRNA synthesis (Wentz *et al*., 1996).

(4) The rotavirus segments are completely base paired and the gene sequences are A+U rich (58% to 67%) (Kapikian, 2001).

Analysis of the viral genome using polyacrylamide gel electrophoresis (PAGE) is

relatively easy and popular for detecting virus and monitoring viral outbreaks and transmission. Thus the electrophoretic pattern of group A rotavirus is composed of four high-molecular-weight dsRNAs (gene 1-4), two middle-size segments (gene 5 and 6), a distinctive triplet of segments (gene 7-9), and the two smallest segments (gene 10 and 11) (Kapikian, 2001).

1.1.4 Genome-Protein Coding Assignment

The coding assignments and many functions of the viral proteins have been determined using *in vitro* translation of viral RNA (McCrae and McCorquodale, 1983), immunological studies with specific antibodies, expression of viral proteins via recombinant DNA and analysis of reassortant viruses (Both *et al*., 1983; Greenberg *et al*., 1983b; Kantharidis *et al*., 1983; Mason *et al*., 1983). Figure 1.2 shows the eleven gene segments and the corresponding viral proteins. Both the genome segments and viral proteins are numbered based on their migration order on PAGE from the slowest to the fastest. But the absolute migration order of cognate genes does vary among viral strains. The identification of cognate genes is made on the basis of hybridization with gene-specific probes or direct sequencing.

1.1.5 Functions of Viral Structural and Nonstructural Proteins

1.1.5.1 Structural Proteins (VPs)

The 11 genome segments encode six structural proteins found in virions (Fig 1.3) and six non-structural proteins, although some viral strains have been reported as lacking the NSP6 open reading frame (Rainsford and McCrae, 2007). The structural proteins are VP1, VP2, VP3, VP4, VP6 and VP7, with VP5* and VP8* being

generated by proteolytic cleavage of VP4. The core particle is composed of VP1, VP2 and VP3 which together act as the virus transcriptional unit. VP4, VP6 and VP7 are the major structural proteins and make up the largest proportion of the virion.

1.1.5.1.1 VP1

VP1 have been detected inside the VP2 core (Patton, 1996). VP1 appears to be the viral RNA polymerase functioning as both the viral replicase and transcriptase (Patton, 1996). Amongst the core proteins only VP1 shows a specific viral RNA binding property (Patton, 1996). Although VP1 is the candidate as the viral polymerase, VP2 has been shown to be required for its replicase activity (Patton *et al*., 1997).

1.1.5.1.2 VP2

Studies have shown that VP2 forms the basic architecture of the core and is capable of forming core-like particles spontaneously when expressed in the insect baculovirus system (Labbe *et al*., 1991). VP2 also binds RNA non-specifically which is thought to facilitate its role in viral replication and encapsidation (Labbe *et al*., 1994).

1.1.5.1.3 VP3

VP3 has been detected inside the VP2 core (Patton, 1996) and acts as a multifunctional capping enzyme possessing the viral guanylyltransferase and methyltransferase activities during virus replication (Chen *et al*., 1999; Liu *et al*., 1992; Pizarro *et al*., 1991).

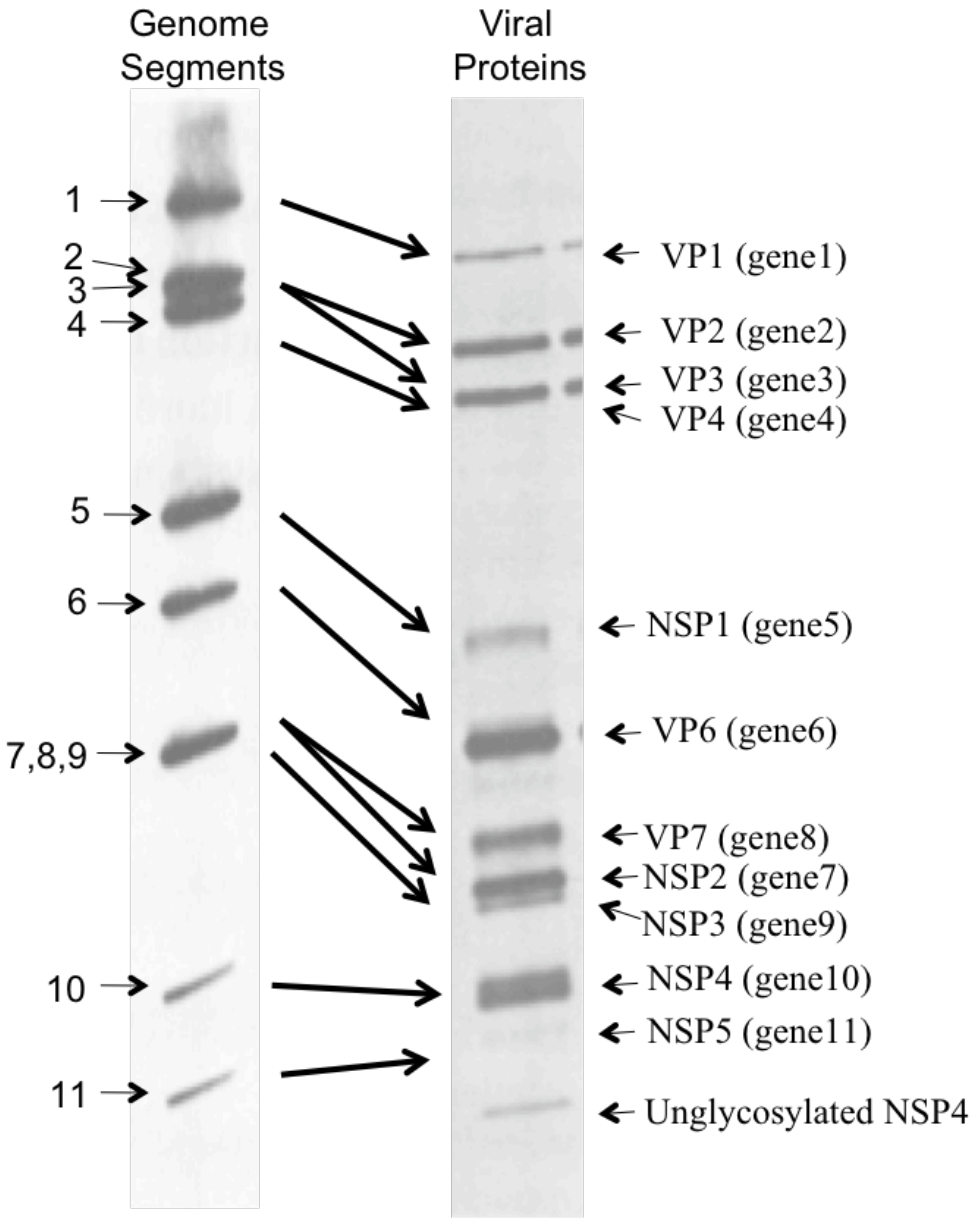

Figure 1.2: Polyacrylamide gel analysis of viral genes and corresponding proteins.

The viral genome RNA segments and proteins shown are for the UKtc strain of bovine rotavirus analyzed by SDS-PAGE. All gene segments are mono-cistronic except for gene 11 which encodes a second out of phase reading frame. The genome segments were from virus-infected cells pulse-labeled at 5-6 hours post infection. The viral proteins were from virus-infected cells pulse-labeled at 6 hours post infection. SDS-PAGE pictures adapted from McCrae (McCrae and Faulkner-Valle, 1981).

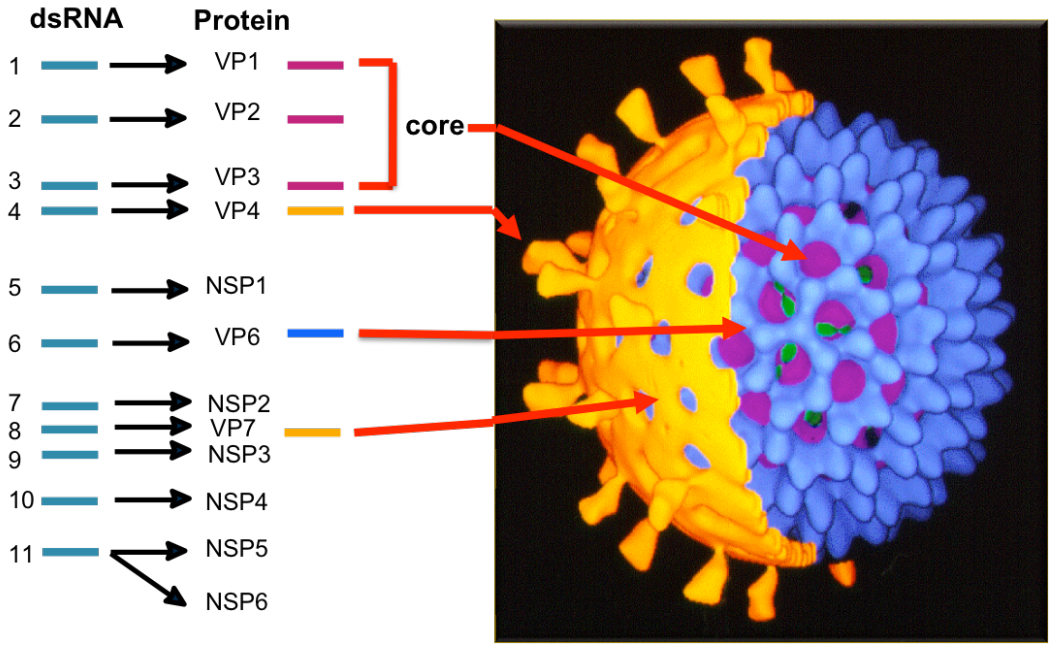

Figure 1.3: Schematic representation of gene-protein coding assignment and location of structural proteins in the virion.

Left: Rotavirus dsRNA genome (UKtc strain) and the proteins encoded in each gene segments. Right: CryoEM reconstruction of the rotavirus particle demonstrating the position of the viral structural proteins in the particle (Prasad *et al*., 1988; Yeager *et al.*, 1990). The outermost layer (VP4 and VP7) is in yellow, the VP6 layer is in blue, the inner core (VP1, VP2 and VP3) is in red.

1.1.5.1.4 VP4

The viral spike protein VP4 is the viral haemagglutinin, which is surprising given its lack of glycosylation, and appears to be a very important virulence factor in mice and piglets (Kalica *et al*., 1983; Offit *et al*., 1986). It also determines host range and cell tropisms (Estes, 2001). The penetration, but not the binding of virus to cells can be greatly enhanced by proteolytic cleavage of VP4 to produce VP5* and VP8*, and this also leads to some increase in virus infectivity (Kaljot *et al*., 1988). Protective immunity in children and animals can be effectively induced by VP4 via the

generation of VP4-specific neutralizing antibody (Estes, 2001).

1.1.5.1.5 VP6

VP6 which forms the middle shell of the virion accounts for about 50% of the total virion protein. It is a hydrophobic protein and very stable after spontaneous trimerization (Gorziglia *et al*., 1985). It is highly immunogenic leading to it being the primary antigen detected in routine diagnosis of rotavirus disease (Estes *et al*., 1987). Surprisingly *in vivo* protection has been observed when two immunoglobulin A antibodies against VP6, which lack virus neutralization activity, are administrated to the luminal side of the intestinal tract (Burns *et al*., 1996). In common with several other major structural proteins of members of the *Reoviridae* (Lopez *et al*., 2005a; Plascencia-Villa *et al*., 2009), VP6 is capable of assembling nano-tubular structures spontaneously in virus-infected cells or when expressed individually in the insect baculovirus system (Lopez *et al*., 2005a; Plascencia-Villa *et al*., 2009). Although the potential role of these structures in infection is currently unknown they have been exploited in the production of a novel nanobiomaterial (Lopez *et al*., 2005a; Plascencia-Villa *et al*., 2009).

1.1.5.1.6 VP7

The N-linked glycoprotein VP7 forms the smooth surface of the outer capsid and accounts for 30% of the total virion protein. It is the G serotype determinant of rotavirus (Greenberg *et al*., 1983a). This fact has stimulated intense investigations of its structure, biosynthesis and function. VP7 is co-translationally glycosylated as it is inserted into the ER membrane (Ericson *et al*., 1983; Kabcenell and Atkinson, 1985). The glycosylation of VP7 involves addition of high mannose oligosaccharides that are processed by trimming. Although VP7 has up to three glycosylation sites, only

two of them are apparently used in different viral strains (Kouvelos *et al*., 1984a; Kouvelos *et al*., 1984b). Studies attempting to understand the ER retention property of VP7 showed that it is an integral membrane protein with a luminal orientation (Kabcenell and Atkinson, 1985). VP7 has also been shown to be the dominant target for cytotoxic T-lymphocyte (CTL) activity in mice indicating its important role in the immune response against rotavirus (Heath *et al*., 1997; Offit *et al*., 1994).

1.1.5.2 Nonstructural proteins (NSPs)

During viral infection, rotaviruses also encode at least five non-structural proteins (NSPs). Although they are not present in viral particle they play very important roles in viral replication, morphogenesis and pathogenesis.

1.1.5.2.1 NSP1

NSP1 (segment 5) is the least conserved protein encoded by rotaviruses (Mitchell and Both, 1990b) and has received considerable attention recently following recognition of its role as an antagonist of the interferon (IFN) signaling pathway (Sen *et al*., 2009). Following viral infection recognition by the host of expressed viral proteins and nucleic acids causes activation of IFN regulatory factors (IRFs) that lead in turn to expression of type I IFNs (IFN-α and IFN-β). NSP1 was first shown to interact with the IFN regulatory factor 3 (IRF3, mediates expression of IFN-α and IFN-β)) in a yeast two hybrid screen (Graff *et al*., 2002). This interaction was subsequently shown to promote proteasome-dependent degradation of IRF3 (Barro and Patton, 2005). In addition NSP1 has also been reported to mediate proteasome dependent degradation of IRF5 and IRF7 (Barro and Patton, 2007). IRF5 functions to up-regulate IFN expression and IRF7 serves as a master regulator of type I IFN

(IFN-α and IFN-β) expression (Honda *et al*., 2005). Role of NSP1 in degrading of IRF5 suggests that it functions to down-regulate expression of IFNs whereas its role in stimulating the turnover of IRF7 suggests that it also functions to suppress the IFN signalling pathway (Barro and Patton, 2007). The NSP1 from the Wa strain has also been showed to prevent nuclear accumulation of the signal transducer and activator of transcription 1 (STAT1) and STAT2 (Holloway *et al*., 2009). This inhibits activation of the expression of many IFN-stimulated genes (ISG) with antiviral properties whose expression in surrounding uninfected cells would normally result in establishment of anti-viral state in the cell population (Holloway *et al*., 2009). Studies have also shown that NF-kB, which plays a key role in anti-viral defenses, is affected by NSP1 through prevention of its activation and nuclear accumulation (Graff *et al*., 2009; Holloway *et al*., 2009). Specifically NSP1 from the porcine OSU strain induces proteasome-dependent degradation of β-transducin repeat containing protein (β-TrCP) (Graff *et al*., 2009). β-TrCP stimulates the degradation of NF-kB inhibitor (IkBα). Therefore increased degradation of β-TrCP leads to a preservation of IkBα which in turn prevents activation of NF-kB (Graff *et al*., 2009). As the molecular mechanism of NSP1 has been investigated in great detail the actual functionality of NSP1 in infected host has been called into question by the observations that bovine UK strain of rotavirus is able to degrade IRF3 in simian COS7 cells but not in mouse fibroblasts and murine NIH 3T3 cells (Sen *et al*., 2009). By contrast mouse EW strain and simian RRV strain of rotaviruses have shown their ability to degrade IRF3 in all of these three cell lines mentioned above (Sen *et al*., 2009). This finding suggests that the phenotype of IRF3 degradation of viral strains is cell line dependent.

1.1.5.2.2 NSP2

A distinct feature of rotavirus infected cells is the formation of cytoplasmic inclusion bodies called viroplasms where viral replication occurs. NSP2 has been shown to be an important component in forming viroplasms by interacting with NSP5 (Eichwald *et al*., 2004; Fabbretti *et al*., 1999). This interaction of NSP2-NSP5 is able to drive formation of viroplasm-like structures without the presence of other viral proteins (Eichwald *et al*., 2004; Fabbretti *et al*., 1999). However when NSP2 is transiently expressed alone it distributes diffusely in the cytoplasm (Eichwald *et al*., 2004; Fabbretti *et al*., 1999). Furthermore NSP2 has been shown to have high affinity to microtubules and this has been proposed to cause the association of viroplasms to the microtubular network and also virus induced microtubule de-polymerization (Cabral-Romero and Padilla-Noriega, 2006; Martin *et al*., 2010). Enzymatic studies have revealed that NSP2 possesses nucleoside triphosphatase (NTPase), RNA triphosphatase (RTPase) and helix-destabilizing activity (Taraporewala *et al*., 1999; Taraporewala and Patton, 2001; Vasquez-Del Carpio *et al*., 2006). These activities indicate that NSP2 also acts as a multi-functional protein involved in genome replication and packaging.

1.1.5.2.3 NSP3

NSP3 was initially reported to function primarily in the shut-off cellular protein expression following viral infection (Padilla-Noriega *et al*., 2002). In eukaryote protein translation, eukaryotic initiation factor 4E (elF4E) first binds to the of 5'-cap structure of mRNA. At the same time the poly A tail at the 3' end of mRNA is recognized by poly A binding protein (PABP). This is followed by the scaffold protein elF4G, bringing elF4E and PABP together through its interaction with them.

This latter interaction causes circularisation of mRNA which is required for efficient initiation of translation (Imataka *et al*., 1998; Preiss and Hentze, 1998; Tarun and Sachs, 1995). To interrupt this process NSP3 is first thought to recognize a minimal consensus sequence GACC at the 3' end of rotavirus mRNAs (Poncet *et al*., 1994). At the same time NSP3 also interacts with elF4G taking the position of PABP so that the PABP and its associated mRNA are evicted from the cellular translation complex resulting in the shut off of cellular protein synthesis (Piron *et al*., 1998). The simultaneous interaction of NSP3 with elF4G and the 3' end of viral mRNA has also been reported as being required for efficient translation of viral mRNA (Vende *et al*., 2000). However this straightforward role for NSP3 has been called into question by studies using RNAi technology to knock down NSP3 expression which had little effect on viral gene expression (Montero *et al*., 2006). Based on these observations the function of NSP3 in promoting the translation of viral proteins requires further investigation. In a separate study, a novel cellular protein, RoXaN associated with NSP3 (Vitour *et al*., 2004). This interaction does not appear to impair the interaction between NSP3 and elF4G and protein complexes of NSP3, elF4G and RoXaN can be found in virus infected cells suggesting the participation of RoXaN in regulation of viral protein expression (Harb *et al*., 2008; Vitour *et al*., 2004).

1.1.5.2.4 NSP4

The most studied NSP is perhaps NSP4 which is encoded by segment 10. This viral protein is both cotranslationally and post-translationally glycosylated. It is ER resident and has been shown to function like a receptor capable of mediating the budding of DLPs through the ER membrane (Au *et al*., 1989; Au *et al*., 1993; Taylor *et al*., 1993). NSP4 has also been shown to be a viral enterotoxin secreted in a

paracrine fashion (Ball *et al*., 1996; Zhang *et al*., 2000). A more detailed discussion of NSP4 will be presented later in this chapter.

1.1.5.2.5 NSP5

NSP5 is one of the two proteins encoded by segment 11. It is both O-glycosylated and phosphorylated post translationally (Afrikanova *et al*., 1996). Protein modification studies have shown that NSP5 possesses auto-kinase activity which leads to its hyper-phosphorylation independent of other viral proteins (Sen *et al*., 2006; Sotelo *et al*., 2010). Interactions of NSP5 with NSP2 and VP2 have been reported to be able to produce the viroplasm-like structures in a calcium dependent manner (Contin *et al*., 2010; Fabbretti *et al*., 1999; Sen *et al*., 2007). Recently the NPS5-NSP2 and NSP5-VP2 interactions have been shown to recruit all the other viral proteins found in viroplasms (Contin *et al*., 2010). These results have been interpreted as indicating that NSP5 plays a key role in the assembly of viroplasms and in recruitment of viroplasmic proteins (Contin *et al*., 2010). The overall role of NSP5 in the viral replication cycle has also been studied by knocking down its expression using RNAi technology (Campagna *et al*., 2005; Lopez *et al*., 2005b). This lead to a reduction in the number and size of viroplasms, an altered intracellular distribution of the other viroplasm-associated proteins, a decreased production of the other structural and non-structural proteins, of genomic dsRNAs, and of infectious viral particles (Campagna *et al*., 2005; Lopez *et al*., 2005b). These observations pinpoint NSP5 as not only functioning to assembly viroplasms but as also being involved in the regulation of viral replication.

1.1.5.2.6 NSP6

Gene segment 11, the smallest genomic RNA segment not only encodes NSP5 but also has an alternative open reading frame, encoding NSP6 in most viral strains. NSP6 is encoded in a +1 alternate reading frame in gene 11 that is positioned completely within the ORF of NSP5. Expression studies of NSP6 showed that it appears to be expressed at a low level, with a high turnover rate also having been detected in a pulse-chase analysis (Mattion *et al*., 1991; Rainsford and McCrae, 2007). Interaction of NSP6 with NSP5 has been demonstrated by using co-immunoprecipitation from cells co-transfected with ORFs of NSP5 and NSP6 and in yeast two hybrid assays; however this interaction could not be confirmed in virus infected cells (Torres-Vega *et al*., 2000). The C-terminal region of NSP5 has been mapped as interacting with NSP6, with this region of NSP5 also having been shown to be involved in both dimerization and its hyper-phosphorylation (Torres-Vega *et al*., 2000). Studies have shown that NSP6 is co-localized with NSP5 to viroplasms in virus-infected cells (Rainsford and McCrae, 2007; Torres-Vega *et al*., 2000). The absence of the start codon of NSP6 in two human strains (Mc323 and 512-C) (Kojima *et al*., 1996; Wu *et al*., 1998), and truncated NSP6 found in both the Alabama strain of lapine virus (Gorziglia *et al*., 1989) and the porcine OSU strain (Gonzalez and Burrone, 1989) has led to the suggestion that NSP6 may play non-essential role in regulation during the viral replication cycle (Rainsford and McCrae, 2007).

1.1.6 Viral Replication Cycle

1.1.6.1 Attachment and Entry

The initial stage in a rotaviral infection is targeting of the virus to tissue and cells.

This virus-tissue/cell interaction that determines both the tissue and cell tropism and host range requires two factors, viral capsid proteins and cell surface molecules (cellular receptors). Investigations focusing on these interactions have primarily been conducted using either the monkey kidney epithelial cell line MA104 and/or the polarized human colon carcinoma cell line Caco-2. Both of these cell lines are highly permissive for rotavirus infection and in the case of Caco-2 cells are thought to reflect the *in vivo* situation. The outermost layer of TLPs made up of VP4 and VP7 as expected has been shown to be involved in the initial binding of the virus to the host cell (Lopez and Arias, 2004). A variety of potential cellular receptors have been reported as being involved in this binding including N-acetylneuraminic acid (sialic acid), several integrins ($\alpha 2\beta 1$, $\alpha v\beta 3$, $\alpha 4\beta 1$ and $\alpha x\beta 2$) and a heat shock cognate (hsc70) (Lopez and Arias, 2004). Turning to the viral molecules involved, studies have shown that the proteolytic cleavage of the VP4 and the glycosylation of VP7 are not essential for this binding (Fukuhara *et al*., 1988; Petrie *et al*., 1983).

Amongst the various potential cellular receptors identified sialic acid has been generally considered to mediate the initial viral attachment to susceptible cells based on the observation that treatment of cells with neuraminidase (NA) or pre-incubation of virus with sialic acid containing compounds both reduced the infectivity of some viral strains (Isa *et al*., 2006; Lopez and Arias, 2004). Viral strains affected by such treatments are classified as NA-sensitive strains and include the simian rotaviruses SA11 and RRV, and the bovine strain NCDV (Isa *et al*., 2006; Lopez and Arias, 2004). By contrast a number of animal virus isolates and most strains isolated from humans are not affected by prior neuraminidase treatment of cells and consequently are classified as NA-resistant strains and these include the human strains Wa and DS-1 (Isa *et al*., 2006; Lopez and Arias, 2004). However this division does not mean

that NA-resistant strains do not use sialic acid for cell attachment but rather that they may use sialic acid located in the internal regions of oligosaccharide structures, like ganglioside GM1. This internal sialic acid is less sensitive or completely insensitive to NA treatment (Lopez and Arias, 2004). Recent studies using NMR spectroscopy, molecular modelling and infectivity competition assays have provided evidence that the sub-terminal sialic acid of ganglioside GM1 was a key determinant for cell-virus recognition of the NA-resistant human strain Wa (Haselhorst *et al*., 2009). This suggests that sialic acid also plays a role in the cell attachment of NA-resistant strains.

There is some evidence that integrins are the subsequent components that virus bind specifically to after initial attachment to cells. To date a number of integrins including α2β1, αxβ2, α4β1 and αvβ3 have been identified as having a role at the post-attachment level (Lopez and Arias, 2004). Expression of integrin α2β1 (VLA-2) in Chinese hamster ovary (CHO) cells allowed virus to enter and replicate 2-10 fold more productively than in parental CHO cells (Ciarlet *et al*., 2002). However VLA-2 alone was not responsible for viral cell attachment and entry (Ciarlet *et al*., 2002). Additional studies have shown that VP4 from a number of rotavirus strains including those from humans, monkeys, and cattle was the viral protein interacting with VLA-2 *in vitro* (Graham *et al*., 2003). This VLA-2-VP4 interaction has been supported by experiments showing that antibodies against different domains of VP4 and anti-peptide against the VP4 interaction domain of VLA-2 both inhibited viral binding to cells expressing VLA-2 (Fleming *et al*., 2007; Graham *et al*., 2004). The relevance of VLA-2 to viral infection *in vivo* has also been investigated in newborn mice infected with RRV. This showed that the expression of VLA-2 in biliary epithelial cells (cholangiocytes) but not in hepatocytes made cholangiocytes rather

than hepatocytes susceptibility to RRV infection. The use of monoclonal antibodies against the α2 unit of VLA-2 has also been shown to reduce the ability of RRV to cause biliary atresia in mice (Jafri *et al*., 2008).

The αvβ3 integrin has also been examined in some detail. Transfection of αvβ3 genes into CHO cells significantly increased their susceptibility to the rotavirus strains RRV, nar3 and Wa (Guerrero *et al*., 2000). The viral protein responsible for αvβ3 binding was identified as VP7 rather than VP4 (Graham *et al*., 2003; Zarate *et al*., 2004).

A recent study using RNA interference based silencing of α2 and β3 in MA104 cells showed a reduction in infectious virus yield of strains RRV and Wa but not UK and TFR-41, providing further support for the α2 and β3 subunits of integrins involvement in viral entry of some viral strains (Isa *et al*., 2009).

Additional members of the integrin family, such as α4β1 and αxβ2 have also been reported to promote viral post-attachment binding (Fleming *et al*., 2007; Graham *et al*., 2005; Graham *et al*., 2003; Graham *et al*., 2004). α4β1 has been shown to interact with VP4 (Graham *et al*., 2005), and its interaction with VP7 has also been suggested by the fact that antibodies directed against VP7 reduced viral binding to α4β1 (Fleming *et al*., 2007). Studies on αxβ2 have shown that it interacts with the amino acid motif GPR in VP7 (Graham *et al*., 2003). Furthermore synthetic peptides containing amino acids GPR have been shown to block the infectivity of virus (Graham *et al*., 2004). Finally heat shock cognate 70 (Hsc70) has been identified as promoting viral entry at a post-attachment step (Guerrero *et al*., 2002). The studies on Hsc70 have shown that it interacts with VP4 and VP6, probably through the peptide binding and ATPase domains of hsc70 (Gualtero *et al*., 2007; Zarate *et al*., 2003) (Perez-Vargas *et al*., 2006).

Thus, to date the study of rotavirus entry has revealed the participation of sialic acid, integrins and hsc70 as cellular receptors and has also suggested that the molecules required for viral entry are viral strain and cell line dependent. It is also possible that there are other cell surface proteins playing indispensable roles in the entry process. Consequently it appears that the molecular mechanism of rotavirus entry is a complex and multistep process demanding the correct organization and interaction between both of the viral surface antigens (VP4 and VP7) and various cell surface receptors.

1.1.6.2 Internalization

Following attachment to the cell surface virus initiates the internalization of the viral particle. Studies using electron microscopy have shown that the viral particles are associated with coated pits and sequestered in a variety of coated vesicles suggestive of receptor-mediated endocytosis being employed for internalization (Ludert *et al*., 1987; Quan and Doane, 1983). Alternatively, using the same experimental technique, it has been proposed that direct plasma membrane penetration is employed by trypsin pre-treated infectious virus particles. By contrast, in these studies untreated noninfectious viral particles were removed from the plasma membrane by endocytosis resulting in a non-productive infection (Suzuki *et al*., 1985). Studies using biochemical approaches have demonstrated that the use of lysosomotropic agents, such as NH_4Cl, chloroquine, methylamine, and amantadine, and of drugs that block the intracellular traffic of endosomes, such as cytochalasin D, dansylcadaverin and bafilomycin A1, have no effect on the viral entry (Bass *et al*., 1995; Cuadras *et al*., 1997; Fukuhara *et al*., 1987; Kaljot *et al*., 1988; Ludert *et al*., 1987). The failure of these treatments argues against endocytosis being the primary route used by virus

to enter the cells. Consequently, direct plasma membrane based entry is perhaps now more favoured as the internalization mechanism of rotaviruses (Sanchez-San Martin *et al*., 2004). Using a combination of biochemical and genetic (over-expression of dominant-negative mutants of the target gene) approaches one study has demonstrated that the entry of virus is not through a well-defined clathrin or caveolin-dependent endocytosis but is rather dependent on functional dynamin in a cholesterol sensitive pathway (Sanchez-San Martin *et al*., 2004). Recently in a comparison of four different strains of rotaviruses, which included the simian strain RRV used in the above studies, hsc70, dynamin, and cholesterol were required for entry of all of the strains. However the human strain Wa, porcine strain TFR-41, and bovine strain UK all appear to enter the cells through clathrin-mediated endocytosis as their infectivity is blocked by the treatment inhibiting this pathway. These three strains of rotaviruses are also consistently sensitive to changes in the endosomal pH (Gutierrez *et al*., 2010). These studies emphasizes the possibility that different viral strains appear to utilize diverse mechanisms (i.e. direct plasma membrane penetration and/or endocytosis) for their internalization, and that the exact mechanism of each pathway still remains unclear.

1.1.6.3 Uncoating

The uncoating process of rotaviruses involves removing the outermost shell made up of VP4 and VP7. This process can be achieved *in vitro* by the use of EDTA or EGTA as chelating agents (Cohen *et al*., 1979). *In vivo*, it is thought that the low levels of calcium concentration in the cells is important to activate this event; the inhibition of uncoating of the porcine strain OSU on MA104 cells by the calcium ionophore A23187 being the experimental basis for this conclusion (Ludert *et al*., 1987). It has

also been reported that the uncoating of the RRV and SA11 strains for virus are not affected by the use of compounds such as the calcium ionophores A23187 and ionomycin or of the endoplasmic reticulum calcium-ATPase inhibitor thapsigargin which increases intracellular calcium levels (Cuadras *et al*., 1997). These different observations being made concerning the importance of calcium levels for viral entry may be accounted for by the different viral strains used in the various studies (Cuadras *et al*., 1997; Ludert *et al*., 1987).

1.1.6.4 Transcription

The product of uncoating associated with virus entry is the double-shelled (DS) particle that is transcription-competent. The transcriptional ability of DLPs has been demonstrated *in vitro* by using treatment with EGTA or EDTA to uncoat the TLP (Cohen *et al*., 1979; Mason *et al*., 1980). To initiate transcription the viral RNA dependent RNA polymerase believed to be VP1 utilizes viral dsRNA to synthesize positive sense single stranded mRNA (Lawton *et al*., 2001). The nascent RNA transcripts are capped at their 5' end by the virion associated guanylyl and methyltransferase activities residing in the virion core protein VP3 to produce mRNAs with a $^{m7}GpppG^{(m)}$ cap at their 5' end (Lawton *et al*., 2001). As the elongation process proceeds, the growing mRNA protrudes from DLPs through channels that penetrate the VP2 and VP6 capsid layers (Lawton *et al*., 2001). On completion mRNA molecules are released into the cytoplasm of the infected cell and a new cycle of transcription begins using the same viral RNA template and enzymes (Lawton *et al*., 2001). Transcript of the 11 segments dsRNA in the DLP involves 12 copies of VP1 and VP3 and is a distinct feature of segmented viruses (Prasad *et al*., 1996). In an early study done using the bovine UKtc strain of rotavirus, the

transcriptional regulation of viral genes has been shown to occur at two levels (Johnson and McCrae, 1989). The first is temporal control, with the genes divided into three categories, the first being genes 1, 2, 6, 8 and 11 whose transcription proceeds at a more or less linear rate throughout the infection cycle (Johnson and McCrae, 1989). The second category includes only gene 7 which accumulates rapidly early in the infection cycle and reaches a plateau at which it is maintained for the rest of the infection cycle (Johnson and McCrae, 1989). The third and final category involves genes 3, 4, 5, 9 and 10 which have low rates of transcription at early times post infection, but the rate increases later in the infection cycle (Johnson and McCrae, 1989). The second level of transcriptional control is a quantitative one, with the greatest accumulation being seen for genes 2 and 7 at 73,000 to 94,000 molecules per cell; a medium level seen in gene 3 at 45,000 molecules per cell and genes 1, 5, 8, 9 and 11 at 30,000 to 36,000; with the lowest levels being seen for genes 4, 6 and 10 at 14,000 to 21,000 molecules per cell (Johnson and McCrae, 1989).

1.1.6.5 Translation

To translate the capped viral mRNA released from DLPs the virus hijacks the translational machinery of the cell, with cellular ribosomes being recruited for synthesis of all 12 of the viral proteins (Patton *et al*., 2006). To regulate viral protein translation NSP3 has been shown to be important in shutting off cellular protein synthesis and enhancing viral protein synthesis by interacting with eIF4G (eukaryotic initiation factor 4G) and RoXaN (rotavirus X protein associated with NSP3) (Harb *et al*., 2008; Padilla-Noriega *et al*., 2002; Piron *et al*., 1999; Piron *et al*., 1998; Vende *et al*., 2000; Vitour *et al*., 2004). However the interaction between NSP3 and eIF4G

only appears to shut off cellular protein synthesis and not contribute to efficient viral protein translation as indicated in NSP3 knock down experiments using RNAi (Montero *et al*., 2006). A study attempting to understand the translational regulation used by bovine strain UKtc rotavirus clearly showed that viral proteins are neither synthesized in equal amounts nor are the amounts similar to that of their corresponding gene transcripts (Johnson and McCrae, 1989). This study showed that VP6 and NSP4 were synthesized in the largest quantities compared to the nine other viral proteins with NSP5 and NSP6 being the least synthesized proteins (Johnson and McCrae, 1989; Rainsford and McCrae, 2007).

1.1.6.6 Genome Replication

Following translation of the viral proteins NSP2 and NSP5 they assemble to form electron-dense cytoplasmic inclusions (viroplasms). These structures are the sites for viral (-)RNA synthesis and the formation of DLPs (Altenburg *et al*., 1980; Fabbretti *et al*., 1999; Petrie *et al*., 1984). It has been proposed that the initial plus sense RNA transcripts made by infecting DLPs translocates to either polysomes for protein translation or viroplasms for negative strand RNA synthesis i.e. genome replication (Patton *et al*., 2006). Further synthesis of viral plus sense RNA for replication has been reported to occur exclusively in viroplasms from newly formed DLPs (Silvestri *et al*., 2004). Packaging of plus sense transcripts into cores and its replication to form dsRNA occur in succession such that no naked dsRNA is formed in the cytoplasm of infected cells (Patton *et al*., 2006).

1.1.6.7 Particle Assembly and Maturation

In virus infected cells DLP particles (VP1, VP2, VP3 and VP6) are formed in

viroplasms and released into the cytoplasm, the NSP4-driven translocation of DLPs across the ER membrane to the ER is followed by their maturation to become infectious TLPs. The viral core (VP1, VP2 and VP3) has been shown to accumulate in viroplasms using electron microscopy (Korolev *et al*., 1981; Suzuki *et al*., 1981). Following expression of viral proteins, recruitment of VP1 and VP2 from the cytoplasm has been reported to depend both on their high affinity to single-stranded RNA and their interactions with NSP2 and NSP5 (Arnoldi *et al*., 2007; Colomina *et al*., 1998; Patton *et al*., 2006). The enriched VP2 forms the structural basis for the viral core and its simultaneous association with VP1 and VP3 leads to the formation of a functional viral core (Zeng *et al*., 1998). The formation of DLPs is achieved by adding VP6 to the viral core. Co-expression of VP2 and VP6 in insect cells results in the formation of DLPs, which is indicative of the intrinsic ability of VP6 to associate with the viral core (Zeng *et al*., 1996). During DLP formation in infected mammalian cells VP6 has been observed in the exterior region of viroplasms (Lopez *et al*., 2005a). This would allow VP6 to associate with newly assembled and translocated cores to form DLPs as they move toward the periphery of viroplasms. NSP4 has been shown to regulate VP6 localization around viroplasms probably by its interaction with VP6, with silencing NSP4 by specific siRNA resulting in the formation of large filamentous arrays of VP6 in the cytoplasm (Au *et al*., 1989; Lopez *et al*., 2005a). The association of VP6-encapsidated DLPs and NSP4 allows the former to bud across the ER into the lumen of the ER, with the DLPs acquiring a lipid envelope during this translocation step (Lopez *et al*., 2005a). The heterotrimeric complex containing NSP4 and the ER lumen resident VP7 and VP4 proteins eventually results in the maturation of DLPs by disassociation of NSP4 and the lipid envelope and the addition of VP7 and VP4 (Lopez *et al*., 2005a). Research

addressing the role of VP7 and VP4 in the process of TLP maturation has been done using specific siRNA knockdown. Silencing VP7 resulted in the accumulation of DLPs in the ER but had no effect on DLP formation. This suggests that VP7 is involved in removing the lipid envelope (Lopez *et al*., 2005a). Knock down of VP4 lead to the appearance of TLPs lacking VP4 spikes suggesting that VP4 is not involved in the budding of DLP into the ER or the removal of the lipid envelope. Thus it appears that VP4 only plays a role in the final step of TLP maturation by forming spikes on the surface of TLP (Arias *et al*., 2004; Dector *et al*., 2002). The silencing of both VP7 and VP4 did not prevent DLPs from entering the ER lumen suggesting that NSP4 alone was sufficient to drive DLPs into the ER lumen.

1.1.6.8 Release of Virions

The mechanism of progeny virion release from cells differs in undifferentiated (MA104) and differentiated (Caco-2) cell lines. In MA104 cells, an undifferentiated cell line, release of virions has been reported to be through cytolysis at the end of the viral replication cycle (Musalem and Espejo, 1985; Perez *et al*., 1998). By contrast in differentiated Caco-2 cells, virions have been shown to be released preferentially from the apical surface of the cell through a vesicular transport process that bypasses the Golgi apparatus (Gardet *et al*., 2007; Jourdan *et al*., 1997). The apical release has been reported to involve actin and lipid rafts (Gardet *et al*., 2007; Sapin *et al*., 2002). However disruption of the cellular skeleton particularly the actin network has been reported in Caco-2 cells at later times in the viral replication cycle (Brunet *et al*., 2000a). Furthermore endogenously expressed or exogenously added NSP4 have also been shown to alter the actin network (Berkova *et al*., 2007). Taken together, these observations in differentiated enterocytes suggest that the release of progeny virions

may be blocked late in the infection cycle because of disruption of the actin network by viral replication in the infected cells. In addition disruption of the actin network in bystander uninfected cells by secreted NSP4 may set a barrier in these cells that will not support progeny virions released following infection.

1.1.7 Rotavirus Disease

1.1.7.1 Symptoms and Clinic Features

Rotavirus infection normally leads to diarrhoea varying from subclinical through mild to severe and finally a lethal dehydrating infection. Rotavirus patients usually have a temperature of 37.9 °C or above (Kapikian, 2001). Vomiting and dehydration often occur with a mean duration of 2.6 days for vomiting. Diarrhoea follows the vomiting where it occurs and lasts for a mean duration of 5 days. In some severe infections, illness progresses to death within 1 to 3 days of the onset of symptoms. It is believed that dehydration, electrolyte imbalance and aspiration of vomit are the main factors accounting for death (Kapikian, 2001). In immunodeficient children a chronic infection with serious symptoms can be established. In such children viral antigen was seen in sections of the liver and kidney and noticeable alterations in the viral genome were found after death of those patients (Kapikian, 2001).

1.1.7.2 Diagnosis and Treatment

The disease symptoms of rotavirus infection are not sufficiently specific to be diagnostic and consequently the identification of viral antigen or genomic RNA is required for diagnosis. To date a number of sensitive and viral strain specific methods have been developed (Kapikian, 2001). The distinctive morphology of the

rotavirus particle means that electron microscopy can be applied for direct detection in 80% to 90% of rotavirus-positive specimens (Kapikian, 2001). Currently the most widely used and promising diagnostic method is RT-PCR. It has allowed detection of virus and gene-typing from 4 to 57 days after the onset of diarrhoea (Richardson *et al*., 1998; Xu *et al*., 1990). Confirmatory ELISA and flow cytometry applied for rotavirus detection have also been reported to have excellent sensitivity (Barardi *et al*., 1999; Eiden *et al*., 1991; Ellens and de Leeuw, 1977). Other routinely used methods such as dot hybridization, counterimmuno-electro-osmophoresis, gel electrophoresis of rotavirus RNA, reverse passive hemagglutination assay (RPHA) and latex agglutination have also been developed in some labs and are the basis for some of the commercial kits available for diagnosing rotavirus infection.

In most cases of rotavirus mediated diarrhoea the patient will normally be recommended to take oral rehydration therapy (ORT) to increase fluid uptake in order to prevent the dehydration associated with vomiting and diarrhoea. If after ORT treatment severe dehydration still persistents then intravenous fluids must be given immediately (Kapikian, 2001).

1.1.7.3 Epidemiology

Although rotaviruses infect people of all ages, infants and young children are those primarily affected by this infection. Infants younger than 6 months are generally protected by maternal derived immunity (Haffejee, 1995). However, when this wanes a high incidence of symptomatic infection occurs covering the 6 to 24 month age group. By 3 years of age more than 90% of children are positive for antibodies against rotaviruses (Huilan *et al*., 1991). In the United States, about 2.7 million episodes of diarrhoea are estimated annually to be associated with rotavirus infection

(Kapikian, 2001). This results in 410,000 visits to a physician, 160,000 emergency room visits, 50,000 hospitalization, and 20 deaths (Kapikian, 2001). Economically this results in over $264 million in medical costs and over $1 billion in social costs (Kapikian, 2001). In developing countries, there are estimated to be approximately 130 million episodes of rotavirus illness with 18 million severe cases and 873,000 deaths (Kapikian, 2001), making rotaviruses globally the most important agent of life-threatening diarrhoea in infants and young children. In adults, infection is common but normally produces minimal or no symptoms due to the high level of immunity from previous infections (Kapikian, 2001).

The faecal-oral route of transmission is the major one seen in rotaviruses. A respiratory route of transmission is suggested by the temporal pattern of disease in temperate zones, with a distinct winter peak of incidence (Brandt *et al*., 1983; Ward *et al*., 1986). Additionally in tropical countries the seasonal pattern does not display uniformity throughout the year but rather shows a peak incidence in the rainy season (Cook *et al*., 1990). Studies have shown that the most efficient way to eliminate virus is treatment with alcohol (70%) with or without savlon which removes over 99% of the virus (Ansari *et al*., 1989). This study also found that routine sanitation methods such as tap water alone or with soap, even savlon in water (1:200) only remove about 80% of the virus (Ansari *et al*., 1989). The remaining 20% of infectious virions after routine washes are sufficient to produce clinical disease as it has been shown that as little as 1 infectious viral particle is capable of causing disease (Graham *et al*., 1987). Therefore, transmission of virus is common and difficult to prevent even in countries with good hygiene practices.

1.1.8 Pathogenesis

In vivo, rotaviruses initialize pathogenesis by infecting mainly mature enterocytes in the mid and upper section of the villi of the small intestine (Kapikian, 2001). Direct observations of the gastrointestinal tract demonstrated subsequent viral replication resulted in lesions in the jejunal mucosa of hospitalized infants and young children (Kapikian, 2001). These lesions include shortening and atrophy of the villi, mononuclear cell infiltration in the lamina propria, irregular microvilli and denudation of microvilli (Kapikian, 2001).

Studies of viral pathogenesis in experimentally infected animals have revealed more details. In calves and piglets showing clinical signs of disease, histopathological studies have revealed thinning of the epithelium cell wall, villous atrophy, shortened villi and conversion of epithelium from columnar to cuboidal (Carpio *et al*., 1981; Collins *et al*., 1989). However the histological change in the intestine could not wholly explain the mechanism of fluid loss and malabsorption as watery diarrhoea was seen in piglets before the detection of extensive intestinal damage (McAdaragh *et al*., 1980). Moreover, infected rabbits showed normal histology with significant alteration in glucose and leucine uptake (Lundgren and Svensson, 2001). Thus the involvement of viral molecules and cellular factors has been extensively investigated. Recently it has become clear that watery diarrhoea is a consequence of disturbances at the cellular and molecular level. Four hypotheses have been put forward to explain the intestinal secretion of fluids and electrolytes:

(A) Diminished absorptive capacity of the intestinal epithelium.

(B) Villi ischemia due to disrupted intestinal microcirculation.

(C) Involvement of the Enteric Nervous System (ENS)

(D) Rotavirus enterotoxin (NSP4)

These four hypotheses have been comprehensively reviewed (Lundgren and Svensson, 2001) and only the last of them will be discussed in detail in this thesis.

1.1.9 Rotavirus Vaccines

In 1998 the first licensed rotavirus vaccine (RotaShield, by Wyeth) was approved by the FDA in the United States. It was a live attenuated vaccine, able to prevent 80-100% of group A rotavirus induced severe diarrhoea, with no statistically significant serious adverse effects having been detected in the clinical trials. However after little more than a year, the vaccine was withdrawn after the discovery of a potential link between intussusception and the first dose of vaccine (Centers for Disease Control and Prevention, 1999).

Despite the disappointment engendered by the withdrawal of Rotashield from the market, there was new hope in 2006 with the announcement of two rotavirus vaccines. Rotarix developed and marketed by GlaxoSmithKline (GSK) is a single serotype, live attenuated human rotavirus vaccine administrated orally. It was shown to prevent G1 and non-G1 (G3, G4 and G9) rotavirus gastroenteritis (McCormack and Keam, 2009; Vesikari, 2008). The other oral vaccine, RotaTeq developed and marketed by Merck, is a live pentavalent vaccine. It contains five rotaviruses generated by reassortment and prevents G1, G2, G3, G4 and P1A induced gastroenteritis and severe disease at 74% and 98% efficacy respectively (Chandran and Santosham, 2008). To date ongoing evaluations of cost-effectiveness and vaccination programs globally show great reductions in clinical and economic burden for both of these vaccines (O'Ryan *et al*., 2009; Weycker *et al*., 2009).

1.2 Non-Structural Protein 4 of the UKtc Bovine Strain (NSP4)

1.2.1 NSP4 Structure and Modification

NSP4, encoded by genome segment 10, is a glycoprotein of 175 amino acids that has been found as an integral protein in the ER membrane. The primary translation product of NSP4 is 20 KDa but it becomes 28 KDa after co-translational and post translational glycosylation and oligosaccharide processing (Kabcenell and Atkinson, 1985). There are three hydrophobic domains (H1-H3) near to the N-terminus of NSP4 with two N-linked high mannose glycosylation sites being in the first of these domains (aa7 to 21). A predicted amphipathic α-helix and a folded coiled coil region are in the middle of the protein. The C terminus that is hydrophilic forms an extended cytoplasmic domain. The H2 transmembrane domain (aa28 to 47) which traverses the ER membrane enables NSP4 to anchor on the ER. The H3 domain (aa67 to 85) appears to lie on the cytoplasmic side of the ER membrane and is associated with DLP binding (Jagannath *et al*., 2006). Glycosylation studies indicate that carbohydrate moieties remain sensitive to endoglycosidase H digestion, and oligosaccharide processing of the Man9GlcNAc carbohydrate added to NSP4 stops at Man8GlcNAc, with the mannose-9 species predominating, indicating that no further trimming occurs in the Golgi (Estes, 2001).

1.2.2 Sequence Conservation

NSP4 is highly conserved across the group A rotaviruses that infect mammals. Detailed computational analysis of NSP4 sequences in GenBank has allowed the recognition of at least four genetic groups of NSP4, with 14 amino acids being absolutely conserved among all group A NSP4 protein. Of the conserved amino acids, two are glycosylation sites, one is in the middle of the transmembrane segment,

seven cross the VP4 binding domain, and five span in the middle of the toxic peptide domain, indicating the functional importance of the conservations (Lin and Tian, 2003). A more recent study detecting adaptive evolution of NSP4 has shown that NSP4 has suffered strong purifying selection across species (Song and Hao, 2009). The requirement for functionally important domains and host adaptive selection of NSP4 may explain the reason for its conservation in different species. In addition, analysis using sequences of human group B rotavirus has shown that despite the absence of primary sequence conservation between group A and B NSP4's, the predicted secondary structural features of the two proteins are highly conserved (Guzman and McCrae, 2005).

1.2.3 Immunogenicity

Immunization with NSP4 has been shown to be able to induce immunity that protects animals and children from viral challenge (Hou *et al*., 2008; Iosef *et al*., 2002; Malik *et al*., 2008). This protection has been seen in experimental animals including neonatal mice and gnotobiotic pig models. In the latter model moderate titres of serum IgM, IgG and IgA antibodies to NSP4 have been detected (Ball *et al*., 1996; Iosef *et al*., 2002). Furthermore anti-NSP4 antibodies have also been reported to be sufficient to block rotavirus-induced diarrhoea in mice (Hou *et al*., 2008). More importantly in children it has been demonstrated that NSP4 induces IgG, IgA and significant IFN-gamma during natural infection (Malik *et al*., 2008; Ray *et al*., 2003; Vizzi *et al*., 2005).

1.2.4 NSP4 Functions

NSP4 possesses pleiotropic properties in both viral morphogenesis and

pathogenesis. On the one hand, it locates to the endoplasmic reticulum (ER) membrane and serves as a receptor for the introduction of viral double-layer particles (DLP) to enter the ER lumen where they can assemble with VP4 and VP7 to produce infectious triple-layer particles (TLP). On the other hand, NSP4 appears to be secreted from infected cells before the release of virus to act in a paracrine fashion as a viral enterotoxin. The sequence elements and functional domains of NSP4 described in the following sections are summarized in figure 1.4.

1.2.5 Morphogenesis

NSP4 plays a crucial role in viral assembly facilitating the budding of viral DLPs into the ER lumen where they form infectious TLPs by the addition of the outer shell proteins (VP4 and VP7). When the budding starts, the C terminal half of NSP4 alone is responsible and sufficient for binding with DLPs (Estes, 2001).The 20 amino acids at the C terminus of NSP4 are involved in binding DLPs and the terminal methionine is essential for binding activity (Taylor, 1992; Taylor *et al*., 1993). As the budding progresses, an enveloped DLP will be generated. To remove this envelope glycosylated NSP4 and VP7 are required (Estes, 2001; Lopez *et al*., 2005a). Subsequent addition of VP4 and VP7 is facilitated by the fact that NSP4 binds VP4 and forms heterooligomers of NSP4, VP4 and VP7 in enveloped DLPs which recruits sufficient VP4 and VP7 to the maturation site of TLP in the ER (Au *et al*., 1993; Estes, 2001). The assembly of the VP7 layer and VP4 spikes has been shown to occur spontaneously at certain concentrations of calcium when these proteins are co-expressed with VP2 and VP6 in insect cells using baculovirus system (Crawford *et al*., 1994). During this process amino acids 73 to 85 and the C terminal (CT) both appear to be important for the oligomerization of NSP4

(Jagannath *et al*., 2006). Studies blocking the synthesis of NSP4 in virus infected cells using RNAi technology have demonstrated that the absence of NSP4 not only leads to disruption of the intracellular accumulation and sub-cellular distribution of several viral proteins and viroplasms but also results in little or no virus particles (neither DLPs nor TLPs) being assembled (Lopez *et al*., 2005a; Silvestri *et al*., 2005). This suggests that NSP4 is functioning in the whole process of viral replication to guarantee the final viral morphogenesis rather than just in the final budding of DLPs and TLP maturation events.

1.2.6 Pathogenesis

The second function of NSP4 that appears to require the protein to be secreted from virus infected cells is its role in viral pathogenesis. NSP4 contributes to the process of diarrhoea directly. It has been characterized as the first and to date the only viral enterotoxin, that can cause diarrhoea in a neonatal mouse model without other components of the virus (Ball *et al*., 1996; Horie *et al*., 1999). Furthermore, the influence of NSP4 in inducing diarrhoea is specific and the alteration in vital amino acids yields an avirulent form of NSP4 that does not induce diarrhoea in newborn mice (Zhang *et al*., 1998). Moreover, amino acids between 112 and 175 of NSP4 have been identified as the key region of the protein involved in the pathogenesis (Zhang *et al*., 2000). The purified peptide (aa112-175) can trigger all the toxic events seen with the intact NSP4 protein (Zhang *et al*., 2000). In infected non-differentiated MA104 cells a peptide cleavage product of NSP4 encompassing this region has been reported as being secreted by the microtubule and actin filament network trafficking pathway rather than the ER-Golgi vesicle-mediated secretion pathway inhibited by brefeldin A (Zhang *et al*., 2000). Further analysis of

possible NSP4 secretion has been done in the polarized epithelial cell line Caco-2 which is thought to more closely mimic the *in vivo* situation. Secretion of NSP4 was detected mainly from the apical surface of this cell line and its secretion was sensitive to treatment of brefeldin A and monensin indicating involvement of the Golgi apparatus during secretion. The form of secreted NSP4 in this second study was full length and fully glycosylated (Bugarcic and Taylor, 2006). These observations are contradictory but they may reflect different strategies of secreting NSP4 in different cell types. Furthermore neither of these studies could exclude NSP4 being in the vesicles disseminated from virus-infected cells described in chapter 5 of the thesis.

The mechanism by which secreted NSP4 destroys epithelial cells through what is currently believed to be a paracrine like pathway has been the focus of much attention. As the release of glycosylated NSP4 occurs before lysis of the infected cell, the secreted NSP4 has been shown to interact with cellular integrins $\alpha1\beta1$ and $\alpha2\beta1$ of bystander cells (Seo *et al*., 2008). These interactions activate a phospholipase C-inositol 1,4,5-triphosphate (PLC-IP3) cascade that stimulates the release of Ca^{2+} from the ER (Dong *et al*., 1997). Calcium imported into the cytoplasm causes an intracellular Ca^{2+}concentration increase due either to Ca^{2+} release from intracellular pools (ER) by IP3 or Ca^{2+} import across plasma membrane via various Ca^{2+}channels (Ruiz *et al*., 2005). Cytoplasmic Ca^{2+}concentrations play an extremely important role in live cells and disrupting them results in dysfunction of crucial cellular molecules and eventually death of the bystander epithelia (Ruiz *et al*., 2005).

Consistent with this role for NSP4, alterations of cellular Ca^{2+} homeostasis can be observed in either rotavirus infected cells or following transfection of an NSP4

expressing plasmid alone (Berkova *et al*., 2003a). However in both cases NSP4 appears to activate an undefined cascade rather than using the PLC-IP3 pathway (Berkova *et al*., 2003b; Dong *et al*., 1997; Michelangeli *et al*., 1991). The expression of NSP4 alone was sufficient to mimic the Ca^{2+} homeostasis changes induced by rotavirus infection in cultured cells (Diaz *et al*., 2008). Silencing of NSP4 in virus infected cells using RNAi technology leads to a reduction in $Ca2^{+}$ levels to those seen in mock-infected cells which has further validated the influence of NSP4 on intracellular calcium homeostasis (Zambrano *et al*., 2008). Mutational analysis using NSP4 expressing cells has demonstrated that the essential domain required for triggering the Ca^{2+} permeability increase may be located in either residues 55 to 69 or the overlapping domain of residues 66 to 83, deletions of which lead to dramatic reductions in cytotoxic activity. However, deletion of residues 1 to 60 including the two glycosylation sites only reduced ^{51}Cr release from cells by approximately 30% and deletion of the region from amino acids 110 to 119 had no affect (Newton *et al*., 1997). It must be recognized however that these deletions in NSP4 may also affect its secondary or tertiary structure or alter its intracellular trafficking pathway. Consequently they need to be interpreted with caution in terms of their ability to reveal the functional region of NSP4 involved in triggering changes in Ca^{2+} permeability. Although the detailed mechanism by which NSP4 regulates intracellular calcium levels has not been completely defined it is clear that NSP4 is the main protein responsible for alteration of calcium levels that facilitates viral replication and participates in viral pathogenesis.

In addition to the pathogenic mechanism that relies on disrupting intracellular calcium levels, other potentially pathogenic strategies have also been proposed.

First, if NSP4 is incubated with polarized epithelium, paracellular leakage mainly through tight-junction-associated protein disruption is observed. Surprisingly, if NSP4 is then removed the original integrity of the epithelium is regained and electrical resistance recovers (Tafazoli *et al*., 2001). Secondly NSP4 appears to act through the enteric nervous system (ENS) to induce Cl^- secretion and hence signal an increase in intracellular calcium concentration (Lundgren *et al*., 2000). This indicates that *in vivo* ENS related cellular components are also involved in the NSP4 pathway (Lundgren *et al*., 2000). Thirdly NSP4 has been reported to up-regulate inducible nitric oxide synthase (iNO) that is responsible for nitric oxide (NO) production in infected mice (Borghan *et al*., 2007). The production of NO has been implicated in affecting both intestinal motility (Hoffman *et al*., 1997) and mucosal permeability (Kubes, 1992) and also acting as a modulator of intestinal ion transport via either its activation of the ENS (Izzo *et al*., 1998) or its direct action on the intestinal epithelium (Borghan *et al*., 2007; Resta-Lenert and Barrett, 2002). Finally supernatants containing secreted NSP4 can induce a Ca^{2+}-dependent microvillar F-actin alteration in uninfected Caco-2 cells (Brunet *et al*., 2000a). Endogenous expression of NSP4 has also been consistently shown to lead to alteration of the actin network organization through the actin remodeling protein cofilin that is also regulated by intracellular calcium levels (Berkova *et al*., 2007). All of these observations may have a role to play in the final symptoms of rotavirus disease and undoubtedly NSP4 has multiple roles in the development of such symptoms.

1.2.7 Intracellular Localization and Interactions with Cellular Proteins

The intracellular localization of NSP4 following both viral infection and transient

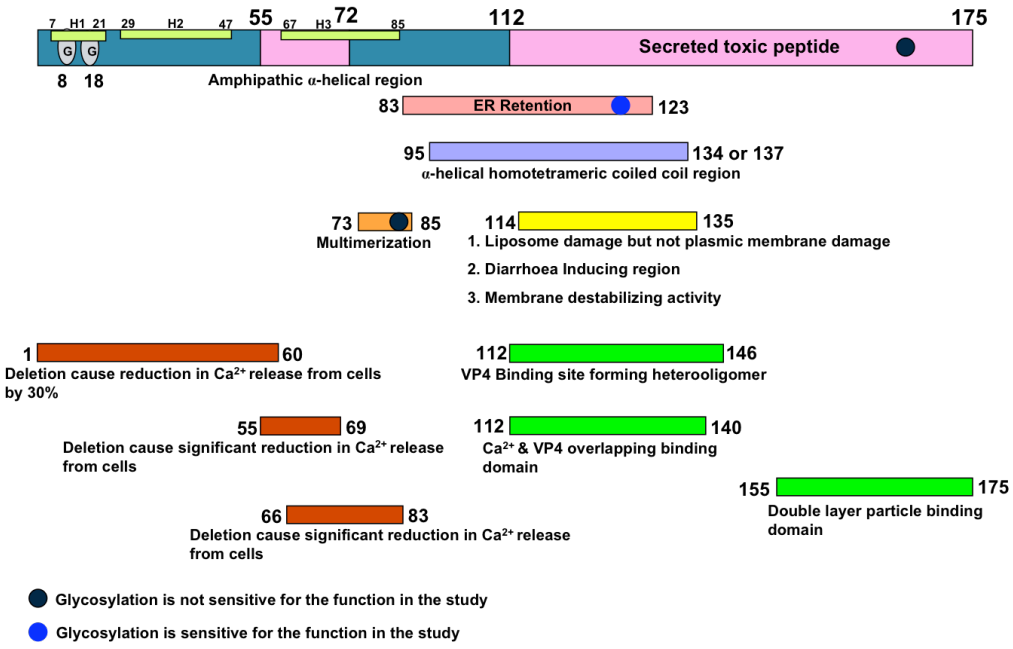

Figure 1.4: Linear schematic of NSP4 and its sequence elements and functional domains.

H1-H3, hydrophobic domains 1 (aa7-21), 2 (aa29-47) and 3 (aa65-85). G, glycosylation sites at aa8 and 18. Amphipathic α-helical region at aa55-72. α-helical homotetrameric coiled coil region at aa95-134 or 137. Secreted toxic peptide at aa112-175 (Zhang *et al*., 2000). Domain at aa83-123 is important for ER retention (Estes, 2001). Multimerization requires aa73-85 (Jagannath *et al*., 2006). Domain 114-135 damages the liposomal membrane but not the cytoplasmic membrane, induces diarrhoea, possesses membrane destabilizing activity (Estes, 2001). Three domains in red (aa1-60, aa55-59 and aa66-83) if deleted resulted in reduction of cytoplasmic Ca^{2+} release from cells (Newton *et al*., 1997). Three domains in green aa112-140, aa112-146 and aa155-175 are important for NSP4-VP4, Ca^{2+} and double layer particle binding respectively (Taylor, 1992; Taylor *et al*., 1993; Au *et al*., 1993; Estes, 2001). Black circle indicates that function does not require glycosylation. Blue circle is indicates that function requires glycosylation.

transfection has been studied to try and gain insights into its function. It is well established that NSP4 is initially synthesized in the ER but it subsequently moves away from the ER to the cytoplasm in which it appears to form vesicular structures similar to viroplasms. Recently these structures have been reported to co-localize

with the autophagosomal marker LC3 but not to co-localize with ER, ERGIC, Golgi, endosomal, or lysosomal markers (Berkova *et al*., 2006). The colocalization of the autophagosomal marker LC3 and viroplasms that has been observed in infected cells does suggest a possible new mechanism for the involvement of NSP4 in virus replication (Berkova *et al*., 2006). Putatively glycosylated NSP4 may play a very important role in assembling of viroplasms as this has been shown to be a calcium-regulated process (Berkova *et al*., 2006). Although the majority of NSP4 has been reported to accumulate in such vesicular structures, a fraction of soluble NSP4 that is full length and glycosylated has also been observed to co-localize with the plasma membrane and to be associated with caveolae (Mir *et al*., 2007; Storey *et al*., 2007). This association has been attributed to the interaction between NSP4 and both the N and C-termini of caveolin-1 (Mir *et al*., 2007; Parr *et al*., 2006; Storey *et al*., 2007). In addition to its interaction with caveolin-1, NSP4 also interacts with the microtubule and extracellular matrix proteins laminin-β3 and fibronectin (Boshuizen *et al*., 2004). Its interaction with microtubules may contribute to the blockage of ER-to-Golgi trafficking *in vivo*, while its interaction with laminin-β3 and fibronectin which are located at the basal side of infected epithelial cells may signify a new mechanism by which rotavirus disease is established (Boshuizen *et al*., 2004; Xu *et al*., 2000).

1.3 Aims

The aim of the thesis are to construct glycosylation mutants of NSP4 and to study the functional difference between the wild type and the mutant NSP4 by observing their intracellular localization and effects on transfected cells; to evaluate the proposed function of NSP4 in infected cells; to construct a protein-protein interaction

screening system which uses full length NSP4 as bait for the isolation of its cellular partners and hence gain a better understanding of the intracellular trafficking and pathogenicity of NSP4.

Chapter 2

Materials and Methods

2.1 Suppliers

General chemicals were obtained from BDH Laboratory Supplies, Fisher Scientific (Loughborough, Leicestershire), Merck Ltd. (Poole, Dorset) and Sigma-Aldrich Company Ltd. (Gillingham, Dorset) and were of analytical or molecular biology grade. All water used was double distilled.

Invitrogen Corporation, R & D Systems Ltd. (Abingdon, Oxfordshire)

TA Cloning™ System, restriction and modification enzymes, *Taq* DNA polymerase, 1Kbp DNA ladder, Lipofectamine™ 2000 Reagent, CellTracker™ Green CMFDA, CellTracker™ Red CMTPX, 1,2-bis (o-aminophenoxy) ethane-N,N,N',N'-tetraacetic acid/Acetoxymethyl (BAPTA/AM), Dynabeads® mRNA DIRECT™ Kit, Alexa Fluor® 594 phalloidin

New England Biolabs (UK) Ltd. (Hitchin, Hertfordshire)

Restriction and modification enzymes

Qiagen Ltd. (Crawley, West Sussex)

MinElute Gel Extraction Kit, QIAGEN Plasmid Mini Kit, QIAGEN Plasmid Maxi Kit

Sigma-Aldrich Company Ltd. (Gillingham, Dorset)

Kanamycin, ampicillin, PAC-1 (final concentration is 5 μM), cycloheximide (final concentration is 20 μg/ml), SigmaSpin™ Maxiprep kit, Apo-TRACE® Apoptotic Cell Staining Kit

Promega (Madison, Wisconsin, USA)

Taq DNA polymerase, reverse transcriptase

MBI Fermentas Life Sciences (Hanover, MD, USA)

Restriction and modification enzymes, GeneJET™ Plasmid Miniprep Kit

Iwaki Glass Co. Ltd. (Tokyo, Japan)

35 mm glass based dishes

Vector Laboratories Ltd. (Peterborough, UK)

VECTASHIELD Mounting Medium

Media Preparation (Department of Biological Sciences, University of Warwick)

LBroth, LB agar plates with 100 μg/ml ampicillin and/or 25 μg/ml kanamycin, GMEM NEAA, DMEM, versene 0.02% in PBS, trypsin 0.25% in Tris saline, phosphate buffered saline (PBS), 10X Tris-Borate-EDTA (TBE), G418, penicillin and streptomycin sulphate, ampicillin, kanamycin

2.2 Materials

2.2.1 Bacterial strains

INVαF' (Invitrogen)

Genotype: F′ *end*A1 *rec*A1 *hsd*R17 (rk-, mk+) *sup*E44 *thi*-1 *gyr*A96 *rel*A1 φ80*lac*ZΔM15Δ(*lac*ZYA-*arg*F)U169 λ-

2.2.2 Cell lines

2.2.2.1 BSR-T7

Baby hamster kidney (BHK) cells, constitutively expressing bacteriophage T7 RNA polymerase (Buchholz *et al*., 1999).

Culture medium: GMEM NEAA + 5% FCS (v/v) + 1 mg/ml geneticin (G418) sulphate.

2.2.2.2 BSC-1

African green monkey kidney cells were grown as previously described (McCrae and Faulkner-Valle, 1981).

Culture medium: GMEM NEAA + 5% FCS (v/v).

2.2.2.3 293T

Human Embryonic Kidney cells, transformed with simian virus 40 (SV-40) T antigen (ATCC# CRL-11268).

Culture medium: DMEM + 10% FCS (v/v).

2.2.3 Viruses

2.2.3.1 Rotavirus UKtc strain

The tissue culture adapted Compton (UKtc) strain of group A bovine rotavirus G serotype 6 (provided by M.A. McCrae, University of Warwick)

2.2.3.2 Vaccinia virus MVA-T7

An attenuated recombinant vaccinia virus encoding bacteriophage T7 RNA polymerase gene (provided by M.A. McCrae, University of Warwick)

2.2.3.3 Reovirus

Human reovirus serotype 3 Dearing strain (provided by M.A. McCrae, University of Warwick)

2.2.4 Plasmids

pCR2.1 and pcDNA3.1 were obtained from Invitrogen (Oxfordshire). pEYFP-N1 was obtained from Clontech (Palo Alto, California, USA). YFP1-ERGIC53 and YFP2-NCFD2 were obtained from Dr Hans-Gerhard Burgert, University of Warwick.

2.2.5 Primers

All PCR primers were synthesized by and purchased from Invitrogen. Fully complementary primer pairs for mutagenesis PCR were designed by SiteFind v4.2 with additional restriction enzyme sites added for convenient mutant screening.

Table 2.2.1 Oligonucleotide primers used in this study

Primer Name	Primer Sequence	Used for
UKtcsite1F	GAT GGA AAA GCT TAC AGA TCT CGC CTA TAC ATT GAG	Forward primer for mutating glycosylation

	TG	site of NSP4 at amino acid 8
UKtcsite1R	CAC TCA ATG TAT AGG CGA GAT CTG TAA GCT TTT CCA TC	Reverse primer for mutating glycosylation site of NSP4 at amino acid 8
UKtcsite2F	GTA ATC ACT CTA ATG GCT AGC ACA TTG CAC ACG	Forward primer for mutating glycosylation site of NSP4 at amino acid 18
UKtcsite2R	CGT GTG CAA TGT GCT AGC CAT TAG AGT GAT TAC	Reverse primer for mutating glycosylation site of NSP4 at amino acid 18
STUENSP4F	AGT GAC TGC AGC AAT GAG GCC TGT TGA GCT GCC GTC GAC	Forward primer for making an *StuI* site at the end of NSP4
STUENSP4R	GTC GAC GGC AGC TCA ACA GGC CTC ATT GCT GCA GTC ACT	Reverse primer for making an *StuI* site at the end of NSP4
STUGFPF	GCG CGT AGG CCT AGC AAG GGC GAG GAA CTG TTC	Forward primer for the amplification of YFP to insert into the end of

		NSP4
STUGFPR	GCG CGT AGG CCT TCA TCA CTT GTA CAG CTC GTC CA	Reverse primer for the amplification of YFP to insert into the end of NSP4
NSP4XhoIF	GCG CGT CTC GAG AAA AGC TTA CCG ACC TCA AC	Forward primer for the amplification of NSP4 coding sequence with *XhoI* site at 5'-end
NSP4XhoIR	GCG CGT CTC GAG TTA CAT TGC TGC AGT CAC TTC	Reverse primer for the amplification of NSP4 coding sequence with *XhoI* site at 3'-end
VP4XhoIF	GCG CGT CTC GAG CTT CGC TCA TAT ACA GAC	Forward primer for the amplification of VP4 coding sequence with *XhoI* site at 5'-end
VP4XhoIR	GCG CGT CTC GAG TCA CAA TCT ACA TTG CAT GAT C	Reverse primer for the amplification of VP4 coding sequence with *XhoI* site at 3'-end

VP6XhoIF	GCG CGT CTC GAG ATG TCC TGT ACT CCT TGT C	Forward primer for the amplification VP6 coding sequence with *XhoI* site at 5'-end
VP6XhoIR	GCG CGT CTC GAG TCA TTT GAC AAG CAT GCT TC	Reverse primer for the amplification VP6 coding sequence with *XhoI* sites at 3'-end
NSP4XhoIF 3.1	GCG CGT CTC GAG ATG AAC AGC ACA TTG CAC ACG	Forward primer for the amplification of NSP4 to insert into the pCDNA3.1 vector
NSP4XhoIF ATG	GCG CGT CTC GAG ATG GAA AAG CTT ACCG	Forward primer for the amplification of NSP4 at the ATG start codon with *XhoI* at 5'-end
YFP2NSP4HheIF	GCG CGT GCT AGC ATG GGC GGT AGG CGT G	Forward primer for cloning YFP2 into pEYFP-N1 vector
YFP2NSP4NotIR	GCG CGT GCG GCC GCT TAC ATT GCT GCA GTC ACT TC	Reverse primer for cloning YFP2 into pEYFP-N1 vector

YFP2PCAsequencingF	ACA ACC ACT ACC TGA GCT ACC	Sequencing forward primer to identify gene in YFP2-cDNA library
pEYFPN1sequenceR	TGA AAT TTG TGA TGC TAT TGC	Sequencing reverse primer to check the end of the gene in YFP2-cDNA library
PCABglII0F	GGA GGT GGT GGG TCC AGA TCT GAA AAG CTT ACC GAC C	Forward primer for making a *BglII* site at the end of the YFP2 sequence so that the downstream insert digested by *BglII* will be joined in the correct (+1) reading frame.
PCABglII0R	GGT CGG TAA GCT TTT CAG ATC TGG ACC CAC CAC CTC C	Reverse primer for making a *BglII* site at the end of the YFP2 sequence so that the downstream insert digested by *BglII* will be joined in the correct (+1) reading frame.

PCABglII+2F	GGA GGT GGT GGG TCC GCA GAT CTA AAG CTT ACC GAC C	Forward primer for making a *BglII* site at the end of the YFP2 sequence so that the downstream insert digested by *BglII* will be joined in the correct (+2) reading frame.
PCABglII+2R	GGT CGG TAA GCT TTA GAT CTG CGG ACC CAC CAC CTC C	Reverse primer for making a *BglII* site at the end of the YFP2 sequence so that the downstream insert digested by *BglII* will be joined in the correct (+2) reading frame.
NotIcDNAdTR	GCG GCT GAA GAC GCG GCC GCT TTT TTT TTT TTT TTT T	PolyT tail reverse primer for converting mRNA into ssDNA
5XhoBglII3	P-GGC CTC GAG AGA TCT GCC	Phosphorylated adaptor for construction of cDNA library (see section 2.3.17.4)

5BglIIXho3	P-GGC AGA TCT CTC GAG GCC	Phosphorylated adaptor for construction of cDNA library (see section 2.3.17.4)

2.2.6 Antibodies

2.2.6.1 Polyclonal mono-specific anti-NSP4 antisera

Produced in rabbit, as described previously in Guzman and McCrae, 2005 and used at 1:200 dilution (provided by M.A. McCrae, University of Warwick).

2.2.6.2 Polyclonal anti-group A rotavirus (UKtc) antisera

Produced in rabbit and used at 1:200 dilution (provided by M.A. McCrae, University of Warwick).

2.2.6.3 Monoclonal anti-β-tubulin antibody

Produced in mouse (Sigma-Aldrich Cat. No. T 5293) and used at 1:500 dilution.

2.2.6.4 Alexa Fluor® 594 goat anti-rabbit IgG (H+L) antibody

(Invitrogen Cat. No. A-11012) used at 1:1000 dilution.

2.2.6.5 Alexa Fluor® 488 goat anti-mouse IgG (H+L) antibody

(Invitrogen Cat. No. A-11001) used at 1:3000 dilution.

2.2.7 Standard Buffers and Solutions

2.2.7.1 Luria-Bertani Broth (LB 10:5:10):

1% (w/v) bactotryptone, 1% (w/v) NaCl, 0.5% (w/v) yeast extract.

2.2.7.2 LB agar:

LB Broth containing 1.5% (w/v) bacto-agar.

2.2.7.3 Phosphate buffered saline (PBS):

137 mM NaCl, 2.7 mM Na_2HPO_4, 1.4 mM KH_2PO_4.

2.2.7.4 Tris-Borate-EDTA (TBE):

90 mM Tris base, 90 mM boric acid, 1 mM EDTA, pH8.0.

2.2.7.5 10X Agarose gel loading buffer:

50% (v/v) glycerol, 0.01% (w/v) bromophenol blue, 0.01% (w/v) xylene cyanol, 2% TBE (v/v).

2.2.7.6 NP40 cell lysis buffer:

100 mM Tris-HCl pH 8.0, 50 mM NaCl, 10 mM EDTA, 0.5% NP40.

2.2.7.7 Paraformaldehyde cell fixing solution:

4% paraformaldehyde (v/v) in PBS.

2.2.7.8 TfbI:

10 mM $RbCl_2$, 10 mM $CaCl_2$, 30 mM potassium acetate, 50 mM $MnCl_2$, 15% (v/v) glycerol, pH 5.8.

2.2.7.9 TfbII:

10 mM $RbCl_2$, 75 mM $CaCl_2$, 10 mM 3[N-morpholino] propanesulphonic acid (MOPS), 15% (v/v) glycerol, pH 6.5.

2.3 Methods

2.3.1 General Molecular Biology

2.3.1.1 Growth of Bacteria

Bacteria were cultured on LB agar plates containing 100 μg/ml ampicillin and/or 25 μg/ml kanamycin or in liquid LB medium containing 100 μg/ml ampicillin and/or 25 μg/ml kanamycin.

2.3.1.2 Small Scale Preparation of Bacterial Plasmids (Mini prep)

Plasmids were purified and re-suspended in water using the MiniprepKit™ (Qiagen) according to the manufacturer's instructions.

2.3.1.3 Large Scale Preparation of Bacterial Plasmids (Maxi prep)

Large scale preparation of plasmid was performed using either the Plasmid Maxi Kit (Qiagen) or the GenElute™ Plasmid Maxiprep Kit (Sigma) following the manufacturer's instructions.

2.3.1.4 Preparation of Plasmids on Cesium Chloride-Ethidium Bromide Gradients

Bacteria (1L) containing plasmids were cultured until the OD_{590} reached 0.6, then chloramphenicol was added to a final concentration of 150 μg/ml and bacterial growth cultured overnight in 37 °C shaking incubator. After overnight culture cells were centrifuged in 500 ml centrifuge bottles at 6000 rpm for 20 mins at 4 ºC. The supernatants were discarded and cell pellets re-suspended in 8.4 ml of 25% sucrose containing 50 mM Tris pH 8.0. 1.4 ml of a 10 mg/ml solution of lysozyme in 50 mM Tris pH 8.0 was added to the resuspended pellets on ice with gentle swirling for 5 mins. Then 4.6 ml of 0.25 M EDTA was added again with gentle swirling for 10 mins. After 10 mins 9.6 ml of lysis mix (500 ml stock made using 50 ml 20% Triton, 125 ml 0.25 M EDTA, 25 ml 1 M Tris pH 8 and 300 ml H_2O) was added slowly with swirling. Chromosomal DNA was then pelleted by centrifugation in Oakridge tubes for one hour at 16,000 rpm (Beckman JA-20 rotor) at 4°C. Chromosomal DNA was hooked out and the remaining supernatants adjusted to 25 ml with H_2O followed by addition of 25 g CsCl and 1 ml 10mg/ml ethidium bromide. Mixtures were then centrifuged in 38 ml Beckman tubes in SW28 rotor and L8 centrifuge at 25,000 rpm 18 °C for one hour. Floating debris was scooped off and discarded. The supernatants were poured into plastic Quick-seal VTi50 tubes, balanced to with 0.1 g and then centrifuged in a VTi50 rotor at 45,000 rpm overnight. Plasmid bands were collected by side puncture into a syringe and extracted with CsCl saturated isopropanol to remove ethidium bromide. Samples were then dialyzed against Tris-EDTA buffer (TE). Following dialysis the plasmid DNA was concentrated by ethanol precipitation (2X). The final plasmid DNA pellets were washed with 80% ethanol, dried, resuspended in ddH_2O and stored at -20ºC.

2.3.1.5 Precipitation of Nucleic Acids

Nucleic acids in aqueous solution were precipitated by addition of 1/10 volume of 3 M sodium acetate pH 5.2 and 2.5 volume of 100% ice-cold ethanol or 0.6 volume of isopropanol. After incubation at -20 ºC for 1 hour precipitated nucleic acids were concentrated using a tabletop microcentrifuge for 10 minutes at 13,200 rpm. Nucleic acid pellets were rinsed in 80% ethanol and air-dried at 37 ºC for 15 minutes.

2.3.1.6 Quantification of Nucleic Acids

Nucleic acids were quantified using both the NanoDrop Spectrophotometer (Thermo Scientific, Wilmington, USA) and agarose electrophoresis.

2.3.1.7 Agarose Electrophoresis

Fractionation of nucleic acids was performed on 0.8 to 1.5% agarose gels containing 0.5µg/ml ethidium bromide in 1×TBE buffer. Electrophoresis was carried out at 100V in 1×TBE buffer. Illumination and digital image capture of nucleic acids was performed using the Bio-Rad Gel Doc XR system and analysis done using the Bio-Rad Quantity One 4.6.3 software.

2.3.1.8 Agarose Gel Extraction of Nucleic Acids

Following agarose gel electrophoresis a desired nucleic acid fragment was isolated using a sterile scalpel blade under UV light, eluted and cleaned using the Qiagen Gel Extraction kit following the manufacturer's instructions.

2.3.1.9 Restriction Enzyme Digestion of Plasmid DNA or PCR Products

Plasmid DNA or PCR Product was incubated with the appropriate enzyme in supplied buffer solution using manufacturer's recommended condition.

2.3.1.10 Polymerase Chain Reaction (PCR)

2.3.1.10.1 Standard PCR

Standard PCRs were carried out in a final volume of 25 μl which included 100 ng of template plasmid DNA, 0.5 μM of each primer and 2 U *Taq* DNA polymerase. The PCR mixture was subjected to 30-40 cycles of 94 ºC for 1 minute, 55 ºC for 1 minute and 72 ºC for 1 minute/kilo-base of amplicon. PCR products were fractionated by agarose gel electrophoresis (see section 2.3.1.7). Individual PCR reactions were optimized by adjusting the final magnesium concentration used.

2.3.1.10.2 Site-Directed Mutagenesis PCR

Mutagenesis PCR was performed with *Pfx* DNA polymerase (2.5 units) to ensure higher fidelity. The PCR reaction (25 μl) with 100 ng of template plasmid DNA and 0.5 μM of each primer was incubated in 94 ºC for 1 minute to fully denature the template DNA and this was followed by 18 cycles of 94 ºC for 1 minute, 55 ºC for 1 minute and 68 ºC for 1 minute/kilo-base of amplicon. Individual PCR reactions were optimized by adjusting the final magnesium concentration used.

2.3.1.11 Dephosphorylation of the 5' Ends of DNA

Removal of 5'-phosphate groups from DNA was catalyzed using shrimp alkaline phosphatase (SAP) (1 units/μg of DNA treated) (Fermentas) in the supplied buffer at

37 ºC for 30 minutes or overnight. Catalysis was inactivated by heating at 65 ºC for 15 minutes.

2.3.1.12 Conversion of 5' Overhang Restriction Enzyme Ends to Blunt Ends

5' Overhangs generated in restriction enzyme digests were filled in using the large fragment of DNA polymerase I (1 unit/μg of DNA treated) (Invitrogen) in the supplied buffer and 0.5 mM of each dNTP at room temperature for 15 minutes. The fill-in reaction was terminated by phenol extraction.

2.3.1.13 DNA Ligation

T_4 DNA ligase (5 units) was used in a final reaction volume of 10 μl containing insert DNA fragment (used in a molar ratio of 10:1 to vector DNA) and dephosphorylated vector DNA (100 ng) at 16 ºC overnight.

2.3.1.14 Transformation of Competent Bacterial Cells by Heat Shock

Competent bacterial cells were prepared as follows:

A single colony of INVαF' was grown overnight at 37 °C in 2 ml LB overnight. This fresh overnight culture was then diluted into 100 ml LB and cultured until the OD_{600} reached about 0.39. The culture was then cooled on ice for 10 mins, and bacteria concentrated by centrifugation in two 50 ml Falcon tubes (of 3300 × g for 10 mins at 4 ºC). The bacterial cell pellet was resuspended in 40 ml TfbI solution on ice for 5 mins. Cells were re-centrifuged as before and resuspended in 4 ml TfbII solution on ice for two hours. Cells were then aliquoted (100 μl/tube) and stored at -70 ºC until used (max 3 months).

Transformation procedure:

Ligation products (see section 2.3.13) or plasmid DNA (100 ng) was transformed to INVαF' competent cells by heat shock (45 seconds in 42 ºC water bath). After a 1 hour incubation at 37 ºC in LB the cells were plated on LB agar plates containing the appropriate selection antibiotics.

2.3.1.15 Transformation of Competent Bacterial Cells by Electroporation

Competent bacterial cells were prepared as follows:

An overnight culture of bacteria was grown in 5 ml of LB. 2 ml of this fresh overnight culture was then added to 200 ml LB in a 1 L flask. This was grown at 37 °C with shaking until the OD_{590} reached ~ 0.4. Cells were then pelleted and washed subsequently in equal, half, quarter volumes, and finally resuspended in 3 ml of chilled H_2O containing 10% glycerol. The washed resuspended cells were aliquoted (100 μl/tube) and stored at -70 °C until used (max 3 months).

Electroporation procedure:

All procedures were carried out on ice. Pre-cooled 0.2 cm cuvettes containing competent cells and DNA (50 μl) were inserted into the cuvette slide of Bio-Rad Gene Pulser system that was set with voltage at 2.5 kV, capacitance at 25 μFD, capacitance extender at 150 μFD and pulse controller at 200 Ohms resistance. The time constant value was used to monitor electroporation, with a reading above 4.6 being deemed as indicating successful electroporation. Cells were then incubated in LB for 1 hour at 37 ºC and then plated on LB agar plates containing appropriate selection antibiotics.

2.3.1.16 DNA Sequencing

The Molecular Biology Service (University of Warwick) provided routine DNA sequencing by using ABI Prism Genetic Analysers. Sequencing data were opened using Chromas Lite 2.0 and analysed using the Clone Manager, SciEd Central, v7.04 software.

2.3.1.17 Construction of cDNA library

2.3.1.17.1 Extraction of mRNA Using Dynabeads® mRNA DIRECT™ Kit

Cellular mRNA was extracted using Dynabeads® mRNA DIRECT™ Kit (Invitrogen) following the manufacturer's instructions.

2.3.1.17.2 Synthesis of The First Strand of DNA from mRNA

mRNA was re-suspended in 10 µl of water at a final concentration of 1 µg/µl. The mRNA was then mixed with 1.5 µl of poly(dT) primer (1 µg/µl) and 1µl of 10 mM dNTP. The mixture was placed at 65°C for 5 mins then on ice for 2 mins. Then 4 µl of 5X first strand Buffer, 2 µl of 0.1M DTT, 1 µl of RNasin and 1.4 µl of SuperScript® II Reverse Transcriptase (RT) were added on ice. The tube was placed in a PCR machine and incubated at 25°C for 10 mins, followed by 47°C for 1 hour. The final product of first strand DNA (ssDNA) synthesis was analysed using agarose gel electrophoresis (see section 2.3.1.7).

2.3.1.17.3 Second Strand Synthesis of ssDNA

DEPC-treated water 93 μl, 5X Second Strand Buffer 30 μl, 10 mM dNTP Mix 3 μl, *E.coli* DNA ligase (10 U/μl) 1 μl, *E.coli* DNA polymerase I (10 U/μl) 4 μl, *E.coli* RNAaseH (2 U/μl) 1 μl were all added to the first strand DNA product described in 2.3.17.2 in a final volume of 150 μl on ice. The mixture was then incubated at 16°C for 3 hours. After this incubation 2 μl (10 U/μl) of T4 DNA polymerase was added and incubation continued for 5 mins. The reaction was stopped by adding 10 μl of 0.5 M EDTA and the synthesized cDNA ethanol precipitated prior to adaptor ligation.

2.3.1.17.4 Adaptor Ligation

The precipitated cDNA was dissolved in 25 μl of water and 5X T4 DNA Ligase Buffer 10 μl, 1 μg/μl phosphorylated adaptor 10 μl, T4 DNA ligase 5 μl were all added on ice to give a final reaction volume of 50 μl. This solution was incubated at 16°C for 16 hours.

2.3.1.17.5 Size Fractionation and Directional Cloning of cDNA into Vector

The cDNA was analysed using agarose gel electrophoresis (see section 2.3.1.7) and fractions separated based on size (0-500bp, 500bp-1Kb, 1Kb-2Kb and above 2Kb). Following gel extraction cDNA (see section 2.3.1.8) was digested with either *XhoI* + *NotI* or *BglII* + *NotI* for 2 hours. Finally the digested cDNA was cloned into pEYFP-N1 vector digested with either *XhoI* + *NotI* or *BglII* + *NotI*.

2.3.1.18 Protein Concentration Determination

Protein concentrations were measured in a standard Bradford assay using reagents purchased from Invitrogen and used according to the manufacturer's instruction.

2.3.2 Mammalian Cell Maintenance, Storage, Transfection and Fixation

2.3.2.1 Maintenance

Cells were grown in appropriate culture medium (see section 2.2.2) at 37 ºC in a 5% CO_2 incubator and were split every 3 to 4 days according to their growth condition. To split cells, they were washed twice with versene followed by incubation with a trypsin/versene (1:5) mixture for 5-10 mins at 37 ºC to detach the adherent cells from the flask surface. Cell suspensions were then centrifuged at 1300 rpm for 3 mins to pellet the cells. The pelleted cells were resuspended in appropriate medium (see section 2.2.2) and re-seeded at the required ratio (1:10 for BSR-T7 cells, 1:4 for BSC-1 cells, 1:10 for 293T cells).

2.3.2.2 Long-Term Storage of Cultured Mammalian Cell Lines

Following routine trypsination of confluent cell monolayers, the cell pellet was resuspended at 10^7 cells/ml in GMEM containing 20% FCS. An equal volume of freezing mixture (4 ml FCS, 4.4 ml GMEM and 1.6 ml DMSO making 10 ml master mixture) was added and the two solutions gently mixed. Cells were stored at -70 ºC for one or two days then moved to liquid nitrogen for long-term storage.

2.3.2.3 Transfection

Transfection of mammalian cells was carried out using Lipofectamine 2000

(Invitrogen). For each well of a 12 well plate, 250 µl of serum free medium was mixed with either 3µl of Lipofectamine 2000 or 2µg of DNA and incubated for 10 mins. The Lipofectamine 2000 and DNA containing solutions were then mixed and incubated at room temperature for 20 mins before being added gently to each well and incubated at 37 °C for 4 hours. The transfection mixture was then replaced by medium containing 5% FCS and incubation at 37 °C continued.

2.3.2.4 Paraformaldehyde Fixation

Mammalian cells were fixed in 4% paraformaldehyde for 10 to 20 mins before being used in downstream applications.

2.3.3 Rotavirus Propagation and Measurement by Plaque Assay

Cell monolayers were washed twice with serum-free medium and inoculated with rotavirus diluted in medium (MOI indicated in the experiments) for 1 hour at 37 °C. The inoculum was then removed by aspiration and cells covered with serum free media at 37 °C until the time of experiment.

The cytopathic effect (cpe) reached 80% after 4-6 days and a sterile rubber policeman was used to harvest the infected cells. The harvested infected cells were then frozen and thawed three times, aliquoted, titrated and stored at -70 °C.

Virus stocks were titrated by plaque assay in BSC-1 cells. Cells grown in 6 well plates were inoculated with serial 10-fold dilutions of rotavirus for 1 hour at 37 °C. The inoculum was replaced with serum free GMEM NEAA and cells incubated for 4-6 days at 37 °C for development of virus plaques. Cell monolayers were fixed with formal-saline (30% v/v formaldehyde in PBS) for 1 hour and stained with 0.1% w/v

crystal violet to visualize viral plaques.

2.3.4 Immuno-fluorescence

Cell monolayers grown on coverslips were either infected with virus or transfected with the relevant plasmid and incubated at 37 °C. The cell monolayers were then washed with serum-free medium twice, fixed in 4% v/v formaldehyde in PBS for 10 mins, permeabilized with 0.5% v/v Nonidet P-40 in PBS for 10 mins at room temperature and finally washed with PBS. Coverslips were blocked with 1% w/v of chicken egg albumin in PBS for 1 hour. Primary antibody diluted to the required dilutions (see section 2.2.6) in PBS was added to the coverslips and incubated for 1 hour at room temperature. Coverslips were washed (3X) in PBS before being incubated with the fluorescently tagged secondary antibody which had again been diluted to the required concentration (see section 2.2.6) in PBS. Finally coverslips were incubated with 4', 6-diamidino-2- phenylindole (DAPI) (10 μl/ml) (Sigma) for 5 mins at room temperature to stain nuclei. The cells were then mounted to glass slides with VECTASHIELD® mounting medium and sealed with nail polish. The coverslips were examined using Leica SP5 inverted fluorescent confocal microscope (Leica Microsystem, Germany).

2.3.5 Apoptosis Assay

Apoptosis is a process of programmed cell death reported in rotavirus infected cells (Martin-Latil *et al*., 2007). Apoptotic cells in this study were analysed using Apo-Trace™ Apoptosis Cell Staining Kit (Sigma) according to manufacturer's instruction.

2.3.6 Confocal Microscopy

Samples were analyzed using the inverted lens of Leica TCS SP5 Confocal Microscope System according to the user manual. All images shown are maximum projection of z-series unless indicated otherwise. Time-lapse imaging was carried out using single dish (35 mm in diameter with 27 mm glass base produced by Iwaki Glass Co. Ltd.) for cell culture with the experimental temperature kept for 37 °C.

2.3.7 Flow Cytometry

Monolayers of cells were washed in PBS (2X) and trypsinized using a trypsin/versene (1:5) mixture with incubation for 5-10 mins at 37 ºC to detach the adherent cells. Cells were pelleted by centrifugation at 1300 rpm for 3 mins. The cell pellet was resuspended in serum free medium (see section 2.2.2) at ~ 4×10^6 cells per 30 µl. Cells were analyzed with a FACScan flow cytometer (BD Biosciences) and 20,000 events were routinely recorded, dot plots and histograms were created and analyzed using the software FlowJo version 8.7 (Tree Star, Inc., Ashland, USA).

Chapter 3

Glycosylated NSP4 and Rotavirus Infection

Stimulated Formation of Cytoplasmic Extrusions

3.1 Introduction

NSP4 is an N-linked non-structural glycoprotein. In virus infected cells an unglycosylated NSP4 precursor is synthesized. Subsequent glycosylation of the precursor occurs in the ER through two N-linked glycosylation sites positioned in the amino terminal half of the protein (Baybutt and McCrae, 1984; Bergmann *et al*., 1989). Pulse-chase studies showed that both the unglycosylated NSP4 precursor and fully glycosylated NSP4 were detectable in virus infected cells (McCrae and McCorquodale, 1982). Furthermore unglycosylated NSP4 was still detectable at the end of a 2-hour chase. By contrast, VP7 the structural glycoprotein of rotavirus was only detectable in its fully glycosylated form in pulse-chase studies (McCrae and McCorquodale, 1982). The fact that two stable forms of NSP4 can be found in virus infected cells provides for the possibility that NSP4s with different glycosylation status may differ in their functionality. The early functional analysis of NSP4 showed that it is an intracellular protein located in the ER together with the autophagosomal marker LC3 and functions to provide translocation of DLPs (double shelled pre-virons) from the viroplasm where they are assembled into the lumen of the ER (Au *et al*., 1989; Bergmann *et al*., 1989; Berkova *et al*., 2006). This function has been shown to required glycosylation of NSP4 as the presence of tunicamycin, an inhibitor of N-linked glycosylation, in the culture medium of infected cells resulted in the accumulation of DLPs in the cytoplasm (Sabara *et al*., 1982). Other functional studies appear to show that extracellular secretion is an important feature of NSP4 that contributes to its role in pathogenesis (Bugarcic and Taylor, 2006; Zhang *et al*., 2000). Detection of only fully glycosylated NSP4 in its secreted form supported the hypothesis that glycosylation is also required for NSP4 to be secreted (Bugarcic and Taylor, 2006). Apparently both of these functions require

glycosylation of NSP4 but they require distinct fates of NSP4 in terms of widely different cellular location. In one case glycosylated NSP4 is an intracellular ER membrane protein interacting with DLPs for translocation and the other case it appears to be secreted to the extracellular environment to exercise its cytotoxicity. Given that NSP4 is found in both glycosylated and unglycosylated form in virus infected cells (McCrae and McCorquodale, 1982), it is possible that the two forms of NSP4 may play different roles in NSP4 function. Consequently comparison of the functioning of unglycosylated and glycosylated NSP4 may reveal whether the dichotomy of NSP4 function can be explained by its glycosylation status. To date the main experimental approach employed in this type of analysis has been the use of the N-linked glycosylation inhibitor tunicamycin. However it has the disadvantage that it will also block glycosylation of cellular proteins and this might affect the observations. The absence of a convenient reverse genetics system for rotaviruses means that analyzing the role of unglycosylated NSP4 in the context of a viral infection is currently not possible. However site directed mutagenesis to remove N-linked glycosylation sites and subsequent analysis of the functioning of NSP4 expressed from mutated c-DNA following transfection can be done and this was the first strategy used in this study.

3.2 Results

3.2.1 Cloning of NSP4 Glycosylation Defective Mutants

Gene 10 of rotavirus strain UKtc (provided by M.A. McCrae, University of Warwick) was in the PCR 2.1 cloning vector and under the control of the bacteriophage T7 promoter. Site-directed mutagenesis PCR was used to mutate the two N-linked glycosylation sites present in the first of the three hydrophobic domains located in the amino terminal half of NSP4. The asparagine residues in each of the N-linked glycosylation sites were mutated to alanines by PCR based site-directed mutagenesis introducing *BglII* and *NheI* restriction enzyme sites for the first and second glycosylation sites respectively. Following mutagenesis the complete sequence of NSP4 was checked to ensure that no additional mutations had been introduced. Figure 3.1 shows that part of the NSP4 cDNA and amino acid sequence where the mutations and the sequence changes were introduced.

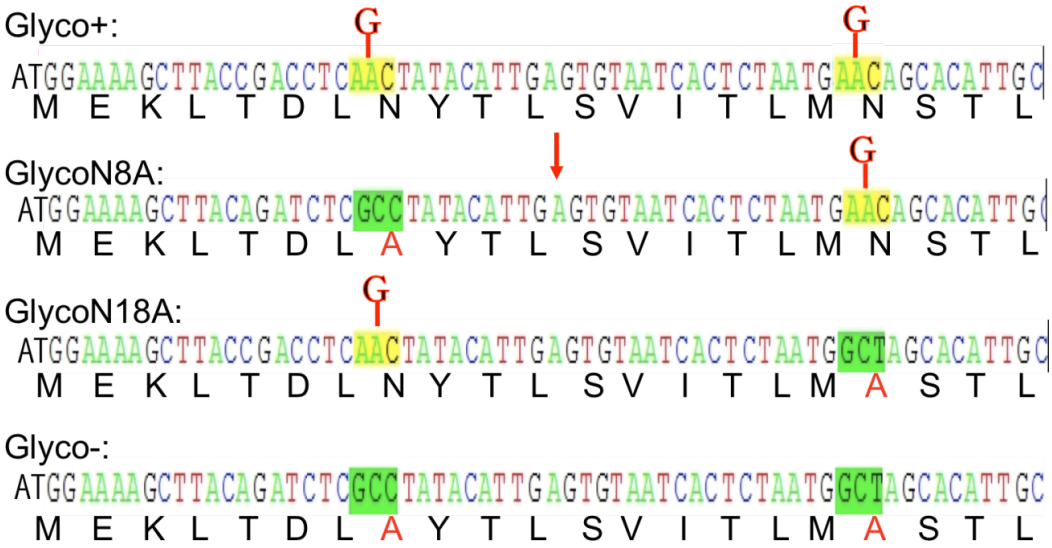

Figure 3.1: Amino terminal region of the NSP4 nucleotide and amino acid sequence covering the region where mutations were introduced.

Glyco+ represents the wild type NSP4 sequence with two N-linked glycosylation sites at amino acid positions 8 and 18. GlycoN8A represents a construct with a mutation from N to A at amino acid position 8 of NSP4. GlycoN18A represents a construct with a mutation from N to A at amino acid position 18 of NSP4. Glyco- represents a construct with mutations from N to A at both amino acid position 8 and 18.

3.2.2 Different Cellular Distributions and Phenotypes of Glycosylation Variants of NSP4 in BSR-T7 Cells

The first series of experiments were done in BSRT7 cells. This cell line was used as it has been engineered to express the bacteriophage T7 RNA polymerase endogenously thereby enabling NSP4 expression from the transfected plasmids since the NSP4 gene was under the control of the T7 promoter. To more fully characterize the intracellular distribution of NSP4, BSRT7 cell monolayers transfected with wild type (glyco+), mono- (glycoN8A and glycoN18A) and double- (glyco-) glycosylation mutants of NSP4 were examined at 7.5, 23, 30 and 40 hours post transfection. A total number of 160 images was taken and analysed. Striking differences were observed between cell samples transfected with wild type, mono- and double-glycosylation mutants of NSP4 at 7.5-h post transfection. In the case of the wild type and mono-glyco mutants intracellular NSP4 containing vesicle-like structures in the cytoplasm (frequently seen) and more strikingly long NSP4 containing 'pseudopodia-like' cytoplasmic extrusions were evident in a small number of cells (Fig 3.2A-F). However, in the double glycosylation site mutant neither of these features was evident (Fig 3.2G and H). At the later time post-transfection (23, 30 and 40 hours) cells transfected with both the wild type and the glycosylation mutants showed a similar intracellular distribution of NSP4 (Fig 3.2I-T).

The striking NSP4 containing cytoplasmic extrusions in cells transfected with wild type NSP4 were analysed in greater detail (Fig 3.3). This confirmed the presence of vesicle-like structures containing NSP4 at the tips of the extrusion (Fig 3.3).

Figure 3.2: Intracellular distribution of wild type (glyco+), mono-glyco mutants (glycoN8A and glycoN18A) and glyco- NSP4 mutant expressed in BSR-T7 cells.

NSP4 was stained with polyclonal rabbit antisera raised against bacterially expressed NSP4 (McCrae and McCorquodale, 1987) followed by Alexa-594-conjugated goat-anti-rabbit secondary antibody as described in Materials and Methods. Nuclei were stained with DAPI again as described in Materials and Methods. (A) Intracellular glyco+ NSP4 containing vesicle-like structure in a cell at 7.5-h post transfection. (B) Long glyco+ NSP4 containing cytoplasmic extrusion in a cell at 7.5-h post transfection. (C and D) Intracellular glycoN8A NSP4 containing vesicle-like structure and cytoplasmic extrusion in cells at 7.5-h post transfection. (E and F) Intracellular glycoN18A NSP4 containing vesicle-like structure and cytoplasmic extrusion in cells at 7.5-h post transfection. (G and H) Glyco- NSP4 expressing cells showing that mutated NSP4 congregates into numerous intracellular spots at 7.5-h post transfection. (I, J, L, M, O, P, R and S) All glyco+, mono-glyco mutants and glyco- NSP4 distribute in numerous intracellular spots at 23 and 30-h post transfection. (K, N, Q and T) All glyco+, mono-glyco mutants and glyco- NSP4 congregate to form larger structures at 40-h post transfection. Time post transfection is indicated in the bottom left corner of each image. Arrowheads indicate NSP4 containing vesicle-like structures and arrows indicate NSP4 containing 'pseudopodia-like' cytoplasmic extrusions. A magnification bar of 5 μm is shown in the bottom right corner of each image.

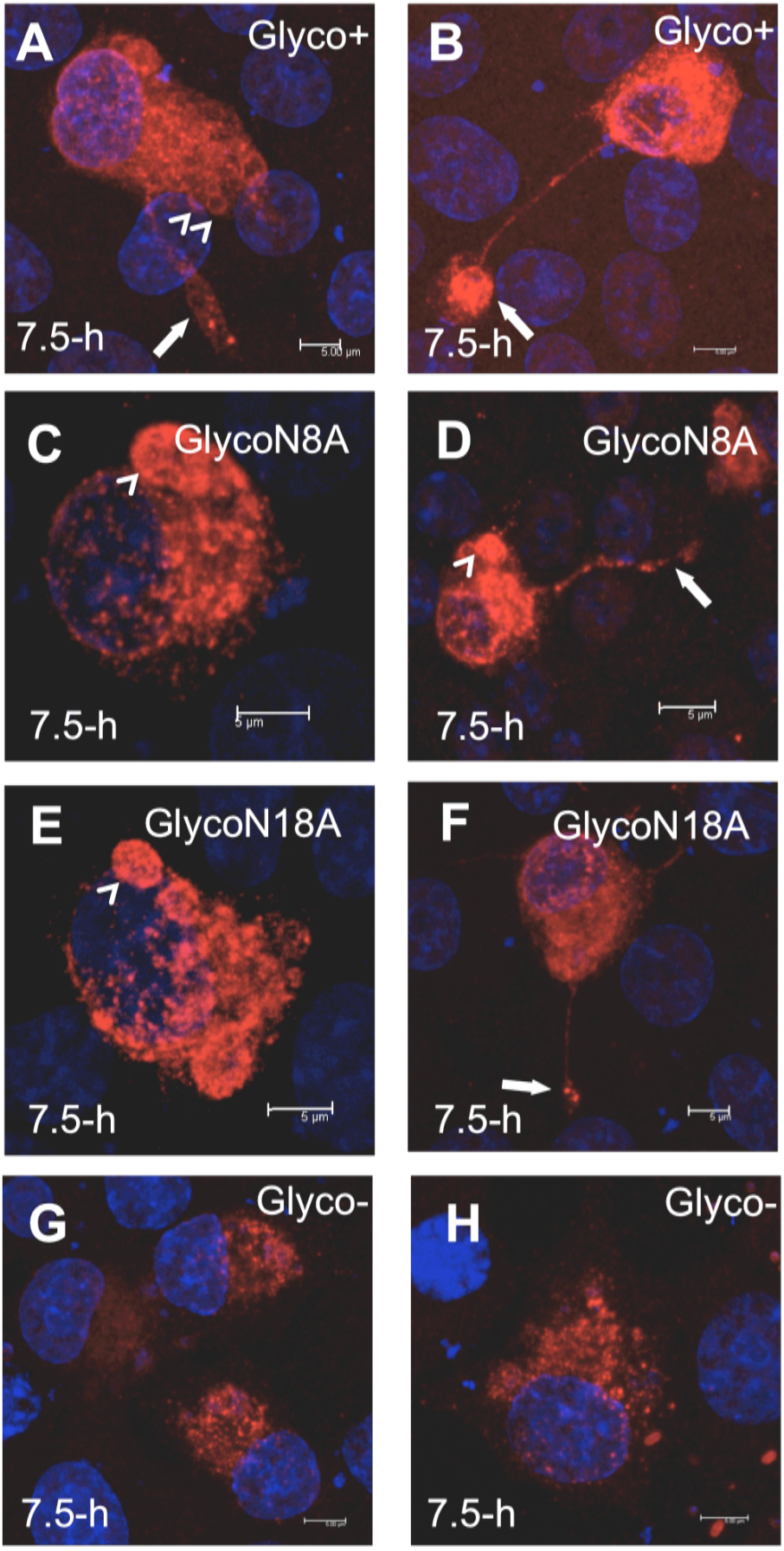
A
Glyco+
7.5-h
5.00 µm
B
Glyco+
7.5-h
C
GlycoN8A
7.5-h
5 µm
D
GlycoN8A
7.5-h
5 µm
E
GlycoN18A
7.5-h
5 µm
F
GlycoN18A
7.5-h
5 µm
G
Glyco-
7.5-h
H
Glyco-
7.5-h

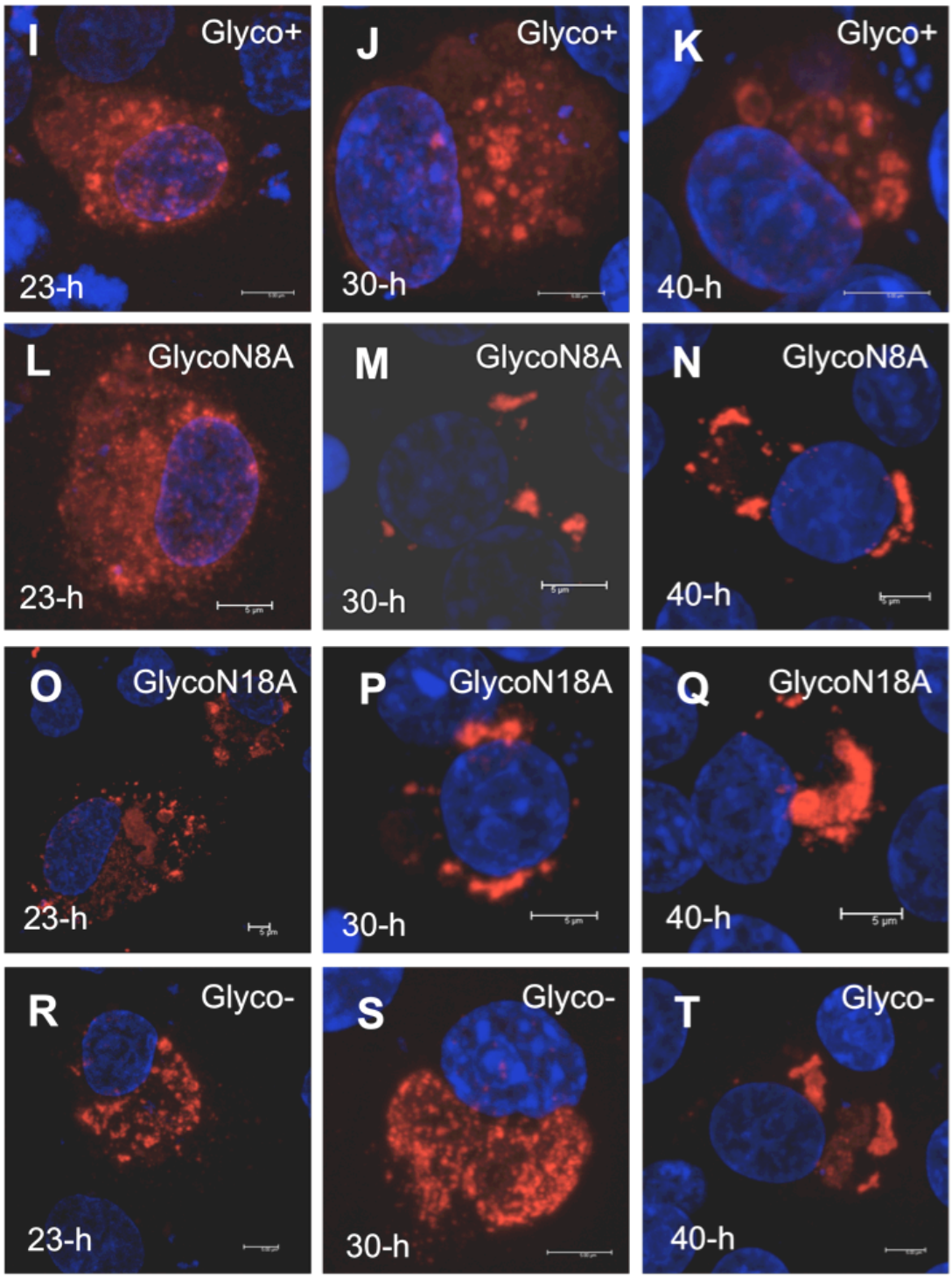
I
Glyco+
23-h
J
Glyco+
30-h
K
Glyco+
40-h
L
GlycoN8A
23-h
M
GlycoN8A
30-h
N
GlycoN8A
40-h
O
GlycoN18A
23-h
P
GlycoN18A
30-h
Q
GlycoN18A
40-h
R
Glyco-
23-h
S
Glyco-
30-h
T
Glyco-
40-h

Figure 3.3: NSP4 containing cytoplasmic projections in glyco+ NSP4 transfected BSRT7 cells.

NSP4 was stained with polyclonal rabbit antisera raised against bacterially expressed NSP4 (McCrae and McCorquodale, 1987) followed by Alexa-594-conjugated goat-anti-rabbit secondary antibody as described in Materials and Methods. Nuclei were stained with DAPI again as described in Materials and Methods. (A) Long projection with narrow connection to the cells main body shown in figure 3.2B, represented here for better comparison. (B) Medium projection. (C) Short projection. Arrows indicate the vesicle-like structures at the tips of the cytoplasmic projections. A magnification bar of 5 μm is shown in the bottom right corner of each image.

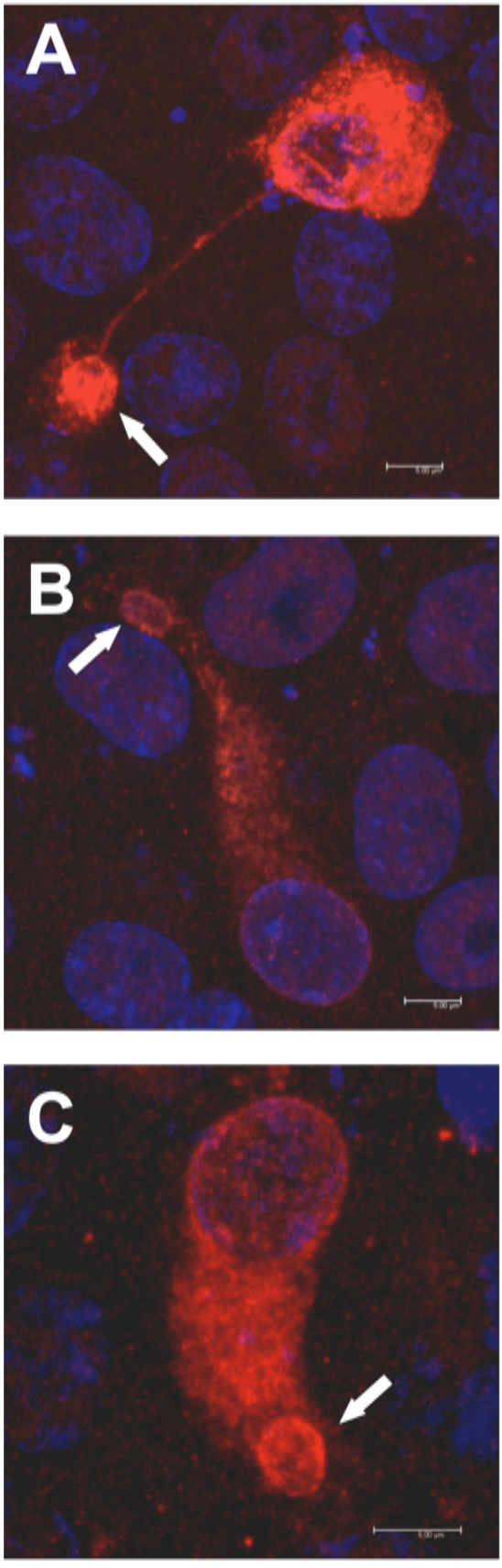
A
B
C

3.2.3 NSP4 Expression in Simian BSC-1 Cells

A significant disadvantage of using the fibroblastic BSRT7 cell line was that this line was derived from baby hamster kidney (BHK) cells and consequently is not permissive for rotavirus infection. This means that the intracellular distribution of the NSP4 expressed from transfected cDNA constructs in these cells could not be easily compared with that seen for NSP4 expressed during virus infection. To investigate whether the striking cytoplasmic extrusions containing NSP4 were also evident in a rotavirus permissive cell line, simian BSC-1 cells that do support rotaviral infection were transfected with the NSP4 plasmids used in the initial experiments done in BSR-T7 cells. However, because these cells do not normally express the bacteriophage T7 RNA polymerase, they also had to be infected with a recombinant vaccinia virus (T7-MVA) to generate the T7 RNA polymerase necessary to drive the expression of NSP4. The infection of cells with T7-MVA was done 4-h after transfection. At 7.5-h following the start of NSP4 expression, the transfected BSC-1 cell monolayers were fixed, stained for NSP4 and observed using confocal microscopy. Images showing long cytoplasmic extrusions of the type seen in BSR-T7 cells were again seen in more than half of the BSC-1 cells expressing glyco+ NSP4 but not with glyco- NSP4 (Fig 3.4). The glycoN8A and glycoN18A cDNA constructs were not tested in these experiments as NSP4 glycosylated at only one of the two N-linked glycosylation sites is not detected following the natural viral infection (McCrae and McCorquodale, 1982).

Figure 3.4: Intracellular distribution of glyco+ and glyco- NSP4 expressed in transfected simian BSC-1 cells at 7.5-h after the switch on of NSP4 expression using T7-MVA.

NSP4 was stained with polyclonal rabbit antisera raised against bacterially expressed NSP4 (McCrae and McCorquodale, 1987) followed by Alexa-594-conjugated goat-anti-rabbit secondary antibody as described in Materials and Methods. Nuclei were stained with DAPI again as described in Materials and Methods. (A and B) BSC-1 cells expressing glyco+ NSP4 showing NSP4 containing long cytoplasmic extrusions. (C) A BSC-1 cell expressing glyco- NSP4 showing cytoplasmic distribution of mutated NSP4 in intracellular spots. Arrows indicate the positions of cytoplasmic projections. A magnification bar of 10 μm in panel A and C, 30 μm in panel B is present in the bottom right corner of each image.

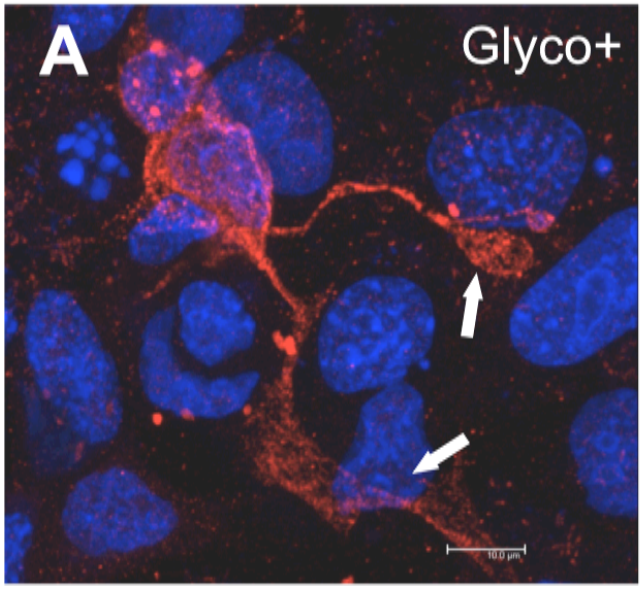
A
Glyco+

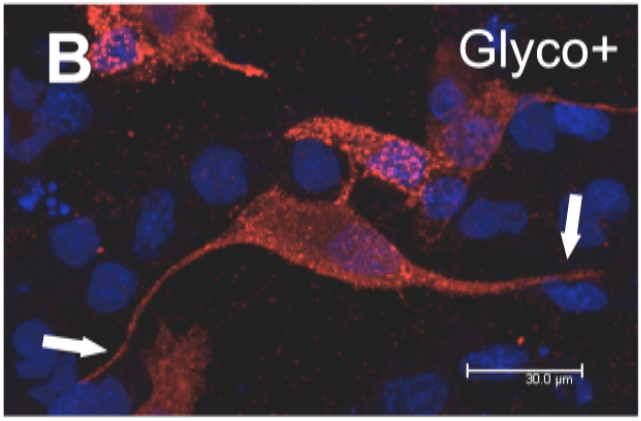
B
Glyco+
30.0 µm

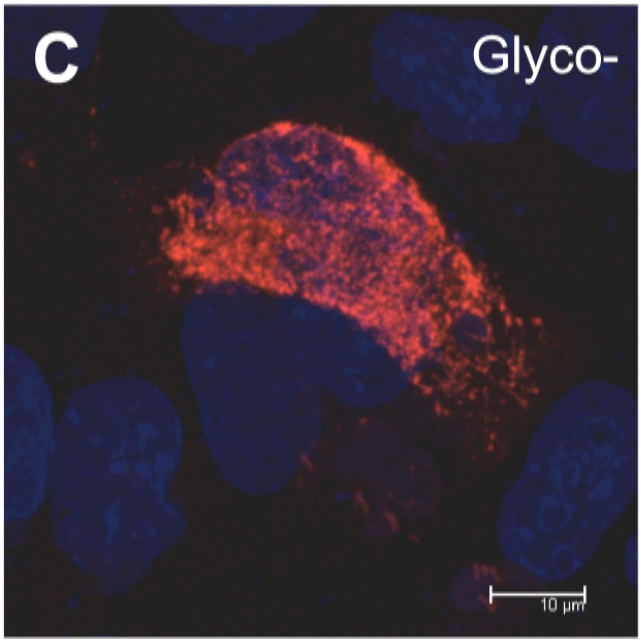
C
Glyco-
10 µm

3.2.4 Cellular Distribution of NSP4 in Virus-Infected Cells

Transfection and expression of glyco+ NSP4 in isolation produced an alteration of cellular morphology. However the participation of other viral proteins during a normal viral infection may affect the effect of expression of glyco+ NSP4. This led us to investigate the relevance of the changes in cell morphology seen when glyco+ NSP4 was expressed in isolation to changes that occur following viral infection. To do this, monolayers of BSC-1 cells were infected at an MOI of 0.2 and fixed at different times post infection. Cells were stained for NSP4 and DAPI before being examined by confocal microscopy. NSP4 expression was first detected at 6 hpi, viroplasms characteristic of rotavirus infection were visible by 8 hpi. The morphology of cells remained smooth at 9 hpi, but significant alterations in cellular morphology could be detected at 10 hpi with small cytoplasmic extrusions being clearly visible. At 11 hpi cytoplasmic extrusions crossing several cellular diameters were clearly evident and cells seemed to lose material from the cytoplasm as less cytoplasm was evident compared to images taken earlier time points post infection (Fig 3.5). These 'snapshot' images showed that the unusual cytoplasmic extrusions seen following expression of NSP4 in transfected cells were also evident in virus-infected cells. However in the case of virus infected cells their appearance was delayed compared to that seen following transfection suggesting that one or more of the viral proteins expressed following infection may regulate the kinetics of NSP4 induced changes in cell morphology.

Figure 3.5: Time course study of BSC-1 cell morphology changes after rotavirus infection.

BSC-1 cell monolayers on coverslips were infected with virus at an MOI of 0.2 and observed at various times post infection (time indicated on top right corner of every image). NSP4 was stained with polyclonal rabbit antisera raised against bacterially expressed NSP4 (McCrae and McCorquodale, 1987) followed by Alexa-594-conjugated goat-anti-rabbit secondary antibody as described in Materials and Methods. Nuclei were stained with DAPI again as described in Materials and Methods. (A) NSP4 staining was first evident at 6 hpi. (B and C) At 8 and 9 hpi viroplasms started to be visible but the individual cell morphology remained smooth and intact. (D) Cells began to change morphology showing short cytoplasmic extrusion at 10 hpi. (E, F and G) Cell morphology changed significantly showing long cytoplasmic extrusions at later times after viral infection. Arrowheads indicate viroplasms and arrows indicate the positions of cytoplasmic extrusions. A magnification bar of 10 μm is present in the bottom right corner of each image.

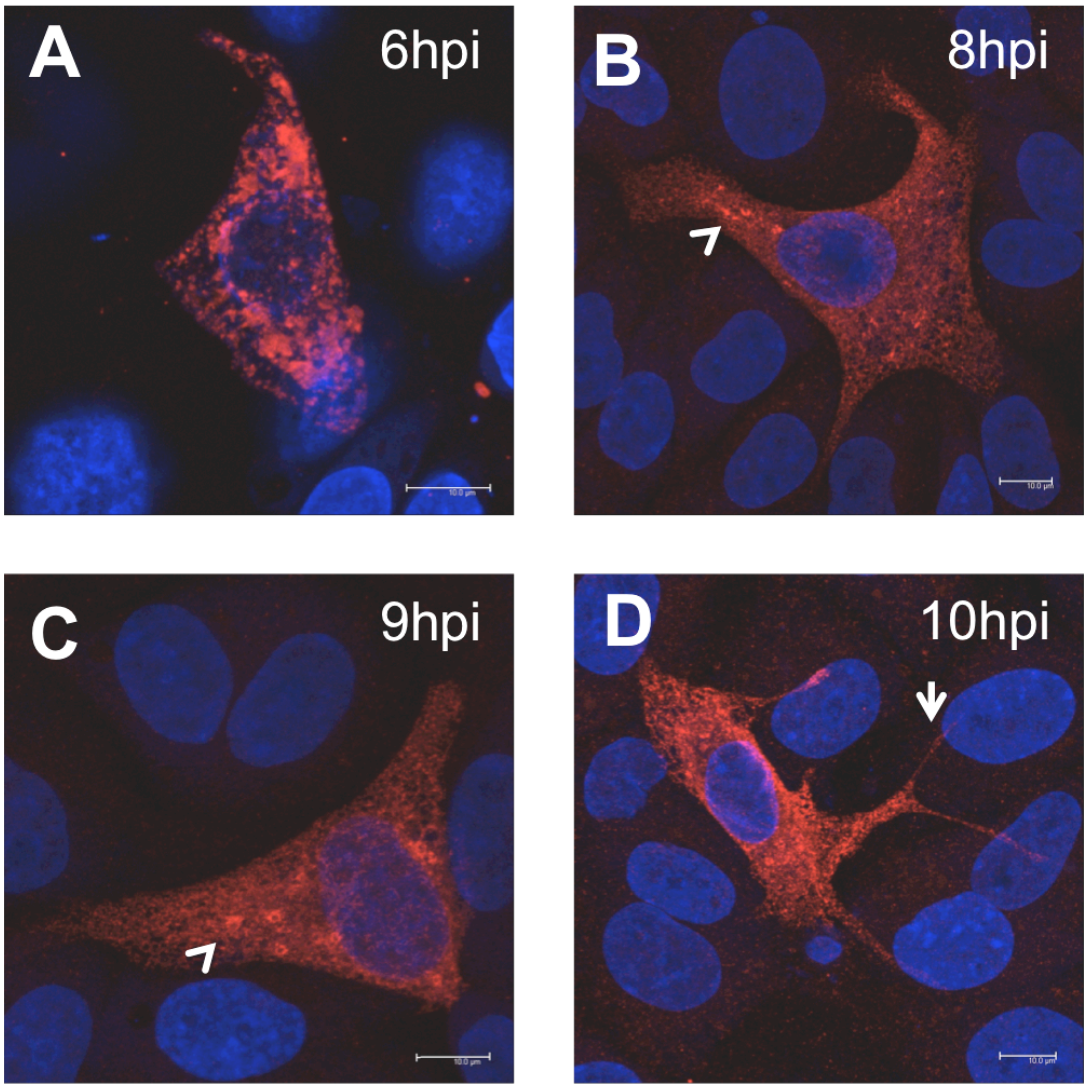
A
6hpi
B
8hpi
C
9hpi
D
10hpi

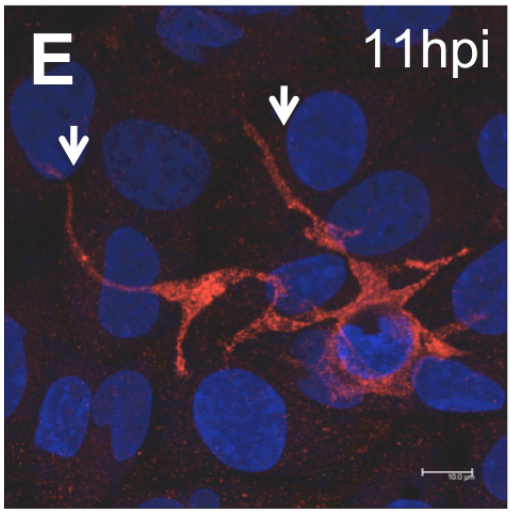
E
11hpi

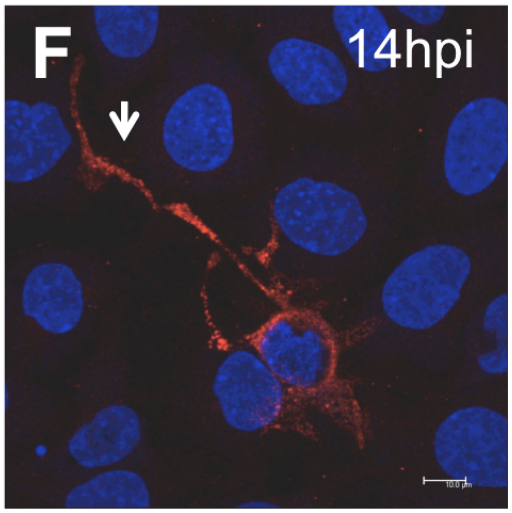
F
14hpi

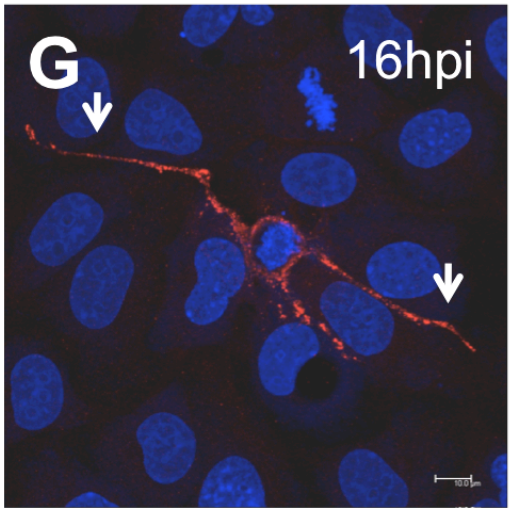
G
16hpi

3.3 Conclusions

The aim of this chapter was to study and compare the intracellular expression pattern of wild type NSP4 and its glycosylation defective mutants constructed by site-directed mutagenesis. Confocal microscopy of BSR-T7 and BSC-1 cells expressing wild type (glyco+) and glycosylation mutants (mono- and double-glycosylation sites mutated) showed that the fully glycosylated (glyco+) and the single site glyco- mutants of NSP4 were able to both localize in vesicular structures in the cytoplasm and to alter cellular morphology as early as 7.5 hours after expression. However neither of these phenomena were seen in cells expressing the double glycosylation site mutant of NSP4. These results suggested that both fully and single glycosylated NSP4 possess the ability to alter cell morphology promoting the formation of long cytoplasmic extrusions. Consistent with these observations glycosylated NSP4 has been reported to stimulate cellular projections in HEK 293 cells (a human embryonic kidney cell line) by increasing intracellular calcium levels to change the actin filament network. Although unglycosylated NSP4 was not analysed in that study (Berkova *et al*., 2007), nevertheless inhibiting increases in intracellular calcium levels either by treatment with tunicamycin or through the use of RNAi (RNA interference) silencing of NSP4 indicate that glycosylation of NSP4 is required for the increase of intracellular calcium concentration in infected cells (Ruiz *et al*., 2005; Zambrano *et al*., 2008). Unglycosylated NSP4 that did not increase intracellular calcium concentrations also did not exhibit the actin network changes seen in cells expressing glycosylated NSP4. Taken together these studies support the observation that only glycosylated NSP4 was able to change cell morphology. Therefore the present study supports the hypothesis that differential glycosylation status of NSP4 affects its function.

Changes in cellular morphology associated with viral infection were also examined to see if there were any similarities to the changes induced by NSP4 expression alone. Confocal microscopy of virus-infected cells showed that at 10-hour post infection cytoplasmic extrusions similar to those seen in transfected cells expressing wild type glyco+ NSP4 were present. The delay in timing (7.5 hours in transfected cells versus 10 hours in infected cells) of appearance of cytoplasmic extrusions indicated that this function of glyco+ NSP4 might be controlled by other viral proteins. However these speculations are based on observations using 'snap-shot' images made by fixing and antibody staining of cells at various times after either transfection or infection and require further investigation to validate them. To avoid the drawbacks of only examining a 'frozen' moment and the possibility of cell fixation destroying fragile cellular structure it was decided that real time confocal microscopy should be exploited as a means of monitoring the dynamics of the changes in cellular morphology in glyco+ NSP4 expressing and virus infected cells.

Chapter 4

Real-time Analysis of NSP4 and Virus Induced Cytoplasmic Extrusions

4.1 Introduction

In both fixed cells expressing solely glyco+ NSP4 and fixed virus infected cells significant alterations in cellular morphology were evident. In both cases long cytoplasmic extrusions were seen. However, to observe the kinetics of these changes in cellular morphology and also to avoid the drawbacks of cell fixation and 'snapshot' imaging of the microscopy in the previous chapter real-time confocal microscopy was investigated. Specifically after either glyco+ NSP4 expression following transfection or viral infection, real-time fluorescent confocal microscopy was used to capture changes in cell morphology highlighted by the presence of either GFP (green fluorescent protein) or YFP (yellow fluorescent protein). Despite the additional information obtained using this approach, it was quickly realized that long exposure of fluorescent molecules to laser light associated with scanning over a longer time frame resulted in both photobleaching of fluorescent molecules and phototoxic damaging to the living cells being observed. Therefore both transmission light confocal microscopy and the use of a resonant scanner were introduced. The transmission light monitoring was aimed at minimizing the phototoxic destruction of cells and the very high resonant frequency (i.e. 8000 Hz) scanning was used to allow high-speed imaging.

4.2 Results

4.2.1 Construction of T7-NSP4-GFP For Real Time Observation Of Glyco+ NSP4 Stimulated Cytoplasmic Extrusions

To facilitate real time monitoring of changes in cell morphology a green fluorescent protein (GFP) sequence was fused onto the 3' end of the NSP4 coding region. To allow the fusion construct to be generated, a *StuI* restriction enzyme site was introduced at the 3' end of the NSP4 open reading franked by site-directed mutagenesis PCR. Then a PCR amplicon consisting of the GFP coding sequence franked by *StuI* restriction enzyme sites was ligated to the 3' end of NSP4 such that the GFP open reading frame was joined in frame to the carboxy terminus of NSP4 to create a fusion protein (Fig 4.1). Transfection of this plasmid construct into BSR-T7 cells resulted in colocalization of NSP4 staining and GFP fluorescence (Fig 4.2). This indicated that GFP fluorescence could be used to represent the intracellular localization of expressed NSP4 to allow real time monitoring of morphologic change in NSP4 expressing cells, thereby overcoming the disadvantages seen when observing the protein in fixed specimens. However, this construct presented a different limitation to that seen in the earlier experiments. An increased incubation time following transfection was required for expression of the NSP4-GFP fusion to accumulate to the point where it could be clearly detected above background fluorescence. This hampered observation of NSP4-GFP positive cells at early times after transfection and no cytoplamic extrusions were seen in BSR-T7 cells at the earliest time post transfection that the NSP4-GFP could be detected which was 24 hours post transfection.

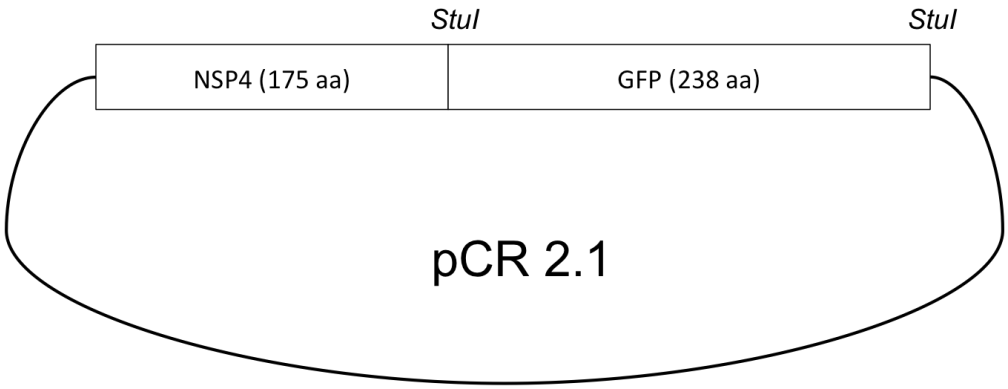

Figure 4.1: Schematic representation of glyco+ NSP4-GFP fusion protein construct.

To construct the NSP4-GFP fusion protein a *StuI* restriction enzyme site was introduced at the 3' end of the NSP4 open reading frame by site-directed mutagenesis PCR. Then a PCR amplicon consisting of the GFP coding sequence franked by *StuI* restriction enzyme sites was ligated to the 3' end of NSP4 such that the GFP open reading frame was joined in frame to the carboxy terminus of NSP4 to create the fusion protein.

Figure 4.2: Colocalization of NSP4 and GFP after 24 hours of expression of the NSP4-GFP fusion protein in BSR-T7 cells.

NSP4 was stained with polyclonal rabbit antisera raised against bacterially expressed NSP4 (McCrae and McCorquodale, 1987) followed by Alexa-594-conjugated goat-anti-rabbit secondary antibody as described in Materials and Methods. Nuclei were stained with DAPI again as described in Materials and Methods. (A) Localization of NSP4 highlighted by NSP4-antibody staining. (B) GFP signal showing intracellular localization of the NSP4-GFP fusion protein. (C) A merged image of panel A and B showing colocalization of NSP4 and GFP in yellow spots. Arrows indicate two specific spots of NSP4 and GFP colocalization. A magnification bar of 5 μm is present in the bottom right corner of each image.

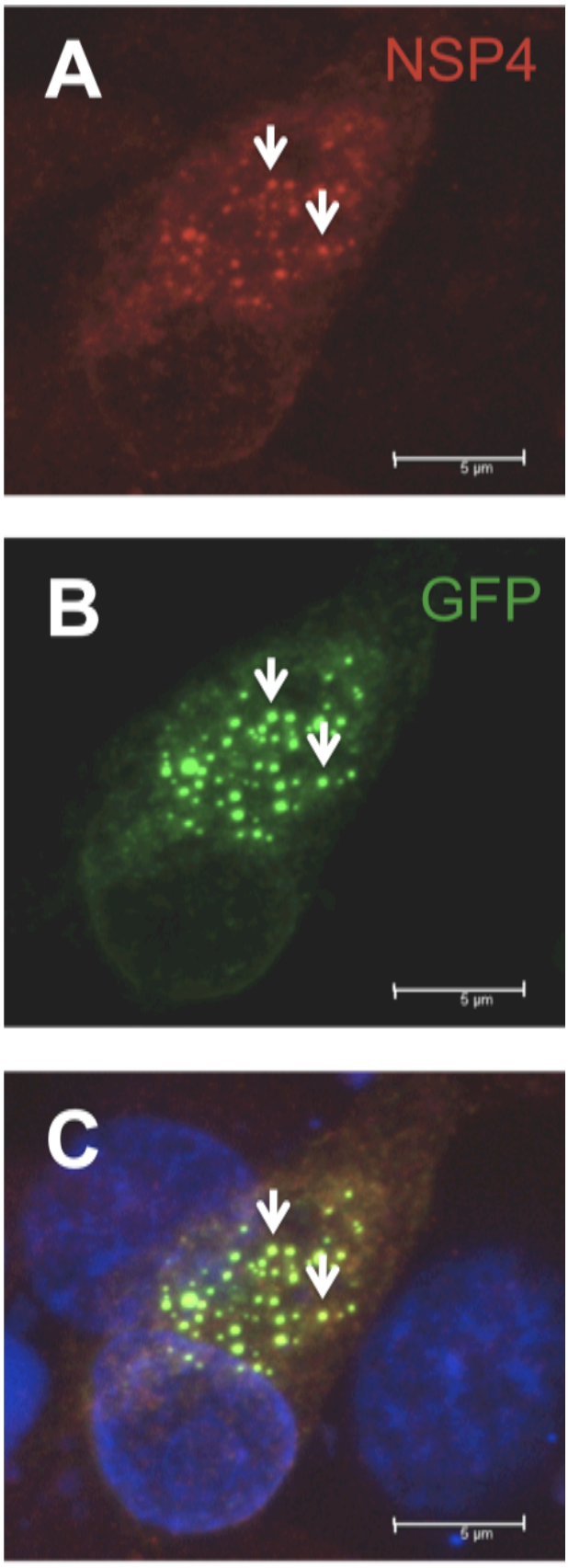
A
NSP4
5 µm
B
GFP
5 µm
C
5 µm

4.2.2 Morphological Observation of Glyco+ NSP4-GFP Expressing BSC-1 Cells

Transfection of the fusion protein plasmid described in 4.2 and subsequent expression of the glyco+ NSP4-GFP fusion protein in BSR-T7 cells demonstrated that GFP fluorescence could be used to monitor the distribution of NSP4 in cells in real time. The fusion protein construct was therefore transfected into rotavirus permissive BSC-1 cells and cells monitored 24 hours after expression of NSP4 was initiated by infection of the cells with MVA-T7 to drive fusion protein expression. This revealed significant changes in cell morphology in all cells positively expressing GFP. Notably in these cells cytoplasmic extrusions also were detected (Fig 4.3). Subsequent real-time observation for 2 hours did not showed any change of these cytoplasmic extrusions. At 48 hours after fusion protein expression was initiated a large proportion of GFP fluorescence positive cells had rounded up and suspended in the culture medium, possibly due to the cytopathology induced by replication of the MVA-T7 vaccinia virus used to drive NSP4 expression.

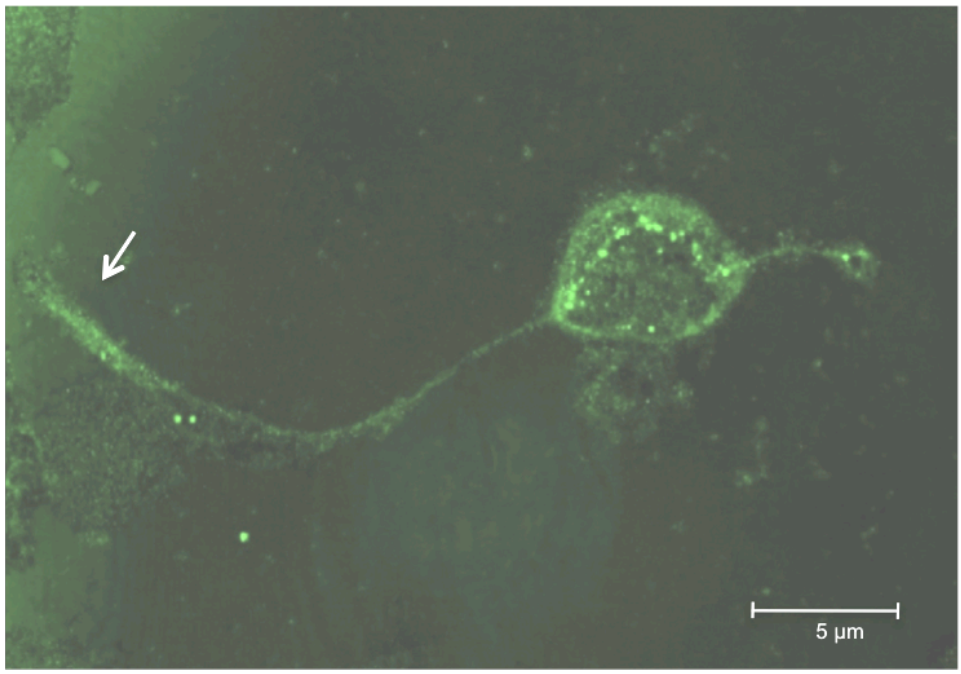

Figure 4.3: Morphologic observation of BSC-1 cells expressing glyco+ NSP4-GFP fusion protein at 24 hours post expression.

BSC-1 cells were transfected with glyco+ NSP4-GFP plasmid and 4 hours later were infected with recombinant vaccinia virus MVA-T7 as described in Materials and Methods. Cells were monitored using confocal microscopy initiated at 24 hours after NSP4-GFP expression began. Arrow indicates a cytoplasmic extrusion. A magnification bar of 5 µm is present in the bottom right corner.

4.2.3 Real-Time Morphological Observation of Virus-Infected BSC-1 Cells

In chapter 3 antibody staining of fixed cells was used to show that viral infection changes cellular morphology to stimulate the formation of long cytoplasmic extrusions at 10 hpi in BSC-1 cells. However dynamic analysis using real-time confocal microscopy was pursued to achieve a better understanding of this novel observation. To do this with maximum efficiency, the effects of viral infection were examined in BSC-1 cells that had previously been transfected with a CMV-YFP plasmid to 'light-up' cellular morphology. Twenty-four hours after transfection, cells were infected with bovine UKtc rotavirus at an MOI of 10. Subsequent real time confocal microscopy of these cells showed that at 14 hours post infection cells began to generate long cytoplasmic extrusions which rapidly elongated and lasted for approximately 1 hour (Fig 4.4). In some cases these extrusions were more than three cellular diameters in length (Fig 4.5).

Figure 4.4: Real-time confocal microscopy examination of a virus-infected cell.

CMV-YFP transfected BSC-1 cells were infected with the bovine UKtc strain of rotavirus at an MOI of 10 as described in Materials and Methods. Observation of cells using real-time confocal microscopy started at 2 hpi with images being recorded every 20 mins. (A and B) At 14 hpi BSC-1 cells began showing a significant change in morphology. (C) The cell started to produce cytoplasmic extrusions. (D) Cytoplasmic extrusions were clearly evident. (E) Cytoplasmic extrusion elongated reaching distant areas and crossing 2 or 3 cellular diameters. (F) Loss of cytoplamic extrusions in the observation area. Time post infection is indicated on the top right corner of each image and arrows indicate an elongating cytoplasmic extrusion. A magnification bar of 40 μm is shown in the bottom right corner of each image.

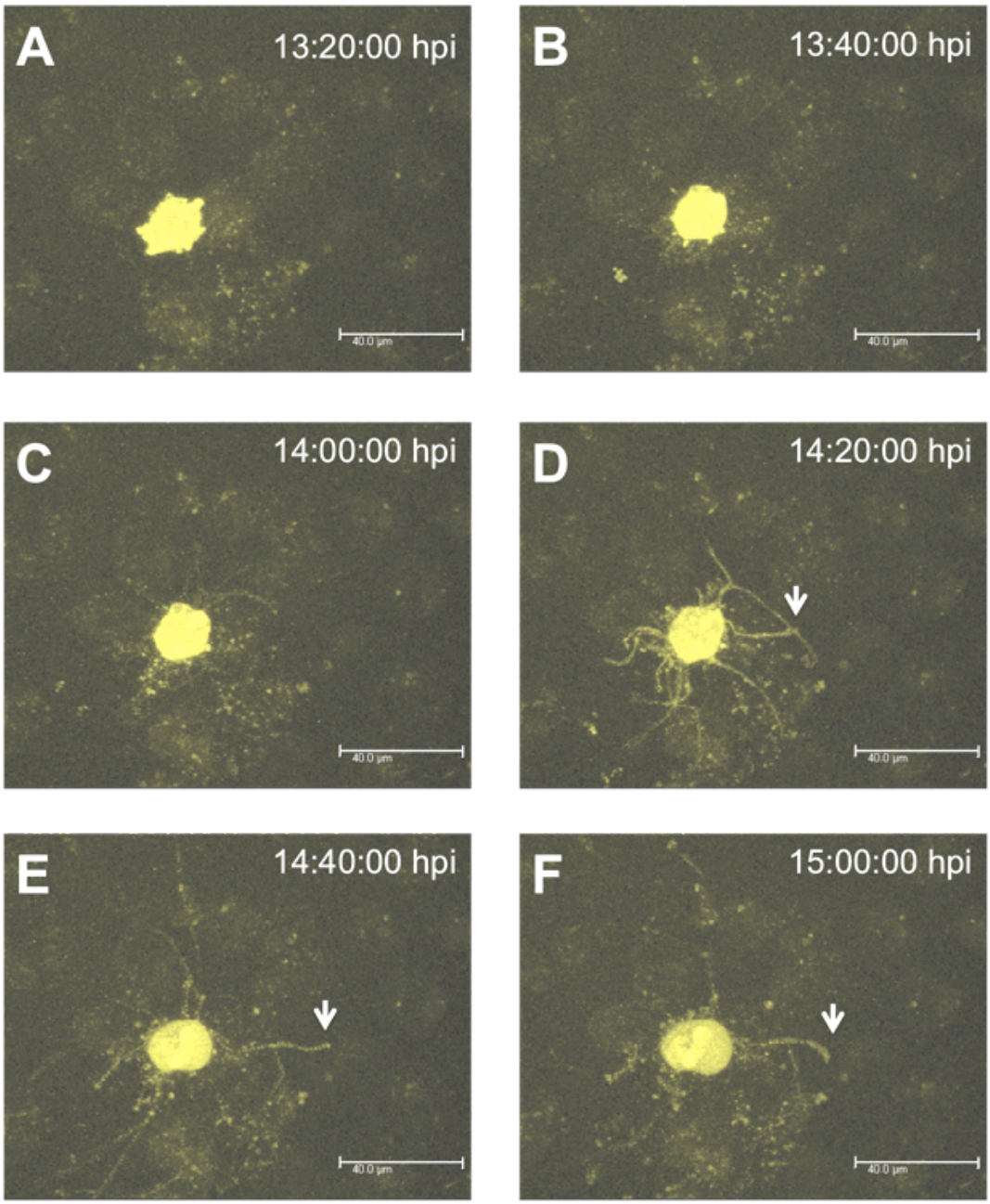
A
13:20:00 hpi
B
13:40:00 hpi
C
14:00:00 hpi
D
14:20:00 hpi
E
14:40:00 hpi
F
15:00:00 hpi

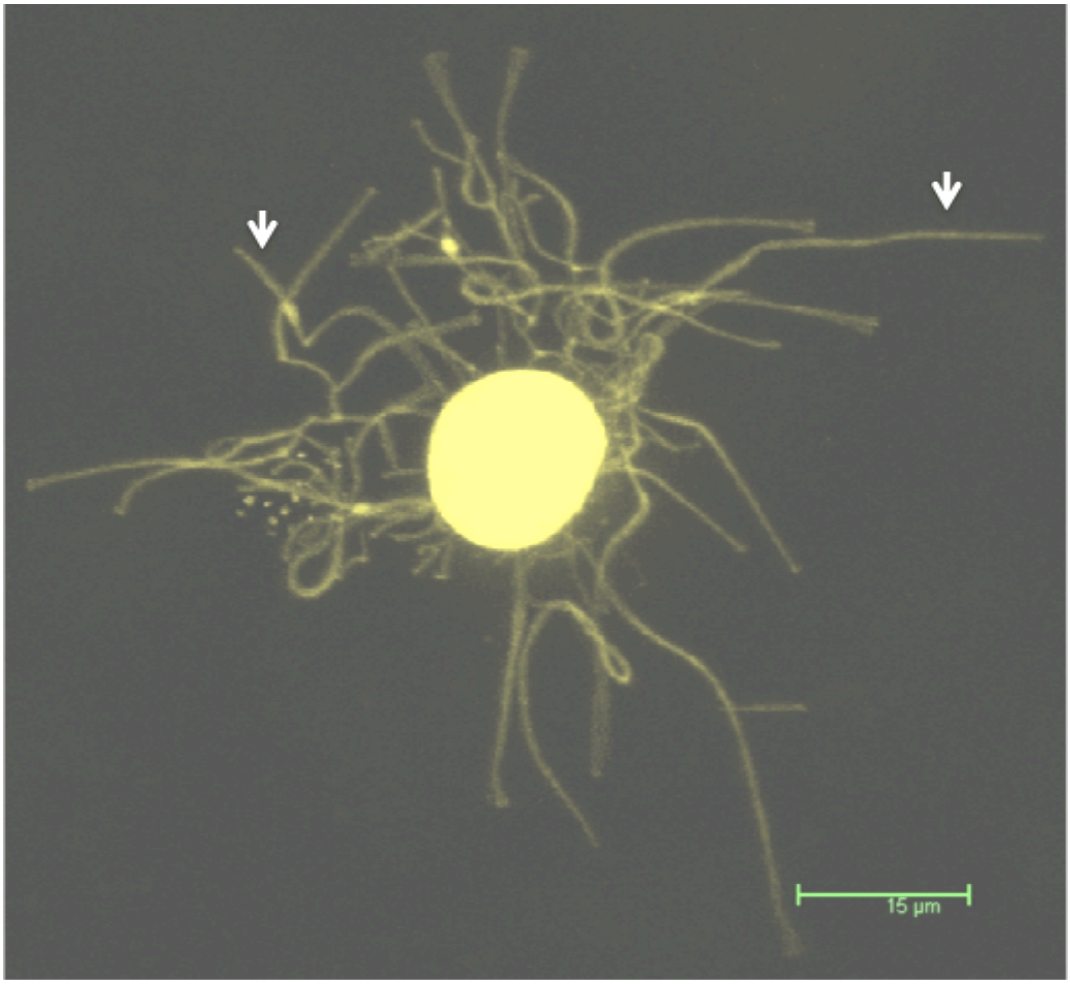

Figure 4.5: Capturing a cell with long cytoplasmic extrusions using real-time confocal microscopy.

CMV-YFP transfected BSC-1 cells were infected with the bovine UKtc strain of rotavirus at an MOI of 10 as described in Materials and Methods. The image was taken using real-time confocal microscopy at 14 hpi. Arrows indicate long cytoplasmic extrusions. The magnification bar is 15 µm.

4.2.4 Monitoring Virus Induced Cytoplasmic Extrusions by Simple Transmission Confocal Microscopy

In section 4.2.3 real time fluorescent confocal microscopy showed that significant changes in cellular morphology with the generation of cytoplasmic extrusions were seen in BSC-1 cells infected with rotavirus beginning at 14 hours post infection. To observe the phenomenon in detail more frequent scanning was required. However when cells are being imaged with fluorescent confocal microscopy long exposure of cells to laser excitation leads to reduced GFP fluorescence as a result of photobleaching and also photo-induced cytotoxicity. Therefore to minimize photo-toxicity and allow closer monitoring of the dynamics of the formation of the cytoplasmic extrusions simple transmission confocal microscopy was employed. In addition a resonant scanner operating at very high scanning frequency was also used to minimize the duration of each scan. BSC-1 cells infected with virus at an MOI of 10 were observed beginning at 12 hpi. Dynamic growth of the cytoplasmic extrusions was recorded, with measurement of the cellular extrusion showing that the extrusion was 32 μm in length when it was initially found (Fig 4.6A). Subsequent active elongation of this extrusion showed that at its maximum the extrusion was 62 μm long and 10 μm wide (Fig 4.6B-F). Its growth speed was about 2 μm/min as it elongated from 32 μm to 62 μm in 15 mins. These simple transmission confocal microscopic observations of cellular extrusion stimulated from virus-infected cells again confirmed the observations made using fluorescent confocal microscopy. It also raised the possibility that these cytoplasmic extrusions might support a novel mechanism to transfer viral material from cell to cell.

Figure 4.6: Real time transmission confocal microscopic examination of virus-infected cells.

BSC-1 cells were infected with the bovine UKtc strain of rotavirus at an MOI of 10 as described in Materials and Methods. Real-time transmission confocal microscopy of the infected cells was started at 12 hpi. (A) A cellular extrusion was initially captured being extruded from a virus-infected cell. (B) The cellular extrusion elongated and reached edge of viewing area. (C, D and E) As the cellular extrusion elongated, the viewing area was moved to fit it in the observation area. (F) Measurement of its maximum length showed that extrusion reached 62 μm.

Images were recorded using a resonant scanner with highest scan speed and took less than one second to collect and single step scan images were taken. The time of recording is indicated on the bottom left of each image and arrows indicate the elongating cytoplasmic extrusion. A 10 μm magnification bar is shown in the bottom right corner of each image.

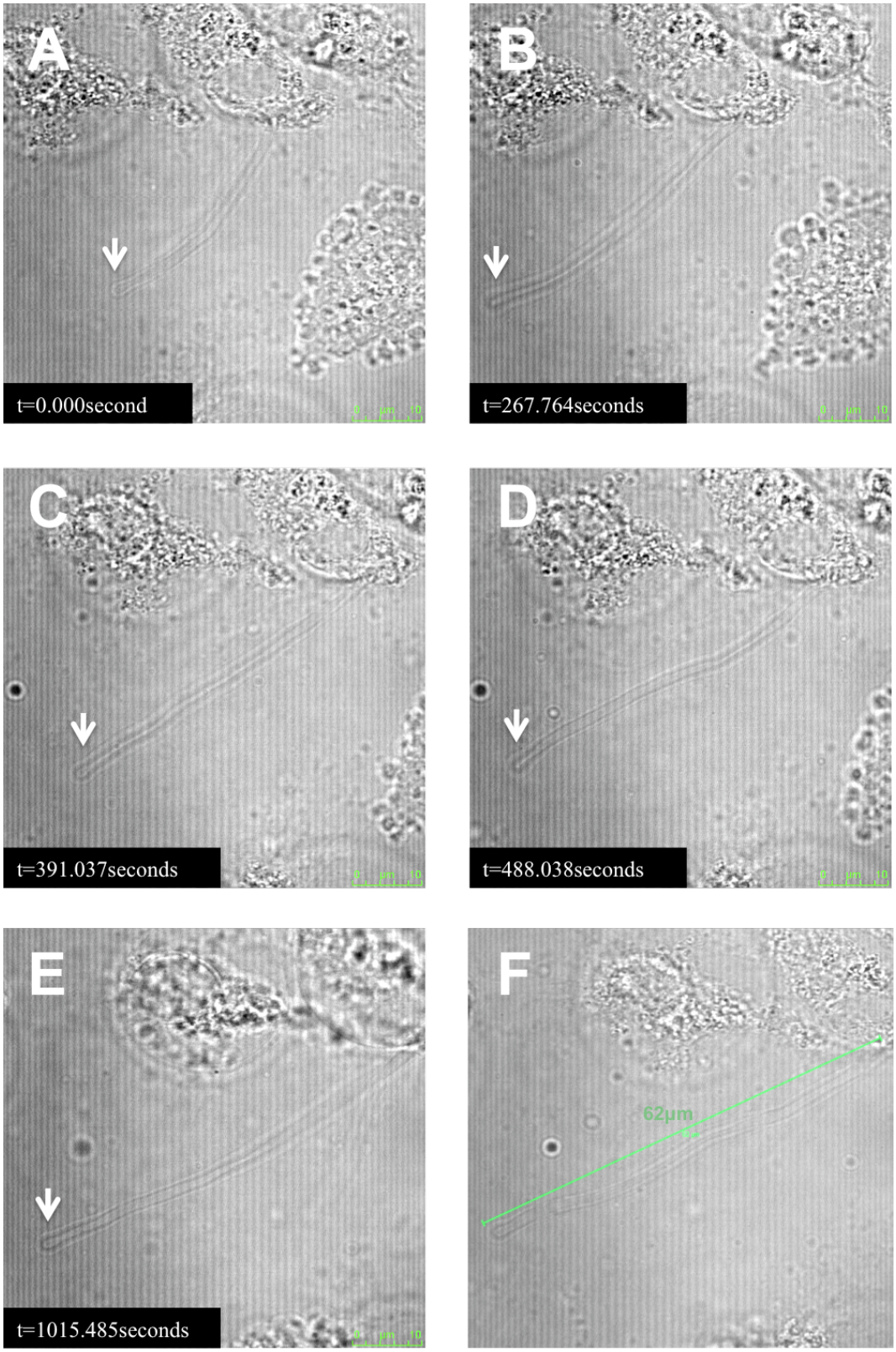
A
t=0.000second
B
t=267.764seconds
C
t=391.037seconds
D
t=488.038seconds
E
t=1015.485seconds
F
62µm

4.2.5 Apoptosis and the Induction of Cellular Extrusions

It is possible that the unusual cytoplasmic extrusions seen in rotavirus-infected cells reflected a general response of cells undergoing viral infection or apoptotic cell death. To test this possibility BSC-1 cells were infected with a different virus (reovirus) or treated with the apoptosis inducing chemical PAC-1 (triggers apoptosis through activating procaspase-3 into caspase-3) and observed with confocal microscopy. Reovirus was chosen to challenge BSC-1 cells as it falls in the same virus family (*Reoviridae*) as rotaviruses and thus shares some similarity in its replication cycle. Monolayers of BSC-1 cells were infected with reovirus type 3 at an MOI of 10 and observed from 12 hpi using real time with transmission confocal microscopy. There were no obvious morphologic changes in the cells and certainly no appearance of long cytoplamic extrusions in the subsequent 4 hours of observation (Fig 4.7). In the case of treatment of PAC-1, which selectively induces caspase-3 dependent apoptosis, on BSC-1 cells Monolayers of BSC-1 cells were challenged by treatment of PAC-1 and observed using transmission confocal microscopy beginning at 1 hour after treatment. Real time observation revealed that during the first 8 hours post treatment cells started to shrink and round up. Additionally the cytoplasm appeared dense and some cytoplasmic fronts making contact with the surface of culture vessel were visible (Fig 4.8A-D). These cytoplasmic fronts were residual from retreat of cytoplasm during apoptosis and lacked progressive growth that differentiated them from cytoplasmic extrusions seen in rotavirus infected cells. In the subsequent 2 hours the membranes of cells showed irregular buds known as blebs and some cytoplasmic vesicles called apoptotic bodies broke apart from cell main body (Fig 4.8E and F). Finally cells burst showing a membranous structure that connected to a fraction of cell debris (Fig 4.8G and H). However at no stage were any of the long

cytoplasmic extrusions seen in rotavirus-infected cells observed.

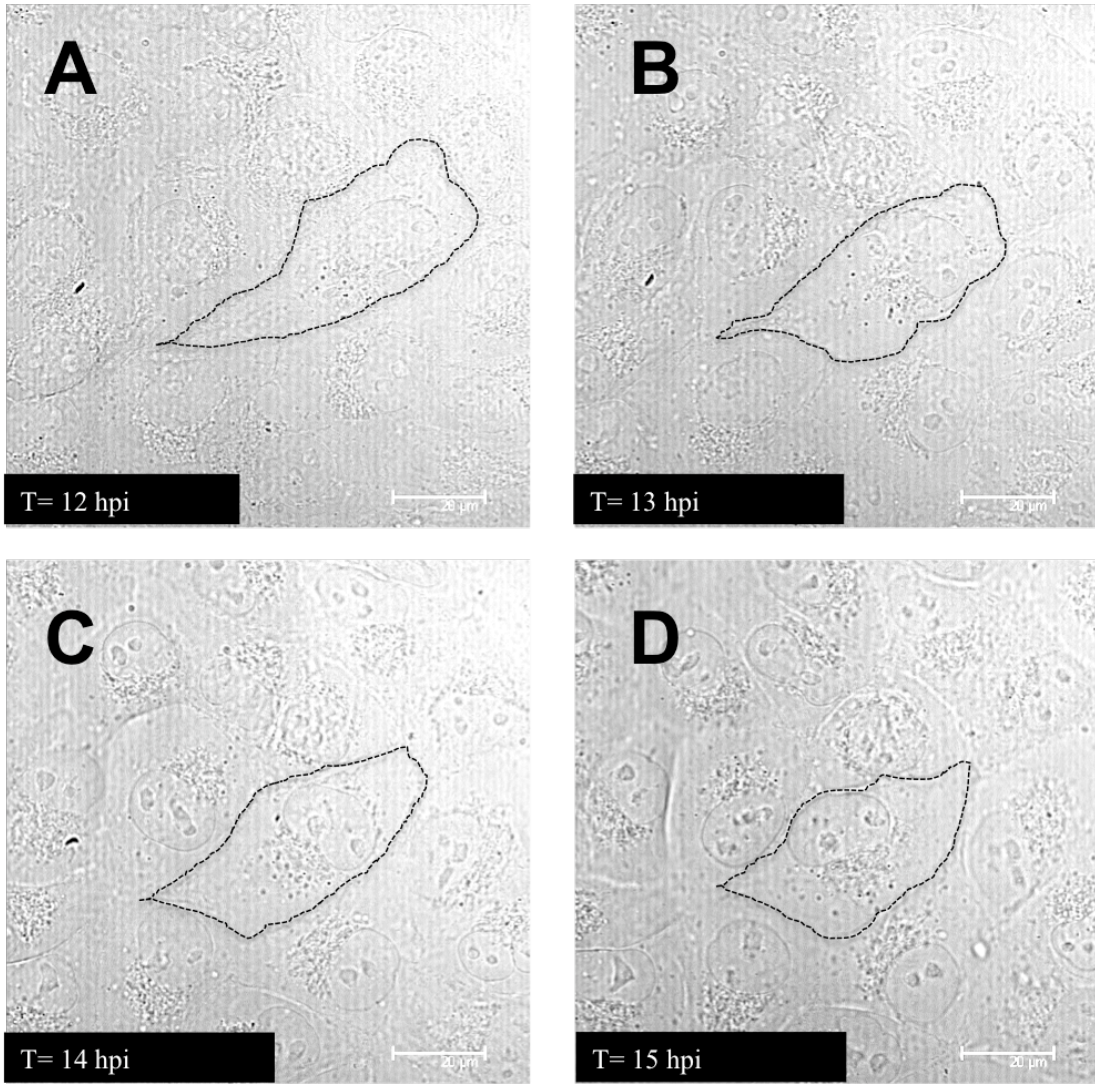

Figure 4.7: Reovirus infection in BSC-1 cells.

BSC-1 cells were incubated in the culture medium containing reovirus at an MOI of 10 until the time of observation. Observation using transmission confocal microscopy was started at 12 hpi. (A) Initial morphology and location of cells at 12 hpi. (B, C and D) Alteration in cellular morphology could be noticed but no appearance of cytoplasmic extrusions seen in rotavirus infected cells. The cellular morphology of a cell in the middle of the images is marked by dashed line indicating continuous change of the cell shape. The time of observation is indicated in the bottom left corner of each image. Single slice images were taken in this experiment. A magnification bar of 20 μm is present in the bottom right corner of each image.

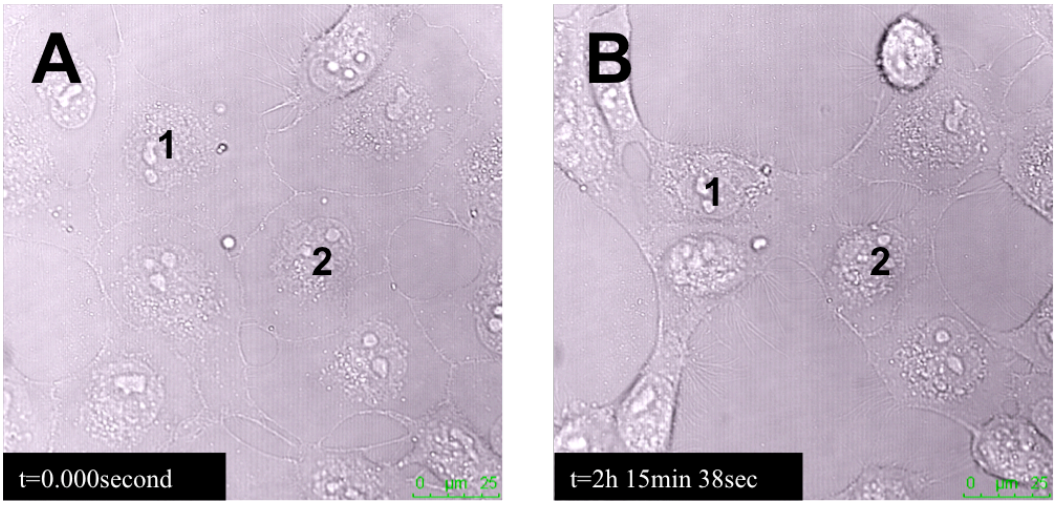

Figure 4.8: Apoptosis stimulated by treatment of PAC-1 in BSC-1 cells.

BSC-1 cells were challenged by adding PAC-1 to the culture medium described in Materials and Methods. Observation using transmission confocal microscopy was carried out one hour after the addition of PAC-1. (A) Initial morphology and location of cells after one hour treatment of PAC-1. Two target cells to be followed through the subsequent images are marked in number 1 and 2 in the image. (B, C and D) Cells appeared to shrink and round up and the cytoplasm appeared dense. (E) Cellular membrane appeared to show irregular buds known as blebs. (F) Cell 1 shows that the cytoplasmic vesicles called apoptotic bodies have broken apart from cell main body whilst cell 2 continued to show blebs on the cell membrane. (G and H) Both cell 1 and 2 burst and show a membranous structure connecting to a fraction of cell debris. Single slice images were taken in this experiment. The time of observation is indicated in the bottom left corner of each image. A magnification bar of 25 μm is present in the bottom right corner of each image.

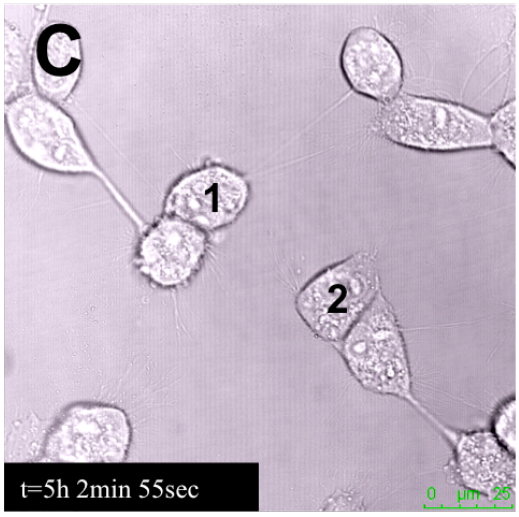
C
1
2
t=5h 2min 55sec
0 µm 25

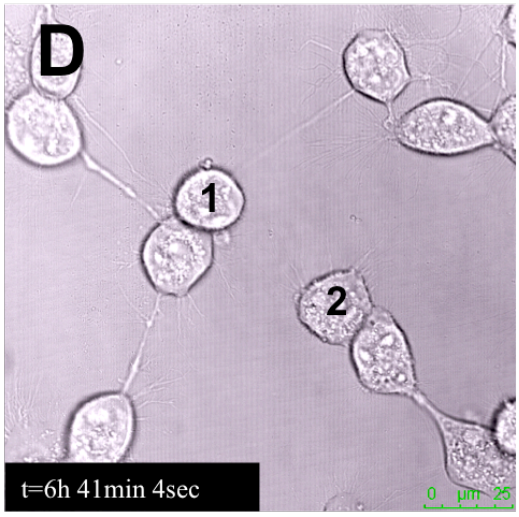
D
1
2
t=6h 41min 4sec
0 µm 25

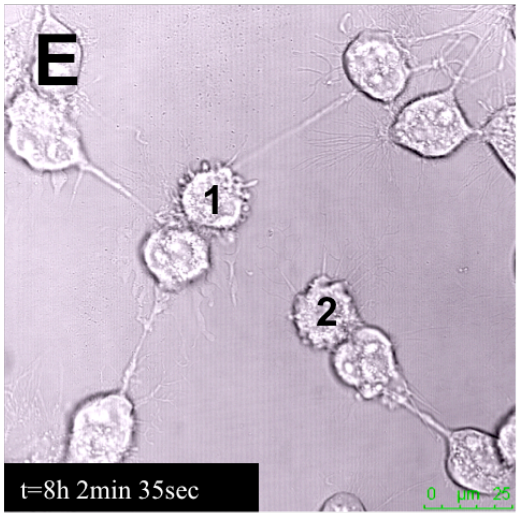
E
1
2
t=8h 2min 35sec
0 µm 25

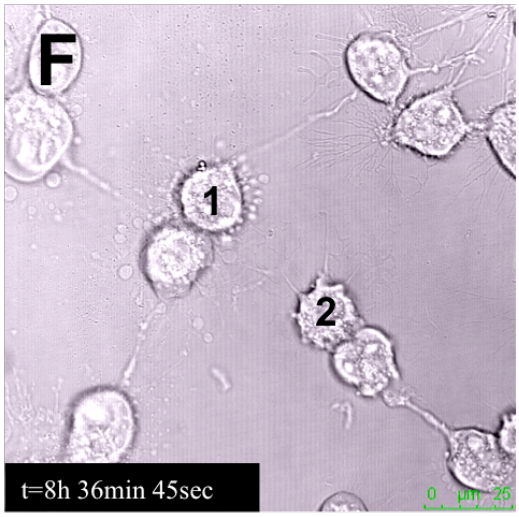
F
1
2
t=8h 36min 45sec
0 µm 25


G
1
2
t=9h 2min 5sec
0 µm 25

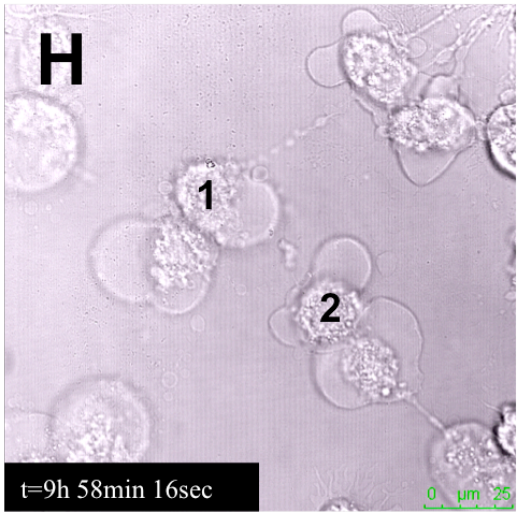
H
1
2
t=9h 58min 16sec
0 µm 25

4.3 Conclusions

The aim of the experiments described in this chapter was to capture a real-time record of the changes in cell morphology seen when NSP4 was expressed in isolation and how such changes relate to those seen for virus-infected cells. Real-time monitoring of BSC-1 cells expressing an NSP4-GFP fusion protein confirmed the capacity of NSP4 to change cell morphology after 24 hours of expression. However observations at earlier times after the start of expression were not possible because of the weak GFP signal which meant that it could not be clearly differentiated from background fluorescence. The relevance of the changes in cellular morphology seen in cells expressing NSP4 in isolation to those seen in rotavirus-infected cells was examined using a combination of real-time fluorescent and transmission confocal microscopy to allow capture of the dynamic changes seen in cell morphology. Fluorescence based confocal microscopy showed that virus-infected cells shrank, rounded up and interestingly generated cytoplasmic extrusions not dissimilar to those seen at early expression times in cells transfected with NSP4 expression plasmid. These cytoplasmic extrusions, that reached several diameters of cell in length, appeared at 14 hpi in the late period of viral infection and disappeared after approximately 1 hour. Subsequent observation using transmission confocal microscopy and a resonant scanner revealed the dynamic growth of the cytoplasmic extrusion in detail and showed their speed of growth was 2 μm/min.

The cytoplasmic extrusions seen in virus-infected cells were novel and to investigate the possibility that they were not linked specifically to rotavirus infection, controls including only uninfected cells, reovirus-infected cells and PAC-1 treated cells were all monitored using real-time transmission confocal microscopy. None of these controls showed any evidence of similar types of cytoplasmic extrusion to those seen

in rotavirus-infected and NSP4 expressing transfected cells. Taken together these observations confirmed the changes in cell morphology seen in the earlier experiments on fixed cells and revealed a novel phenomenon of changes in cell morphology in rotavirus-infected cells. In viral infection the appearance of such cytoplasmic extrusions was delayed until 14 hpi whereas they were seen at 7.5 hours post transfection in cells transfected with glyco+ NSP4 construct and infected with MVA-T7. This suggests the possibility that other viral proteins might regulate the function of NSP4 to delay timing in NSP4 induced cytoplasmic extrusion that provided sufficient time for virus replication.

Chapter 5

Functional Investigation of Virus Stimulated Cytoplasmic Extrusions

5.1 Introduction

Study of the changes in cell morphology induced by rotavirus infection showed that cells produced cytoplasmic extrusions at late times in the virus replication cycle that usually finishes within 16 hours with gradual cell lysis form 10 hpi in BSC-1 cells. The next objective was to investigate the potential functions of these cytoplasmic extrusions. Building on the initial observations it was hypothesized that they may be responsible for disseminating NSP4 to bystander uninfected cells where the protein could exhibit its cyto-toxicity. To test this hypothesis green and red Cell Tracker dyes were employed. The purpose of using Cell Trackers was to allow separate staining of virus-infected and uninfected cells in mixed populations, thereby allowing them to be discriminated from each other. The hope was that by observing such mixed and separately tagged populations the transfer of cellular material from infected to uninfected cells could be monitored. Cell Tracker dyes are non-fluorescent probes prior to entering cells, which when added to the culture medium are able to pass freely through the cell membrane. However once inside the cell they react with intracellular thiols and transform into fluorescent and cell-impermeable reaction products. Consequently they will not transfer to adjacent cells in a culture even if released by cell lysis.

5.2 Results

5.2.1 Spread of NSP4 Cytotoxicity Through Virus Induced Cytoplasmic Extrusions

To investigate possible transfer of cellular material between cells through rotavirus induced cytoplasmic extrusions, populations of BSC-1 cells were split into two populations and separately stained with green or red fluorescent Cell Tracker dyes. In control experiments it was found that the pattern of cell staining with these two dyes differed, with the green Cell Tracker staining the whole cytoplasm whereas staining with the red Cell Tracker was focused near the nuclei of cells (Fig 5.1). A fraction of each of the stained cell populations (i.e. either green or red) was then infected with the UKtc strain of bovine rotavirus at an MOI of 10. Virus-infected cells labeled with one Cell Tracker were then mixed with uninfected cells stained with the other Cell Tracker at a ratio of 2:5. Examination of these cell mixtures started at 14 hours post infection and in both cases cytoplasmic extrusions were seen (Fig 5.2 and 5.3). In the case of the mixture containing green infected and red uninfected cells, cytoplasmic extrusions protruding outward from green infected cells were clearly observed (Fig 5.2C, D and E). Direct contact of these extrusions with bystander cells was not seen in these real time experiments, but rather the cytoplasmic extrusions broke apart into small and mobile membranous vesicles (Fig 5.2F). However in the case of the mixture of red infected cells and green uninfected cells, the cytoplasmic extrusions from the red infected cells were seen to make direct contact with uninfected green cells (Fig 5.3A, B and C). In addition obvious red cytoplasmic material was seen in those green cells having direct contact but not in other bystander green cells indicative of a transfer of cytoplasmic material from an infected red cell into an uninfected green cell (Fig 5.3A, B and C). Extending the real

time observation of this mixture showed that the cytoplasmic extrusions also scattered into small vesicles (Fig 5.3D and E) in this case, one red vesicle from a virus-infected cell was clearly evident on the surface of an uninfected green cell (Fig 5.3F).

Figure 5.1: Cell Trackers staining of Mock infected BSC-1 cells.

BSC-1 cells were divided into separate wells of a culture dish and stained with either green or red Cell Tracker. After one hour of incubation cells were washed extensively, mixed, and incubated at 37 ºC for 24 hours. Subsequent observations were made using these live i.e. unfixed cells. (A) BSC-1 cells fluorescing in the green channel demonstrated that green Cell Tracker stained the whole cytoplasm of cells. (B) BSC-1 cells fluorescing in the red channel demonstrated that red Cell Tracker stained an area surrounding nuclei. (C) A merged image of panel A and B that showing that the Cell Trackers were distinguishable from each other. A magnification bar of 20 μm is present in the bottom right corner of each image.

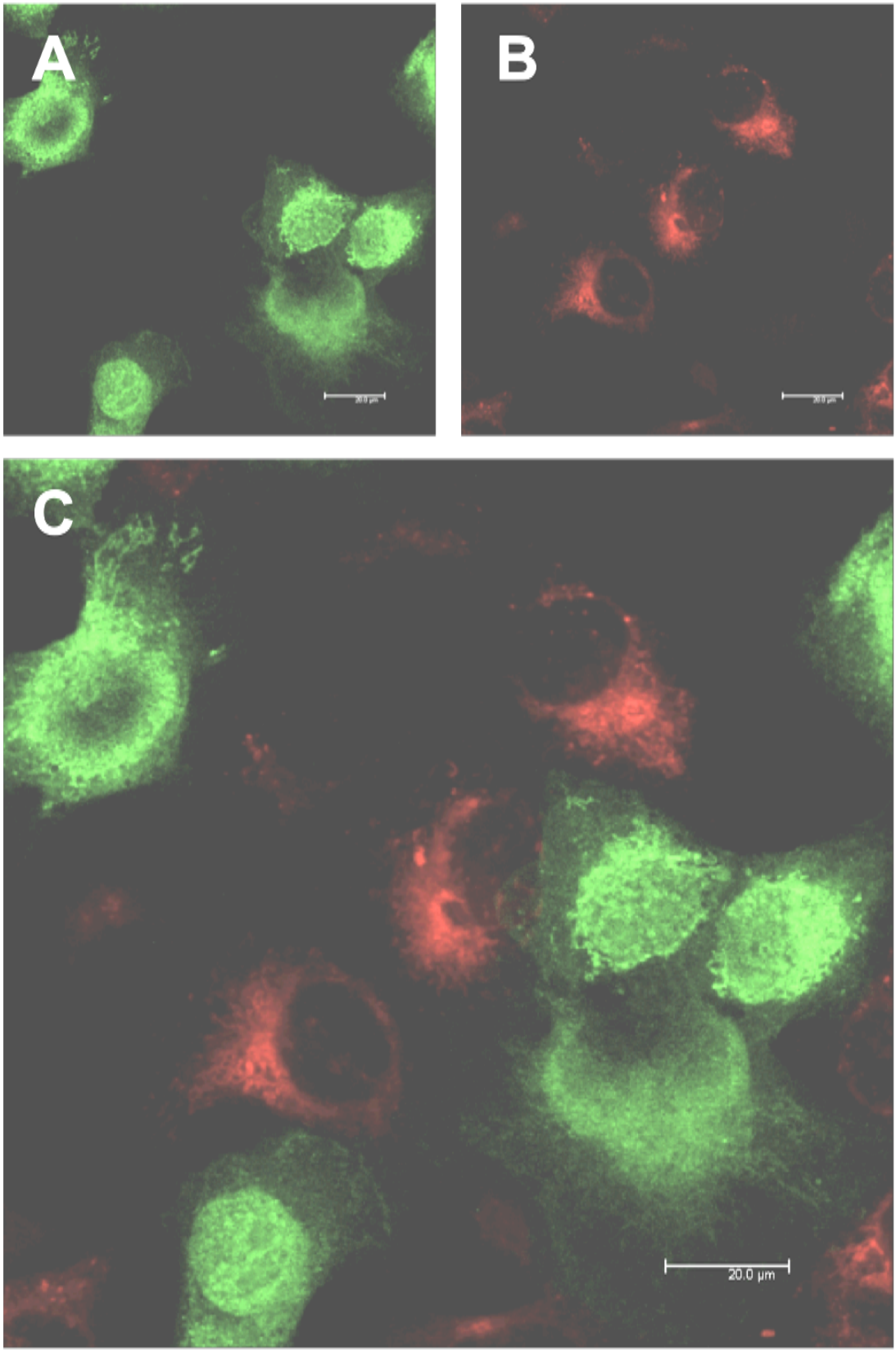
A
B
C
20.0 µm

Figure 5.2: Detection of cytoplasmic extrusions in cells stained with green Cell Tracker after virus infection.

BSC-1 cells were divided into separated wells of a culture dish and stained with either green or red Cell Tracker dye. The cell population stained with green Cell Tracker was then infected with bovine UKtc rotavirus at an MOI of 10. After 1-hour incubation the cell populations were washed extensively, mixed and cultured for 14-hour at 37 ºC before confocal microscopic examination was started. (A) Overview of mixed cells in fluorescent channel with a specific green virus-infected target cell marked with red square. (B) Overview of mixed cells in transmission light channel showing the same green target cell labeled with a red square. (C, D and E) After cytoplasmic extrusions had been detected in the target cell, observation at higher magnification revealed the dynamics of extrusion formation in real-time. (F) The cytoplasmic extrusions broke into small vesicles. Time of recording is showed in the bottom left of image B-F. Arrows indicate cytoplasmic extrusion and arrowhead indicates a scattered vesicle. Fluorescent image and transmission record were taken a single step scan image by scan crossing the middle of cells. A magnification bar of 10 μm is present in the bottom right corner of each image.

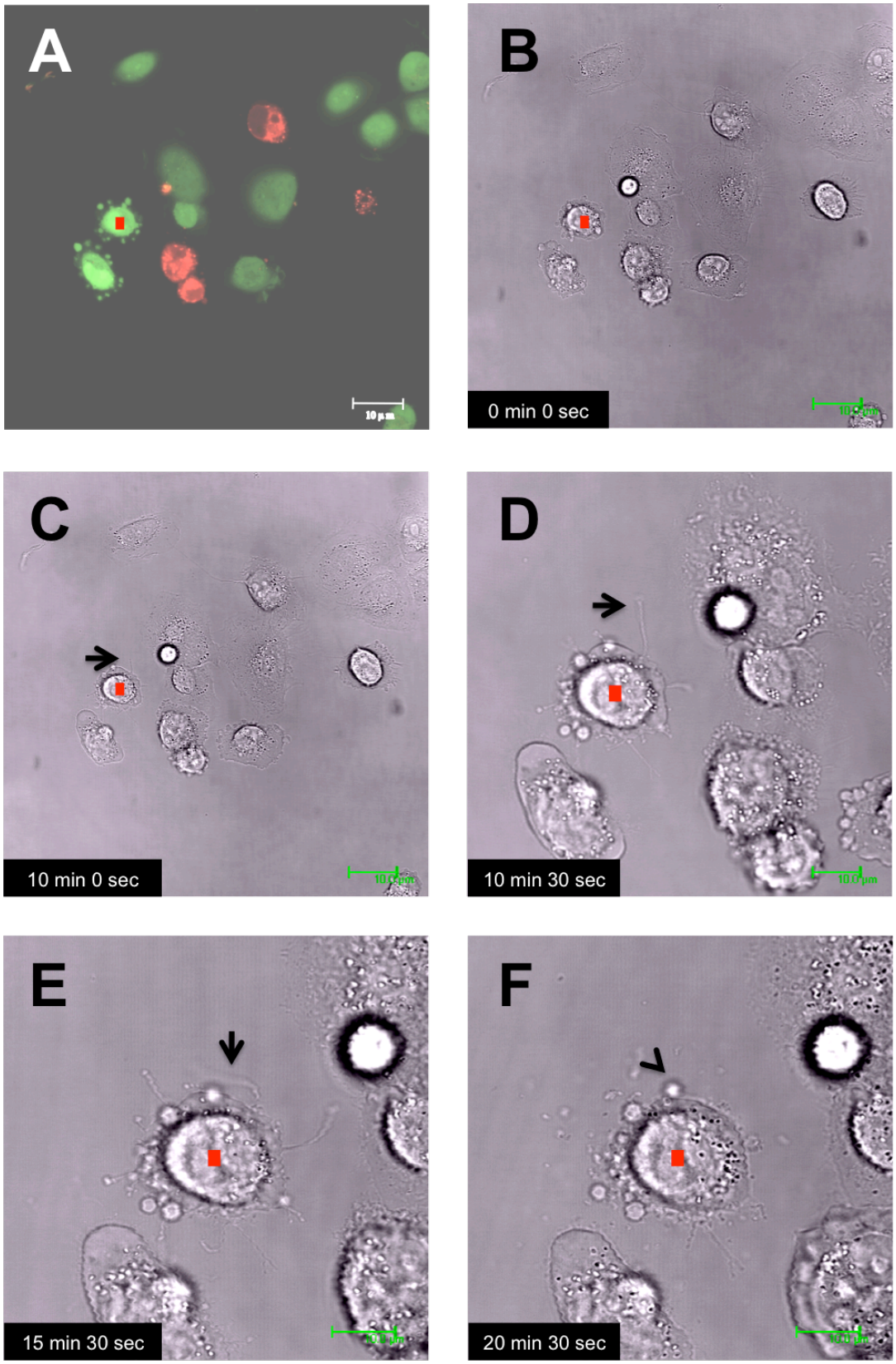
A
B
0 min 0 sec
C
10 min 0 sec
D
10 min 30 sec
E
15 min 30 sec
F
20 min 30 sec

Figure 5.3: Observation of cytoplasmic extrusion in red Cell Tracker staining cell after viral infection.

BSC-1 cells were divided into separate wells and stained with either green or red Cell Tracker. Cells stained with red Cell Tracker cells were also infected with bovine UKtc rotavirus at an MOI of 10. Following one hour of incubation at 37 ºC cells were washed extensively, mixed, and cultured for a further 14-hour at 37 ºC before real time confocal microscopy was started. (A) Overview of mixed cells in fluorescent channel showing a red infected cell (marked by green square) already showing cytoplasmic extrusions, one of which has established contact with a green uninfected cell (surrounded by red circle). (B) Overview of mixed cells showing only red fluorescence with red Cell Tracker present in the green target cell (red circle) indicating transfer of material from the red cell (green square) to the green cell (red circle). For comparison there was no detectable red Cell Tracker present in two other nearby uninfected green cells (surrounded by white circles in panel A and B). (C) Overview of mixed cells using transmission light microscopy indicating the position of the target cells highlighted in A and B. (D and E) Real time observation revealed that the cytoplasmic extrusion making contact with the green cell (red circle) broke apart and also that other cytoplasmic extrusions broke into small vesicles. (F) Fluorescent detection using stacked images to show a physical contact between a red vesicle and the cytoplasmic membrane surface of the green cell and its intracellular red Cell Tracker at the end of recording. Time of recording is in the bottom left of image C-E. Green square indicates the red target cell having cytoplasmic extrusion. Arrow indicates cytoplasmic extrusion and arrowhead indicates a scattered vesicle. Fluorescent images (A-E) were taken a single step scan crossing the middle of cells. A magnification bar of 10 μm in image A-E and 5 μm in image F is indicated in the bottom right corner.

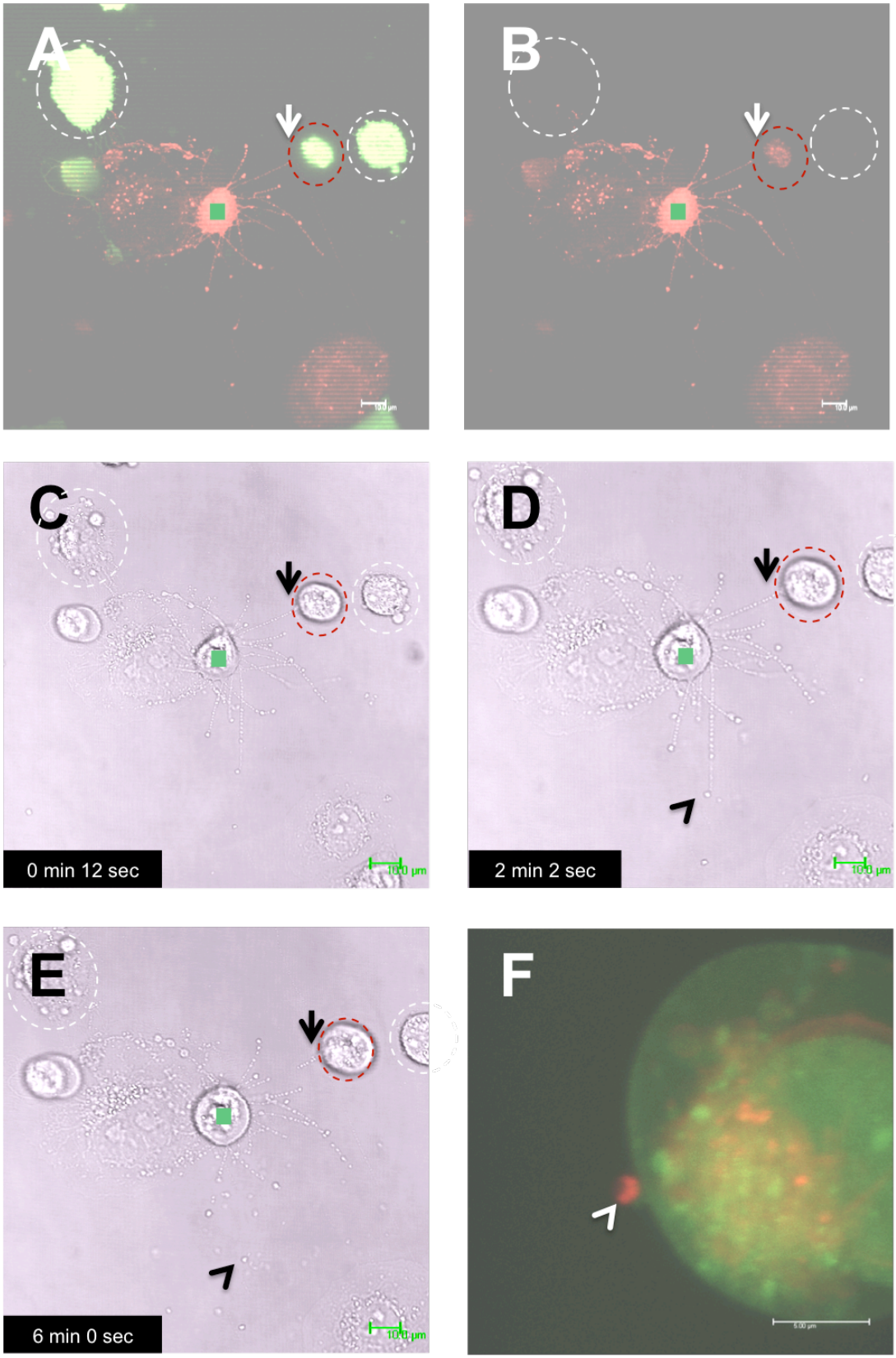
A
B
C
0 min 12 sec
D
2 min 2 sec
E
6 min 0 sec
F

Further detailed examination of scattered small vesicles generated by infected cell populations carried out at 16 hours post infection revealed in the case of green virus-infected and red uninfected cell mixtures the presence of scattered green vesicular structures surrounding red cells (Fig 5.4). Internalization of such vesicles was however much more clearly seen on mixing virus-infected red cells with uninfected green cells (Fig 5.5).

The observation of fluorescent Cell Tracker transferred from infected cells to uninfected cells implied that NSP4 had also been transferred. To investigate this more definitively infected BSC-1 cells with no staining were mixed with green-staining virus non-permissive cells (BSR-T7). The use of BSR-T7 cells as recipient was to mimic the non-permissive cells below the top of the villi *in vivo* to acquire NSP4 transferred from virus infected cells at the tip of the villi. Subsequent staining with NSP4 antibody revealed the dissemination of NSP4-containing structures from infected BSC-1 cells on the cytoplasmic membrane surface of green BSR-T7 cells at 16 hours post infection (Fig 5.6). Attempts to address whether the scattered NSP4 had entered green BSR-T7 cells were not conclusive. This was because simple interpretation of the experiment was confounded by the observation that the exposure of BSR-T7 cells to high titre rotavirus resulted in a few cells in the population becoming infected. Thus on staining cells using specific antibody against NSP4 it was not possible to definitely distinguish between internalized NSP4 and the NSP4 that may have been expressed in the cells following their infection by exogenous virus released from the virus-infected cells. However our observations support a new model for the spread of NSP4 cytotoxicity through virus induced cytoplasmic extrusions to produce membranous vesicles that deliver NSP4 from virus-infected cells to surrounding uninfected cells.

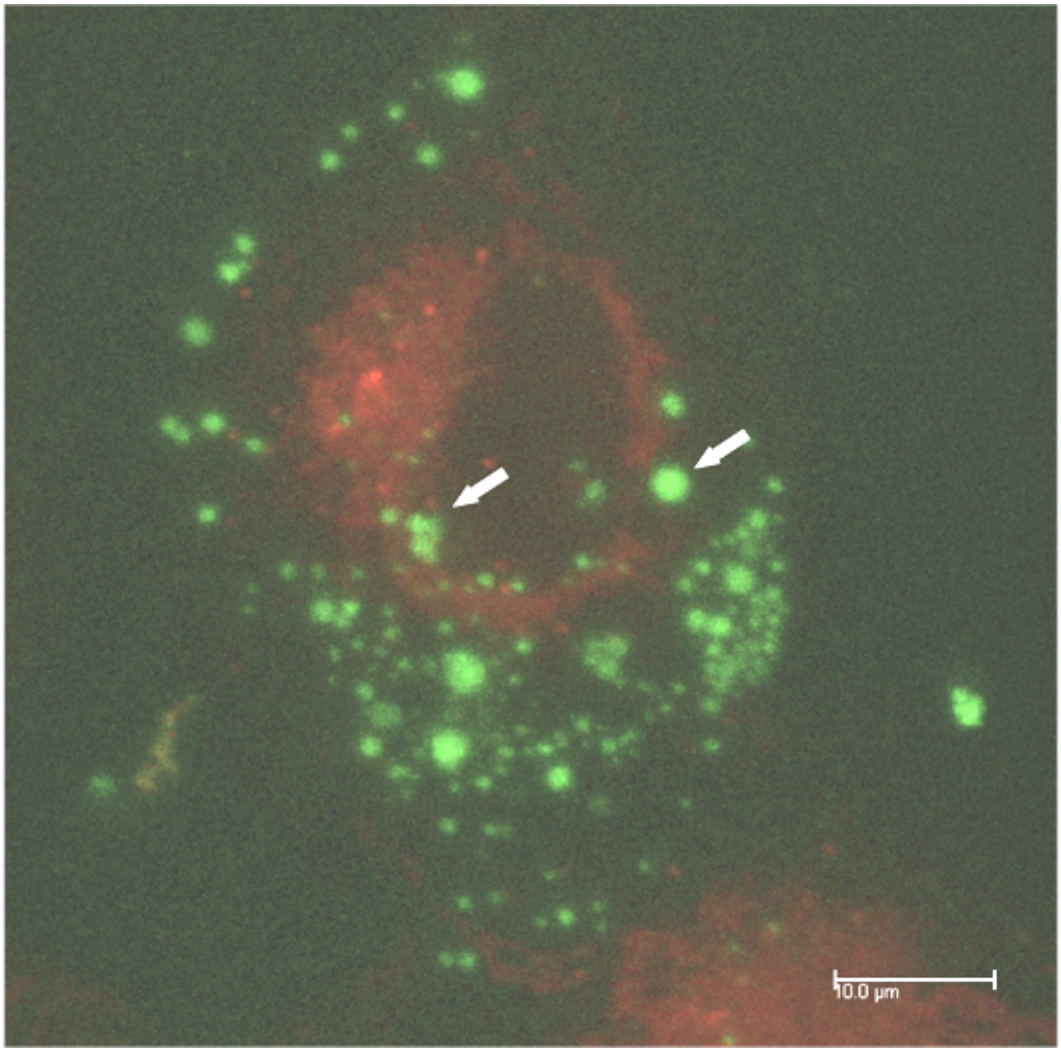

Figure 5.4: Dissemination of material from virus-infected cell to uninfected cell.

BSC-1 cells were divided into separated wells of a culture dish and stained with either green or red Cell Tracker dye. The cell population stained with green Cell Tracker was then infected with bovine UKtc rotavirus at an MOI of 10. After 1-hour incubation the cell populations were washed extensively, mixed and cultured for 14-hour at 37 ºC before confocal microscopic examination was started. The image shows a uninfected cell stained with red fluorescent Cell Tracker acting as recipient of vesicular structures from virus-infected cell stained with green Cell Tracker. Arrows indicate vesicular structures from the green virus-infected cell. A magnification bar of 10 µm is present in the bottom right corner.

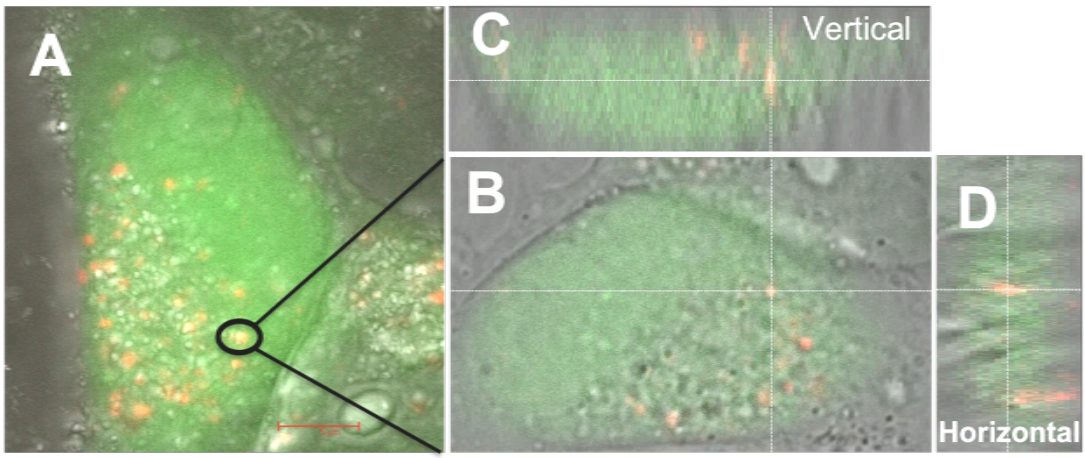

Figure 5.5: Internalization of material from a virus-infected cell to a uninfected cell.

BSC-1 cells were divided into separate wells and stained with either green or red Cell Tracker. Cells stained with red Cell Tracker cells were also infected with bovine UKtc rotavirus at an MOI of 10. Following one hour of incubation at 37 ºC cells were washed extensively, mixed, and cultured for a further 14-hour at 37 ºC before real time confocal microscopy was started. Panel A shows already internalized vesicular structures from a infected red cell into an uninfected cell marked with green Cell Tracker. Panel B shows intracellular location of a vesicular structure with vertical view (panel C) on its top and horizontal view (panel D) on its right. Panels B, C and D are single slice images crossing the cell. A magnification bar of 5 μm is present in the bottom right corner of panel A.

Figure 5.6: Dissemination of NSP4 from virus-infected cell to uninfected cell.

BSC-1 cells, infected with bovine UKtc rotavirus at an MOI of 10 for 1 hour, were mixed with BSR-T7 cell stained with green Cell Tracker. Following 16 hours of incubation at 37 ºC cells were fixed, stained with polyclonal rabbit antisera raised against bacterially expressed NSP4 (McCrae and McCorquodale, 1987) followed by Alexa-594-conjugated goat-anti-rabbit secondary antibody (red staining) as described in Materials and Methods. (A) A max projection of z-stack image shows that NSP4-containing vesicular structures were disseminated from infected non-fluorescent BSC-1 cells on the surface of a group of green Cell Tracker stained BSR-T7 cells. (B-D) Single slice images crossing the cells from top (B) to bottom (D) show that the NSP4-containing vesicular structures are closely associated with the cytoplasmic membrane of a group of green Cell Tracker stained BSR-T7 cells. Arrows indicate NSP4 containing vesicular structures. A magnification bar of 10 μm is present in the bottom right corner of each image.

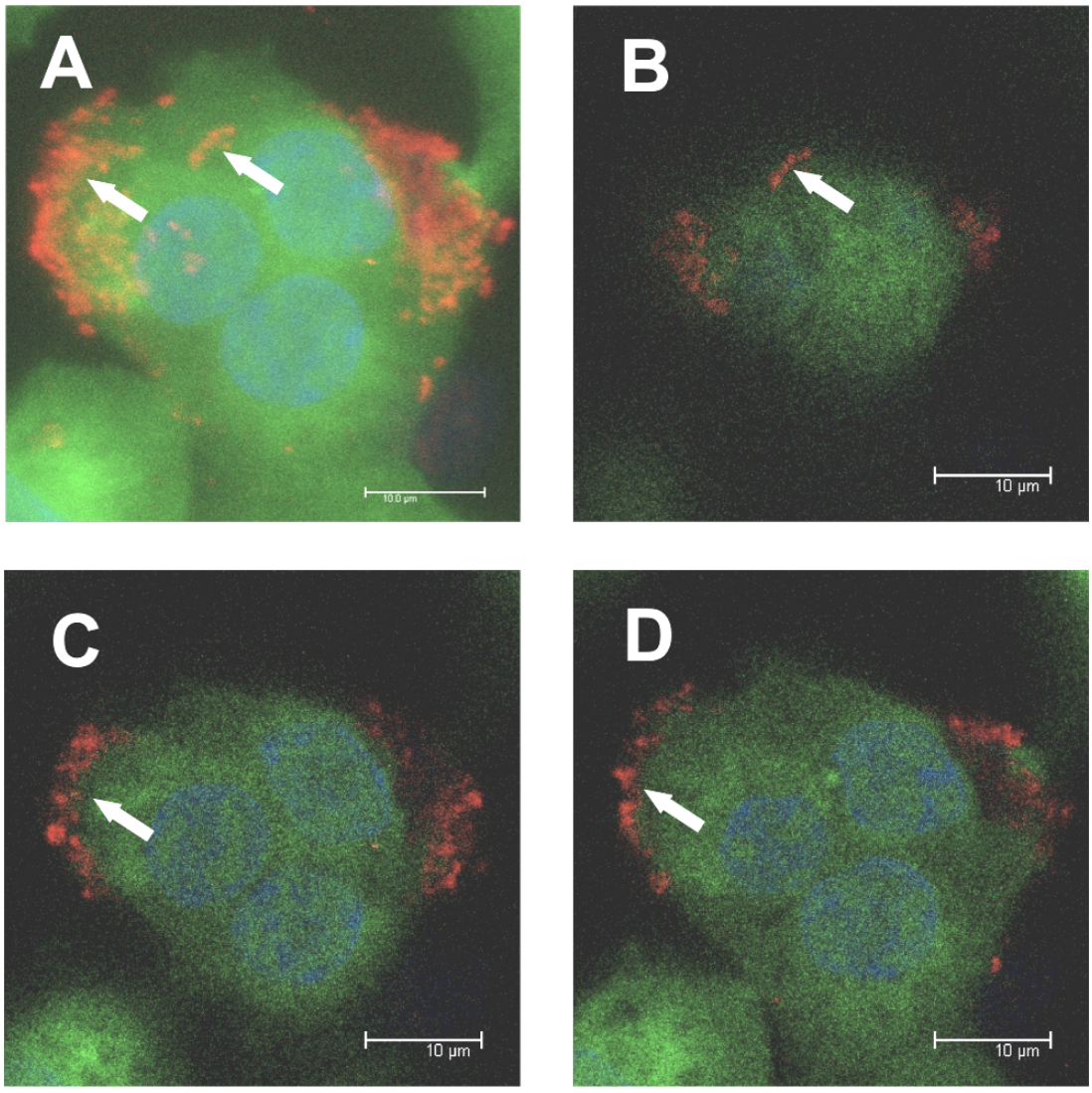
A
10.0 µm
B
10 µm
C
10 µm
D
10 µm

5.3 Conclusions

The aim of the experiments described in this chapter was to study the potential function of the cytoplasmic extrusions seen in virus-infected cells. Through the use of impermeable Cell Tracker dyes for imaging of virus-infected cells such cytoplasmic extrusions were seen to scatter into small vesicles that disseminated onto the surface of and were internalized into bystander cells. Subsequent detection of NSP4 containing vesicular structures on the plasma membrane of BSR-T7 cells implied that NSP4 could also be disseminated in a similar manner. These observations allow a new hypothesis to be proposed covering the mechanism by which rotavirus might spread its cytotoxicity through a population of cells. It is proposed that this involves cytoplasmic extrusions mediating a direct cell-to-cell transfer of cytoplasm from virus-infected cells to these surrounding uninfected cells thereby delivering sufficient cyto-toxin (NSP4) to surrounding cells to kill them over a large area. The advantage of this hypothesis compared to that involving NSP4 being secreted from infected cells might be that NSP4 could still anchor on membrane derived from the ER to exercise its paracrine-like secretion. This provides an explanation of how an ER resident protein such as NSP4 can be transported to cellular environments other than those in which it was synthesized.

Taken together the observations in this chapter support the hypothesis that dissemination of NSP4 from infected cells to bystander cells is possible through membranous vesicles released from virus induced cytoplasmic extrusions.

The changes in cell morphology seen in these experiments imply that the cyto-skeleton has undergone radical reorganization in cells expressing NSP4 or infected with virus. Therefore analysis of the cyto-skeletal network was undertaken to achieve a better understanding of the processes underpinning the formation of

cytoplasmic extrusions.

Chapter 6

Analysis of Cytoskeletal changes in Transfected Cells Expressing NSP4 or Cells Infected with Rotavirus

6.1 Introduction

Eukaryotic cells have a cytoplasmic skeleton composed of actin filaments, intermediate filaments and microtubules to maintain their cell morphology and support special structures such as flagella, cilia and lamellipodia. The alterations seen in the cytoplasmic morphology of either NSP4 expressing or rotavirus-infected cells implied that the cyto-skeleton of such cells had been affected. Calcium dependent rearrangement of the actin network leading to generation of cellular projections has been reported following NSP4 expression in both HEK 293T cells (human embryonic kidney cell line) and MA104 cells (rhesus monkey kidney cell line) (Berkova *et al*., 2007). Virus infection of MA104 cells has also been reported as leading to modification of actin filaments (Berkova *et al*., 2007). Furthermore in infected polarized Caco-2 cells (human colorectal carcinoma cell line) both actin and microtubules were changed in a calcium dependent manner (Brunet *et al*., 2000a; Brunet *et al*., 2000b). By contrast a disorganization of vimentin, a member of the intermediate filament family of proteins, has only been detected in undifferentiated (i.e. non-polarized) Caco-2 cells and CV-1 cells (cercopithecusaethiops monkey kidney cell line) (Brunet *et al*., 2000a; Brunet *et al*., 2000b; Weclewicz *et al*., 1994). These observations on cyto-skeleton albeit done primarily in cell lines other than those employed in this study give further support to the hypothesis that disorganization of the cyto-skeleton contributed to the cytoplasmic extrusions seen in NSP4 expressing or virus-infected BSC-1 cells used in the present study. The effect of NSP4 expression on actin filaments has already been investigated (Berkova *et al*., 2007). Therefore in this study the analysis focused on cellular microtubules and the effects of glycosylation of expressed NSP4 and virus infection of BSC-1 cells on these components and more generally the cytoskeleton using confocal microscopy.

6.2 Results

6.2.1 Microtubule Disruption and Re-assembly in BSC-1 Cells Expressing Glyco+ or Glyco- NSP4

The alteration of cellular morphology seen earlier in this study in cells expressing glyco+ NSP4 indicated that NSP4 was potentially capable of changing the cellular skeletal network. Changes in F-actin have been studied and proposed to be linked to changes in intracellular calcium concentration and cofilin-1 (Berkova *et al*., 2007). However the effects of NSP4 expression on the microtubule network have not been studied previously. To avoid any side effects from the infection of cells with the use of MVA-T7 to drive NSP4 expression, both glyco+ and glyco- NSP4 cDNAs were cloned into the pcDNA3.1 cloning vector that employs the immediate early promoter of cytomegalovirus (CMV) to drive protein expression. To study the effect of NSP4 expression on microtubules, BSC-1 cells were separately transfected with the two plasmids and cells were fixed and stained with NSP4 and β-tubulin antibodies at 24-h and 48-h post transfection. Confocal microscopy showed that expression of both glyco+ and glyco- NSP4 leads to the disassembly of microtubules at 24-h post transfection (Fig 6.1A and B). This disassembly appeared to initiate primarily from the centre of the cell. Interestingly prior to complete destruction of the microtubular network, a reforming of microtubules was evident at the periphery of cells independent of the centrosome (Fig 6.1C and D). In this experiment even though different expression levels of NSP4 were observed in cells at different stages of the microtubular disassembly (Fig 6.1B and C). It was impracticable to interpret from fixed sample that cell-cell transfer of NSP4 resulted in the difference of NSP4 expression levels. At 48-h post transfection a greater proportion of cells expressing NSP4 showed complete disruption of the microtubule network compared to that seen

at 24-h post transfection (data not shown).

Figure 6.1: Examination of the microtubule network after glyco+ and glyco- NSP4 expression in BSC-1 cells.

NSP4 was stained with polyclonal rabbit antisera against NSP4 followed by Alexa-594-conjugated goat-anti-rabbit antibody as described in Materials and Methods. Microtubules were stained by polyclonal mouse anti-β-tubulin antibody followed by Alexa-488-conjugated goat-anti-mouse antibody as described in Materials and Methods, finally nuclei were stained with DAPI as described in Materials and Methods. (A and B) Microtubules were completely destroyed in cells expressing either glyco+ or glyco- NSP4 but remained intact in other bystander cells indicated by arrow. (C and D) Prior to complete destruction of the microtubule network in cells expressing either glyco+ or glyco- NSP4 disassembly of the microtubule started from centre of the cytoplasm and re-polymerization of the microtubules appeared to form a ring structure at the cell periphery. NSP4 stained in red and β-tubulin stained in green.

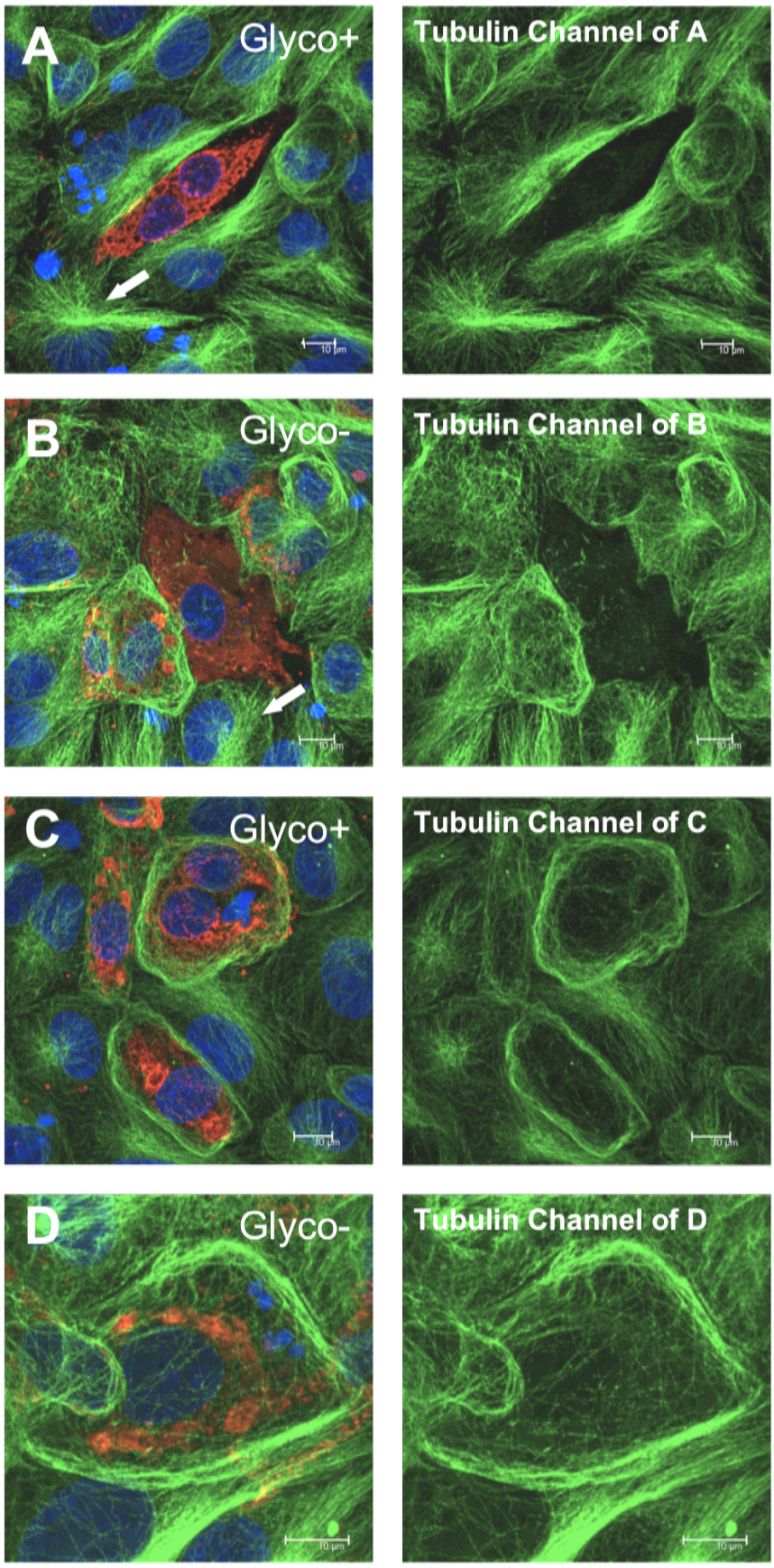
A
Glyco+
Tubulin Channel of A
B
Glyco-
Tubulin Channel of B
C
Glyco+
Tubulin Channel of C
D
Glyco-
Tubulin Channel of D

The NSP4 mediated destructive effect on the microtubule network was studied further by examining the effect of manipulating intracellular calcium concentrations and also the functionality of the centrosome. The reason to investigate the effect of intracellular calcium levels was that actin breakdown in NSP4 expressing cells and both actin and microtubule network damage in virus-infected cells have been reported to be dependent on intracellular calcium levels (Berkova *et al*., 2007; Brunet *et al*., 2000a; Brunet *et al*., 2000b). To investigate whether elevation of intracellular calcium was a factor contributing to the NSP4 driven breakdown of the microtubule network in our study EGTA and BAPTA/AM, both calcium chelator, were added together to the culture medium of transfected BSC-1 cells. Confocal microscopy showed that treatment with both compounds did not prevent the destruction of the microtubule network in NSP4 expressing cells at 24-hour post transfection suggesting that NSP4 driven elevation of intracellular calcium was not involved in the microtubule disassembly (Fig 6.2).

In healthy mammalian cells the microtubule network grows from a cellular organelle localized near the nucleus called the centrosome. However following NSP4 expression polymerization of microtubules at the periphery of cell occurred and this appeared to lack a starting centre. This implied that some functionality of the centrosome had been disrupted by NSP4 expression. To further investigate the possible role of centrosomal functionality nocodazole that prevents microtubule re-polymerization by binding to free tubulin subunits was added to BSC-1 cells expressing either glyco+ or glyco- NSP4 at 24 or 48 hours post transfection. Subsequent removal of medium containing nocodazole and washing of the cells allowed centrosome dependent reformation of the microtubule network in untransfected cells within 10 mins but not in transfected cells expressing NSP4. In

this latter case the microtubule network re-polymerized independently of the centrosome and again distributed in a ring surrounding the centre of the cell (Fig 6.3). This suggested that NSP4 expression resulted in either inhibition of the centrosome functioning as a microtubule polymerization centre or microtubular de-polymerization was occurring faster than its polymerization from the centrosome in the centre of cells. It also suggested that expression of NSP4 caused microtubule polymerization in a centrosome-independent manner at the cell periphery.

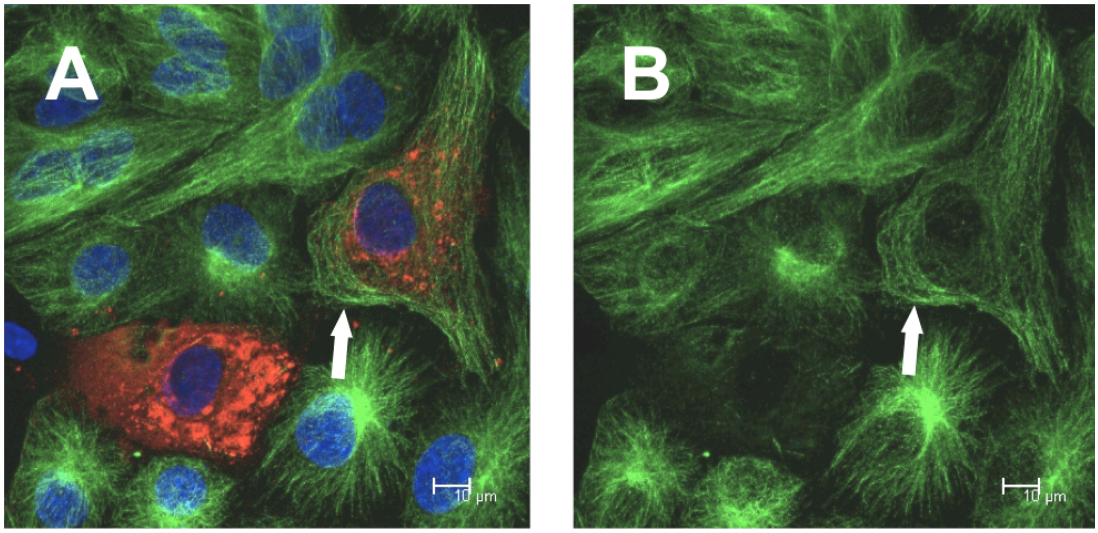

Figure 6.2: The microtubule network in cells expressing glyco+ NSP4 after treatment of EGTA and BAPTA/AM.

BSC-1 cells were transfected with a glyco+ NSP4 construct for 4 hours and subsequently incubated with culture medium containing EGTA (3mM) and BAPTA/AM (75 µM) for 24 hours prior to fixation. NSP4 was stained with polyclonal rabbit antisera against NSP4 followed by Alexa-594-conjugated goat-anti-rabbit antibody (red staining) as described in Materials and Methods. Microtubules were stained by polyclonal mouse anti-β-tubulin antibody followed by Alexa-488-conjugated goat-anti-mouse antibody (green staining) as described in Materials and Methods, finally nuclei were stained with DAPI as described in Materials and Methods. (A and B) EGTA and BAPTA/AM treatment did not prevent disassembly of the microtubule and re-polymerization of the microtubule at the periphery of the cell expressing NSP4. Arrows indicate the re-polymerized microtubule at the periphery of a NSP4 expressing cell. A magnification bar of 10 µm is present in the bottom right corner of each image.

Figure 6.3: Recovery of microtubules in a glyco+ NSP4 expressing BSC-1 cells after treatment of nocodazole.

BSC-1 cells were transfected with a glyco+ NSP4 construct for as described in Materials and Methods. 24 hours after transfection cells were treated for one hour with nocodazole (15 mg/ml final concentration). Following washes (5X) to remove the nocodazole and 10 mins incubation in nocodazole free medium to allow polymerization of microtubules, cells were fixed, stained and examined by confocal immunofluorescent microscopy. NSP4 was stained with polyclonal rabbit antisera against NSP4 followed by Alexa-594-conjugated goat-anti-rabbit antibody. Microtubules were stained by polyclonal mouse anti-β-tubulin antibody followed by Alexa-488-conjugated goat-anti-mouse antibody; finally nuclei were stained with DAPI all as described in Materials and Methods. (A) Recovery of microtubule polymerization appeared to occur independent of centrosome and form ring-like structure in the cytoplasm in a NSP4 expressing cell. (B) Green fluorescent channel showing the ring-like structure of microtubule formed in the NSP4 expressing cell, by contrast a cell indicated by arrow shows normal microtubular network recovery with a microtubules oriented centre. (C) Red fluorescent channel shows expression of NSP4 in the cell with re-arranged microtubules in ring-structure. (D) Control image showing disassembly of the microtubule caused by treatment of Nocodazole prior to washing out the drug. A magnification bar of 10 μm is indicated in the bottom right of each image.

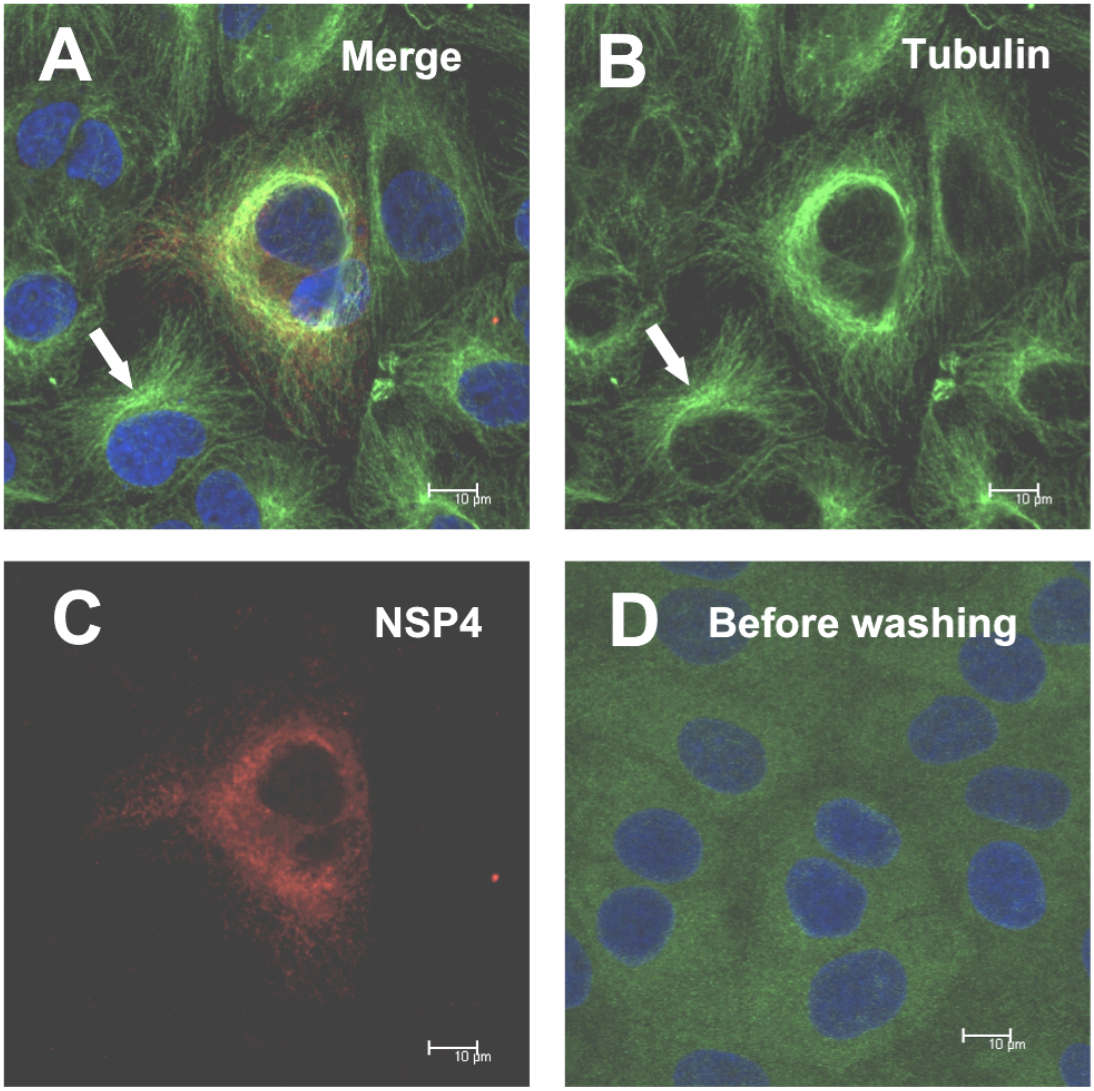
A
Merge
B
Tubulin
C
NSP4
D
Before washing
10 μm

6.2.2 NSP4 Expression Did Not Induce Apoptosis And Necrosis

The pattern of destruction of the microtubule network starting with disassembly from the centre of the cytoplasm and re-polymerization at the periphery of the cell has been proposed as one of the cellular defense mechanisms seen in apoptotic cells (Moss *et al*., 2009; Sanchez-Alcazar *et al*., 2007). Furthermore induction of Bax dependent apoptosis through the mitochondrial pathway has been reported to occur following rotavirus infection (Martin-Latil, Mousson *et al*. 2007). This lead us to investigate whether an NSP4 induced pro-apoptotic signaling might be responsible for the pattern of changes seen in the microtubules in transfected cells. To do this expression plasmids carrying either glyco+ or glyco- NSP4 were transfected into HEK 293T cells. Subsequent FACS (fluorescence activated cell sorting) analysis of NSP4 expressing cells using an apoptotic cell staining kit (Apo-TRACE) at 24 and 48 hours post transfection did not appear to show any apparent induction of either apoptosis or necrosis when compared with controls transfected with the empty pcDNA3.1 plasmid used for the NSP4 constructions. By contrast treatment of cells with PAC-1, a recognized apoptosis inducer, showed a significant induction of both apoptosis and necrosis (Fig 6.4).

Figure 6.4: Induction of apoptosis in PAC-1 treated but not in glyco+ and glyco- NSP4 expressing 293T cells.

293T cells were transfected with the indicated plasmid or treated with medium containing PAC-1 at a final concentration of 5 μM. Cells were stained using Apo-Trace and analysed by FACS (as described in Materials and Methods) at 24 and 48 hours post transfection or treatment. Cell only: Cells without treatment showing their apoptotic status after culture for the indicated times. pcDNA3.1: Cells transfected with pcDNA3.1 cloning vector used in constructing both glyco+ and glyco- NSP4 expression plasmids. Glyco+: Cells transfected with glyco+ NSP4 construct. Glyco-: Cells transfected with glyco- NSP4 construct. PAC-1: Cells treated with PAC-1 at the start of the experiment.

Examination of apoptosis and necrosis at 24 hours in A and 48 hours in B after transfection or chemical treatment. Significant induction of apoptosis and necrosis only seen in cells treated with PAC-1 but not in cells transfected with either glyco+ or glyco- NSP4. A total number of 20,000 cells were analysed in each sample. Transfection controls were included in this experiment: 1. Cells were transfected with pEGFP-N1 and examined at 24 hours post transfection using UV-light microscopy to confirm transfection efficiency above 70% by looking at GFP fluorescence on the cell monolayer. 2. Cells were transfected with either glyco+ or glyco- NSP4 construct, fixed and stained with anti-NSP4 sera at 24 hours post transfection. Specific antibody staining against NSP4 in these cells confirmed positive expression of NSP4 in more than 70% of the cell population.

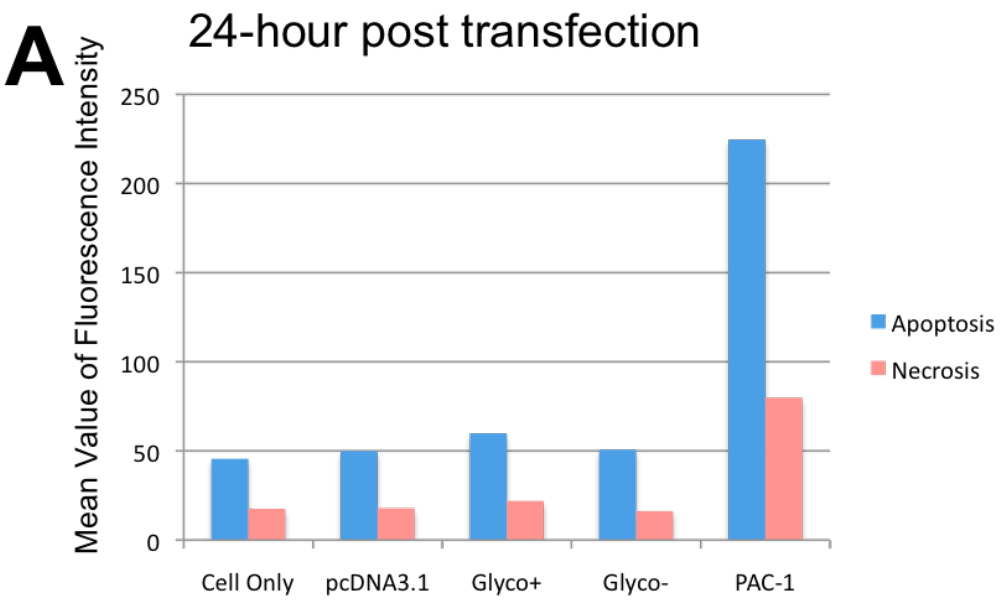
A
24-hour post transfection
Mean Value of Fluorescence Intensity
250
200
150
100
50
0
Cell Only
pcDNA3.1
Glyco+
Glyco-
PAC-1
Apoptosis
Necrosis

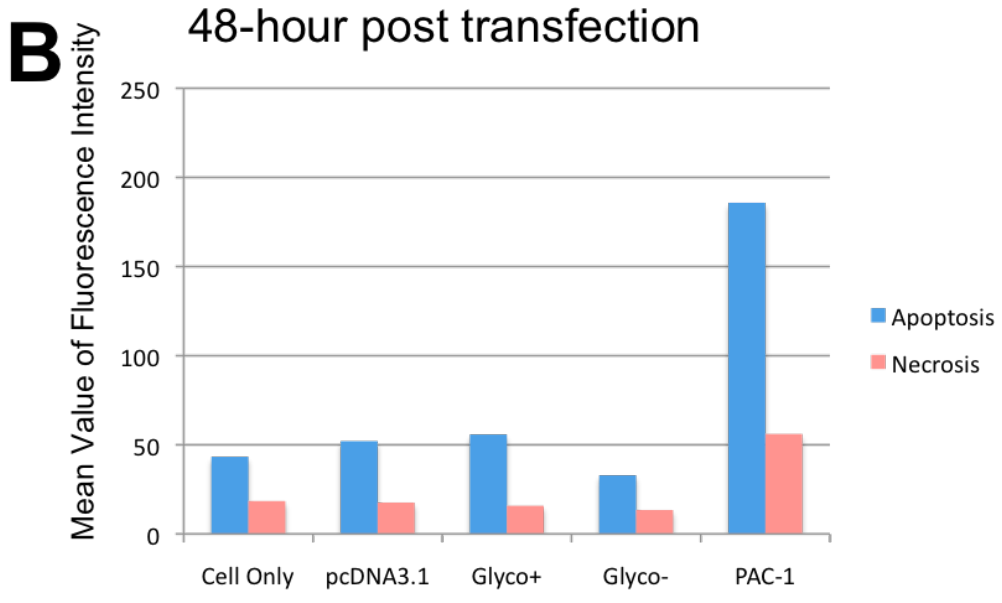
B
48-hour post transfection
Mean Value of Fluorescence Intensity
250
200
150
100
50
0
Cell Only
pcDNA3.1
Glyco+
Glyco-
PAC-1
Apoptosis
Necrosis

6.2.3 Disruption of The Microtubular Network In Virus-Infected Cells

Expression of NSP4 in isolation led to the disassembly of the microtubular network in transfected cells and re-polymerization of microtubules into a ring-like structure at the periphery of the cells apparently independent of centrosome function. To examine whether these changes in the microtubular network also occurred during viral infection, BSC-1 cells were infected with rotavirus and fixed and stained for NSP4 and β-tubulin at 15 hpi. Confocal microscopy showed virus replication in cells also resulted in complete destruction of the microtubular network (Fig 6.5). Notably in some virus-infected cells re-polymerization of microtubules into a ring-like structure at the cell periphery (Fig 6.5) similar to that seen in cells expressing only NSP4 was also observed. This similarity of microtubular modification between cells transfected with NSP4 and those infected with virus suggested that the viral NSP4 protein might also function to disrupt microtubular network following viral infection.

Figure 6.5: Destruction of microtubular network in virus infected BSC-1 cells.

BSC-1 cells were infected with rotavirus at an MOI of 1 and fixed using paraformaldehyde at 15 hpi as described in Materials and Methods. NSP4 was stained with a polyclonal rabbit antisera against NSP4 followed by Alexa-594-conjugated goat-anti-rabbit antibody, microtubules were stained by a polyclonal mouse anti-β-tubulin antibody followed by Alexa-488-conjugated goat-anti-mouse antibody, finally nuclei were stained with DAPI all as described in Materials and Methods. (A) Green fluorescent channel showing the microtubular network of a cell monolayer infected with virus. (B) Red fluorescent channel showing staining of NSP4 to distinguish infected and uninfected cells. (C) Merge of Panels A and B showing both microtubular network and NSP4 staining pattern in cells.

The white square area in panel C was enlarged to produce panels D, E and F. (D) Green fluorescent channel showing complete destruction of the microtubular network in the cell labeled 1 and the destruction of the network from the centre of the cytoplasm and re-polymerization forming a ring-like structure at the cell periphery in the cell labeled 2. (E) Red fluorescent channel showing staining of NSP4 to indicate infected cells. (F) Merge of Panels D and E to show both microtubular network and NSP4 staining pattern in cells. A magnification bar of 10 μm is indicated in the bottom right corner of each image.

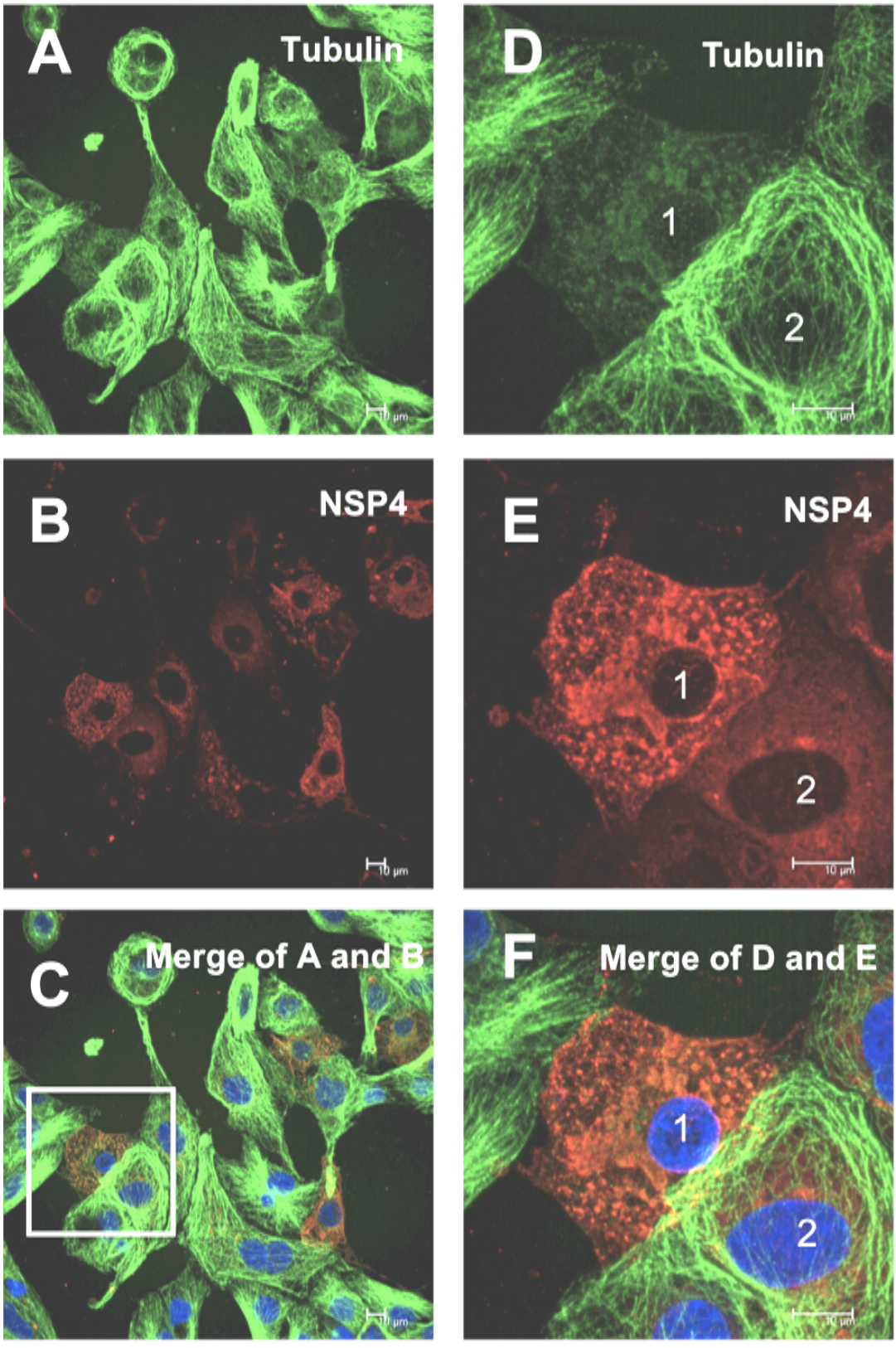
A
Tubulin
D
Tubulin
1
2
B
NSP4
E
NSP4
1
2
C
Merge of A and B
F
Merge of D and E
1
2

6.2.4 Detection of β-Tubulin and F-Actin in Virus Induced Cytoplasmic Extrusions

Analysis of cells expressing NSP4 both in isolation and following viral infection revealed similarities in the disruption of the microtubular network. However no obvious cytoplasmic extrusions were observed in these experiments. This may have been due to the fragility of these cytoplasmic extrusions resulting in their destruction during the two cycles of antibody staining (first cycle for NSP4 antibody staining and second cycle for β-tubulin antibody staining). To overcome this difficulty and allow observation of the cellular components in the extrusions induced by viral infection, BSC-1 cells infected with virus were fixed for one hour at 14 hpi and only stained using β-tubulin antibody. Staining of F-actin was carried out by covering the cells with PBS containing Alexa-594-conjugated phalloidin. These treatments minimized the number of washes used, as it was the washing procedures that were suspected of disrupting the fragile cellular extrusions induced by viral infection. Confocal microscopy of samples prepared using this gentler procedure revealed that β-tubulin and F-actin were reorganised and concentrated in the cytoplasmic extrusions (Fig 6.6). This suggested that β-tubulin and F-actin might be acting to provide a vesicle transport track and cytoskeleton to allow the radial transport of NSP4 containing vesicles seen at the tips of the cytoplasmic extrusions in earlier experiments.

Figure 6.6: Detection of tubulin and actin in cytoplasmic extrusions induced by virus infection of BSC-1 cells.

BSC-1 cells, were infected with rotavirus at an MOI of 10, and fixed at 14 hpi as described in Materials and Methods β-tubulin and F-actin were stained using polyclonal mouse anti-β-tubulin antibody followed by Alexa-488-conjugated goat-anti-mouse antibody and Alexa-594-conjugated phalloidin respectively. Finally nuclei were stained with DAPI all as described in Materials and Methods. (A) Green fluorescent channel showing the staining of concentrated β-tubulin in cytoplasmic extrusions. (B) Red fluorescent channel showing the presence of concentrated F-actin also in cytoplasmic extrusions. (C) Merge of Panels A and B showing an overlay of both β-tubulin and F-actin in cytoplasmic extrusions. Arrow indicates a cytoplasmic extrusion containing clear staining of both β-tubulin and F-actin. A magnification bar of 10 μm is shown in the bottom right corner of each image.

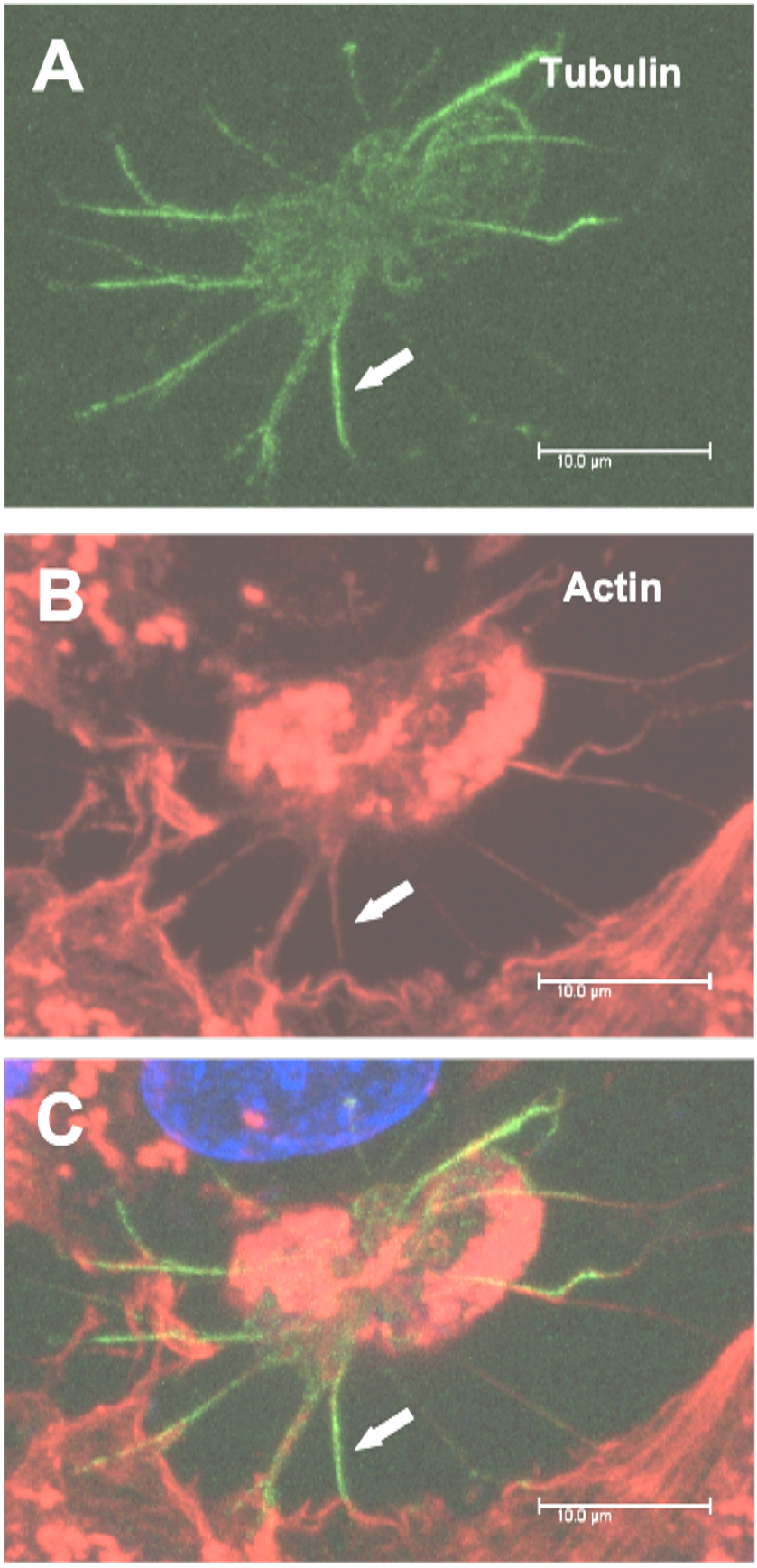
A
Tubulin
10.0 µm
B
Actin
10.0 µm
C
10.0 µm

6.2.5 Effect of Cytoskeleton Disrupting Chemical on The Cytoskeleton Network in Virus-Infected Cells

The importance β-tubulin functionality in supporting cytoplasmic extrusions was studied by using nocodazole and colchicine. Interestingly in the presence of nocodazole or colchicine the β-tubulin in virus-infected cells could still re-polymerize into long tubular structures in the cytoplasm of infected cells (Fig 6.7E). Furthermore staining of such cells with anti-viral antibodies showed that viral protein did localize with these tubular structures but use of mono-specific anti-NSP4 sera showed that NSP4 did not specifically localize to these structures (Fig 6.8).

Figure 6.7: Virus induced microtubule re-polymerization in the presence of nocodazole.

BSC-1 cells, with or without viral infection at an MOI of 10, were treated with nocodazole from 0 hpi. At 10 hpi cells were fixed and stained using polyclonal mouse anti-β-tubulin antibody followed by Alexa-488-conjugated goat-anti-mouse antibody and nuclei were stained with DAPI all as described in Materials and Methods. (A) Overview of an intact microtubular network in a control cell monolayer without viral infection or nocodazole treatment. The white square in panel A marks a region that is enlarged in panel B. (C) Complete destruction of the microtubular network following nocodazole treatment in uninfected cells. The white square in panel C marks a region that is enlarged in panel D. (E) Reformation of de-polymerized microtubules into long tube structures in the cytoplasm of the cell following viral infection and in the continuing presence of nocodazole. Arrow indicates a reformed microtubular tube. A magnification bar of 10 μm is present in the bottom right of each image.

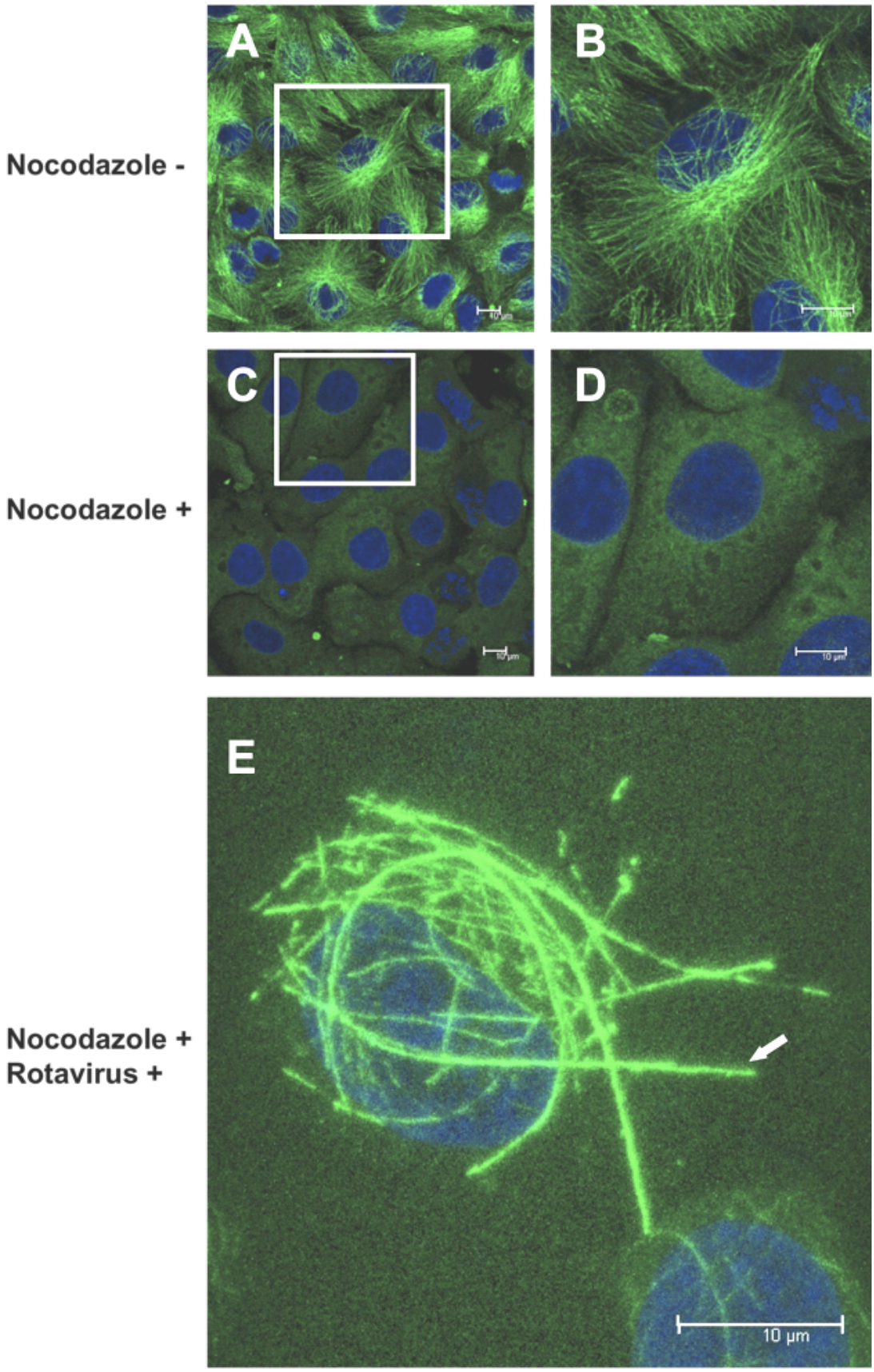
Nocodazole -
A
B
Nocodazole +
C
D
Nocodazole +
Rotavirus +
E
10 µm

Figure 6.8: Colocalization of reformed tubular structure with viral proteins but not NSP4 in cells treated with nocodazole and infected with virus at 10 hpi.

BSC-1 cells, were infected with virus at an MOI of 10, and overlaid with medium containing nocodazole and cultured at 37ºC for 10 hours before being fixed as described in Materials and Methods. Cells were stained with either a polyclonal rabbit antisera against viral structural proteins or a polyclonal mono-specific NSP4 sera followed by Alexa-594-conjugated goat-anti-rabbit antibody as described in Materials and Methods. Microtubules were stained with a polyclonal mouse anti-β-tubulin antibody followed by Alexa-488-conjugated goat-anti-mouse antibody, finally nuclei were stained with DAPI all as described in Materials and Methods. (A) Green fluorescent channel showing reformed microtubular bundles in virus-infected cells in the continued presence of nocodazole. (B) Red fluorescent channel showing the localization of viral proteins to tubular structures. (C) Merge of Panels A and B showing colocalization of microtubular bundles and viral proteins in yellow. (D) Green fluorescent channel also showing reformed microtubular bundles in virus-infected cells in the continued presence of nocodazole. (E) Red fluorescent channel showing NSP4 staining in virus-infected cells. (F) Merge of Panels D and E showing the absence of colocalization of microtubular bundles and NSP4. Arrow indicates a bundle containing both tubulin and viral protein. A magnification bar of 10 μm is indicated in the bottom right corner of each image.

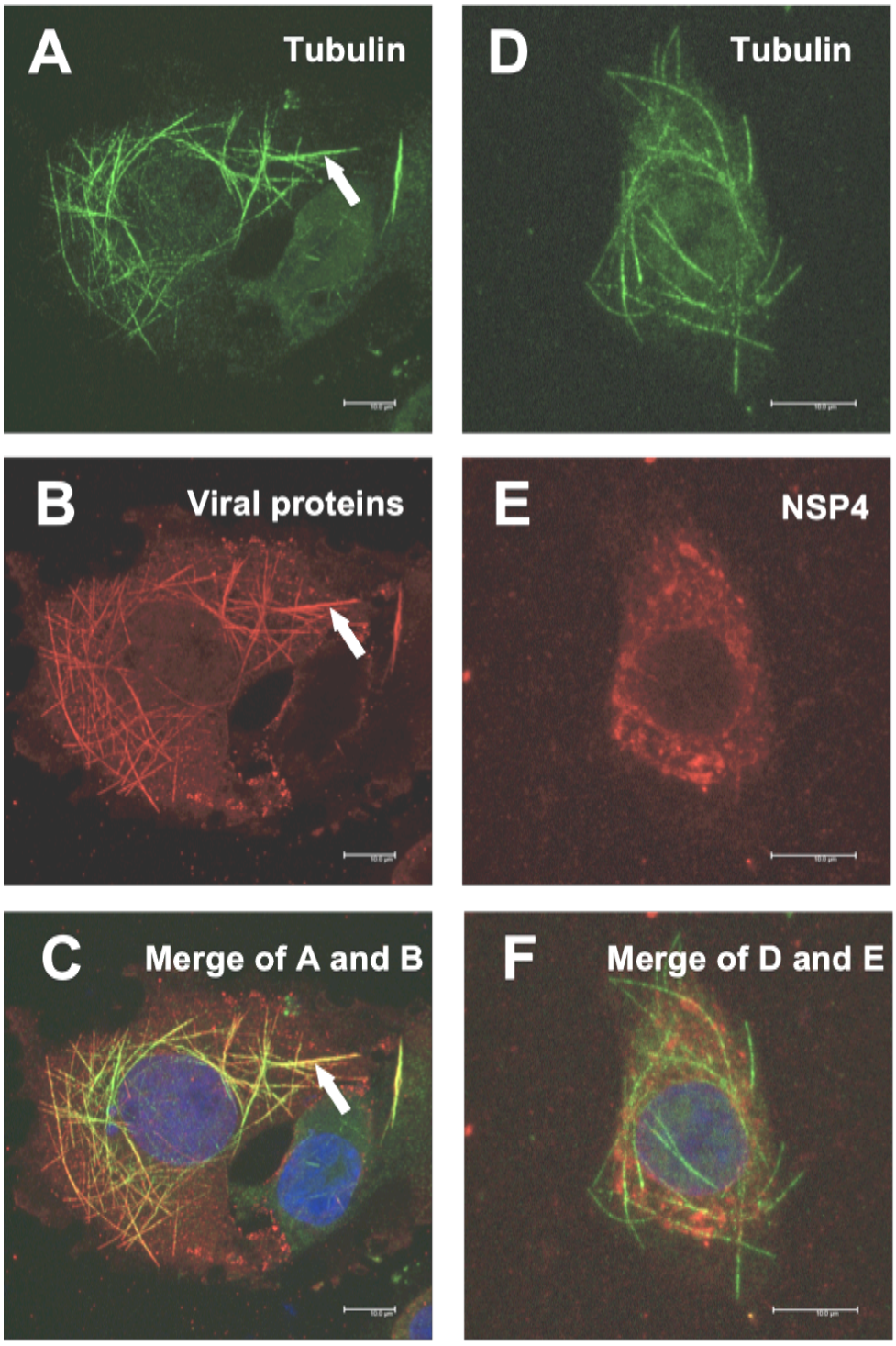
A
Tubulin
D
Tubulin
B
Viral proteins
E
NSP4
C
Merge of A and B
F
Merge of D and E

6.2.6 Kinetics of Nocodazole Induced Microtubular Tubes In Virus-Infected Cells

The observation on reformed microtubule tubes after treatment with nocodazole or colchicine in infected cells indicated that accumulation of viral proteins following viral replication led to the aggregation of microtubules into tubular structures even in the presence of microtubule inhibitors. Thus to further support the hypothesis that aggregation of microtubules was a result of accumulation of viral proteins following viral replication, studies on these re-assembled microtubules were conducted. To do this BSC-1 cells infected with virus were fixed at different times post infection and examined by confocal microscopy. This showed that short tubes containing both β-tubulin and viral proteins could first be detected in about 1% of infected cells at 6 hpi (Fig 6.9A-F). At 8 hpi more tubes of medium length were seen in the cytoplasm of about 5% of infected cells (Fig 6.9G-I). A large number of long tubes were evident in the cytoplasm of about 40% of infected cells at 10 hpi (Fig 6.9J-L). These observations demonstrated that the formation of the tubulin containing tubes in virus-infected cells treated with nocodazole was a gradual process associated with the accumulation of viral proteins. It also showed the ability of viral proteins to cause aggregation of free tubulin generated in cells expressing NSP4 even when treated with nocodazole.

Figure 6.9: Kinetics of formation of microtubule and viral proteins containing bundles in virus-infected BSC-1 cells.

BSC-1 cells, were infected with rotavirus at an MOI of 10, and treated with nocodazole from 0 hpi. Virus-infected cell monolayers were fixed at different times post infection as described in Materials and Methods. Viral proteins were stained with a polyclonal rabbit antisera against viral structural proteins followed by Alexa-594-conjugated goat-anti-rabbit antibody as described in Materials and Methods. Microtubules were stained with a polyclonal mouse anti-β-tubulin antibody followed by Alexa-488-conjugated goat-anti-mouse antibody. Finally nuclei were stained with DAPI all as described in Materials and Methods. Panels A, B and C show no detectable microtubules or viral protein containing tubes at 4 hpi. Panels D, E and F show very short tubes indicated by arrows could be detected in about 1% of infected cells at 6 hpi. Panels G, H and I show medium length tubes were clearly seen in about 5% of infected cells at 8 hpi. Panels J, K and L show longer tubes were evident in about 40% of infected cells at 10 hpi. A magnification bar of 10 μm is indicated in the bottom right corner of each image.

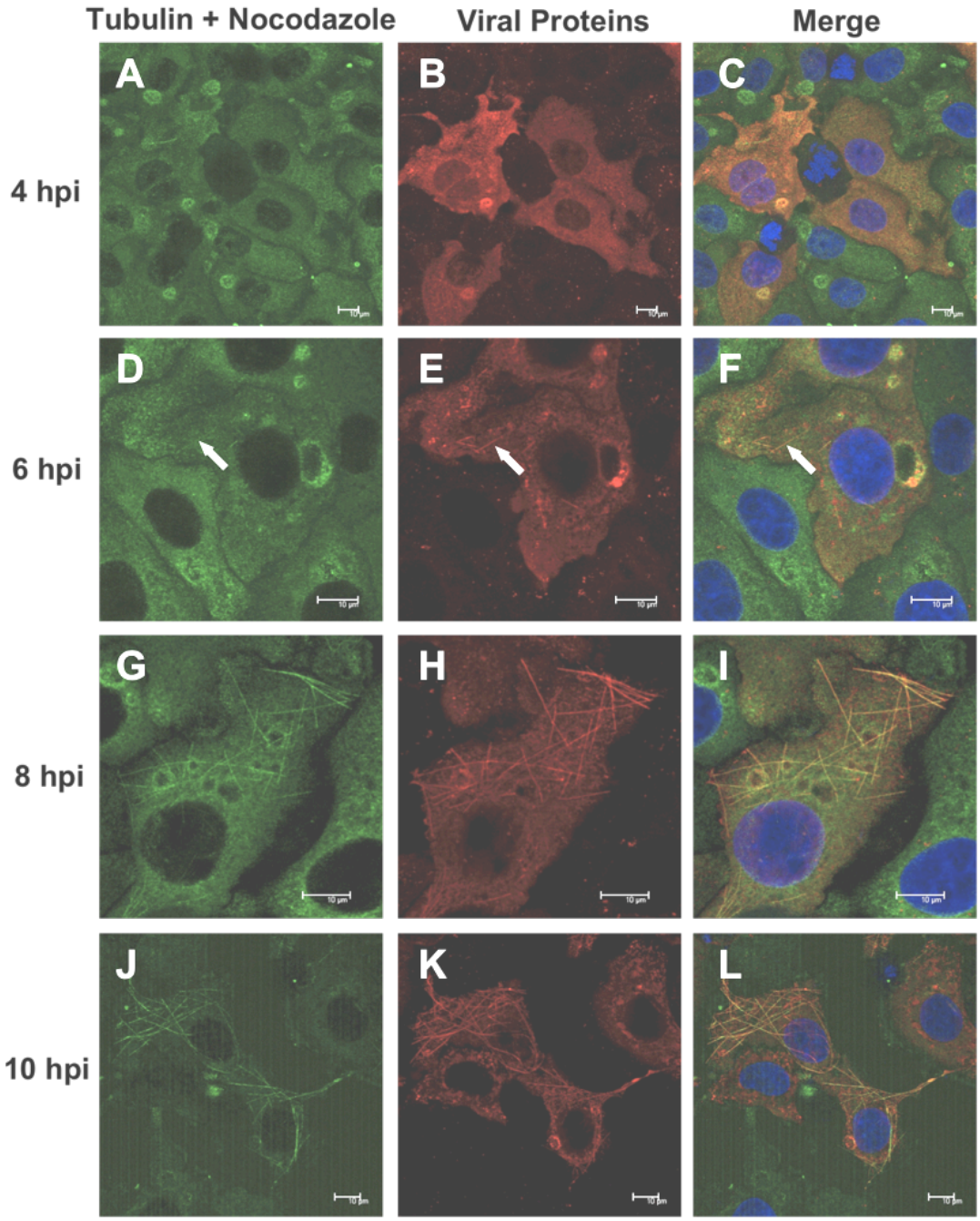
Tubulin + Nocodazole
Viral Proteins
Merge
4 hpi
6 hpi
8 hpi
10 hpi
A
B
C
D
E
F
G
H
I
J
K
L

6.2.7 Effect of Cycloheximide and Tunicamycin Treatment On The Formation of Tubulin Containing Tubes Seen in Virus-infected Cells Treated With Nocodazole

The association of viral proteins with tubulin containing tubes in virus-infected cells treated with nocodazole implies that they have an important role in the re-formation of microtubular tubes. The involvement of glycosylation in the process of forming these tubes was also studied, even though no colocalization of NSP4 with the tubes had been detected. To do this virus-infected BSC-1 cells were overlaid with medium containing nocodazole. Medium containing either cycloheximide, an inhibitor of protein synthesis, or tunicamycin was then added to cell monolayers at different times post infection. Cell monolayers were fixed, stained with anti-virus antibody and β-tubulin antibody, and examined by confocal microscopy. The use of cycloheximide showed that formation of tubes containing viral structural proteins was blocked when it was added before 8 hpi (Fig 6.10B). This indicated that viral protein synthesis was important for tubes containing re-polymerized β-tubulin. Treatment with the glycosylation inhibitor tunicamycin at any time post infection completely inhibited formation of the reassembled microtubular tubes (Fig 6.11). This suggested inhibition of glycosylation could affect the formation of microtubular tubes in virus-infected cells treated with nocodazole (Fig 6.11D) but did not significantly affect the formation of virus structural proteins containing tubes (Fig 6.11E). This result is reminiscent of that seen in NSP4 transfected cells, where glycosylation was found to be dispensable for disruption and re-polymerization of microtubules. However the difference here was that the virus-infected cells were treated with tunicamycin which not only affected glycosylation of NSP4 but also glycosylation of cellular and other viral proteins. Thus there was no clear correlation

between observations done in cells transfected with constructs encoding different glycosylation version of NSP4 and virus-infected cells treated with nocodazole and tunicamycin.

Figure 6.10: Inhibition of the assembly of viral proteins containing tubes in virus-infected BSC-1 cells treated with both nocodazole and cycloheximide.

BSC-1 cells were infected with rotavirus at an MOI of 10 and treated with nocodazole. Culture media were replaced by cycloheximide (20 μg/ml) containing media at 6, 8 and 9 hpi. At 10 hpi cells were fixed and viral proteins were stained with a polyclonal rabbit antisera against viral structural proteins followed by Alexa-594-conjugated goat-anti-rabbit antibody (red staining) as described in Materials and Methods. Nuclei were stained with DAPI all as described in Materials and Methods. Panel A shows a complete inhibition of the formation of viral proteins containing tubes in a virus infected and nocodazole-treated cell with treatment of cycloheximide at 6 hpi. Panel B shows that block of viral protein synthesis resulted in formation of short viral proteins containing tubes in a virus infected and nocodazole-treated cells with cycloheximide treatment at 8 hpi. Panel C shows a great number of long viral proteins containing tubes were observed in a virus infected and nocodazole-treated cell with treatment of cycloheximide at 9 hpi. Arrowhead indicates a short viral proteins containing tube. Arrow indicates a long viral proteins containing tube. A magnification bar of 5 μm is present in the bottom right corner of each image.

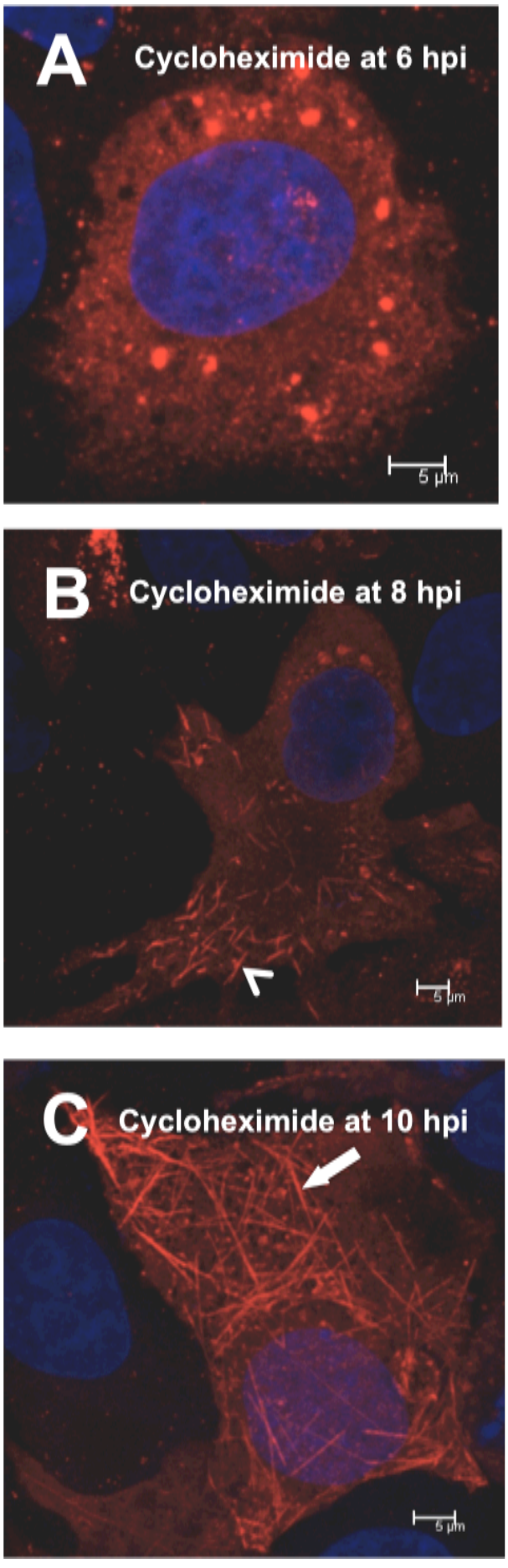
A
Cycloheximide at 6 hpi
5 µm
B
Cycloheximide at 8 hpi
5 µm
C
Cycloheximide at 10 hpi
5 µm

Figure 6.11: Inhibition of the assembly of microtubular tubes in virus-infected BSC-1 cells treated with both nocodazole and tunicamycin.

BSC-1 cells infected with rotavirus at an MOI of 10 and treated with nocodazole were cultured in media with or without tunicamycin at 0 hpi. At 10 hpi cells were fixed and viral proteins were stained with a polyclonal rabbit antisera against viral structural proteins followed by Alexa-594-conjugated goat-anti-rabbit antibody as described in Materials and Methods. Microtubules were stained with a polyclonal mouse anti-β-tubulin antibody followed by Alexa-488-conjugated goat-anti-mouse antibody. Finally nuclei were stained with DAPI all as described in Materials and Methods. Panel A shows the formation of microtubular tubes in cells infected with virus and treated with nocodazole. Panel B shows the formation of viral proteins containing tubes in virus-infected cells and treated with nocodazole. (C) Merge of Panels A and B showing colocalization of both microtubules and viral proteins in tube structures. Panel D shows inhibition of the formation of microtubular tubes in virus-infected cells treated with both nocodazole and tunicamycin. Panel E shows the formation of viral proteins containing tubes could still be detected in virus-infected cells treated with both nocodazole and tunicamycin. (F) Merge of Panels D and E showing only the formation of viral proteins containing tubes could be detected in virus-infected cells treated with both nocodazole and tunicamycin. A magnification bar of 10 μm is present in the bottom right corner of each image.

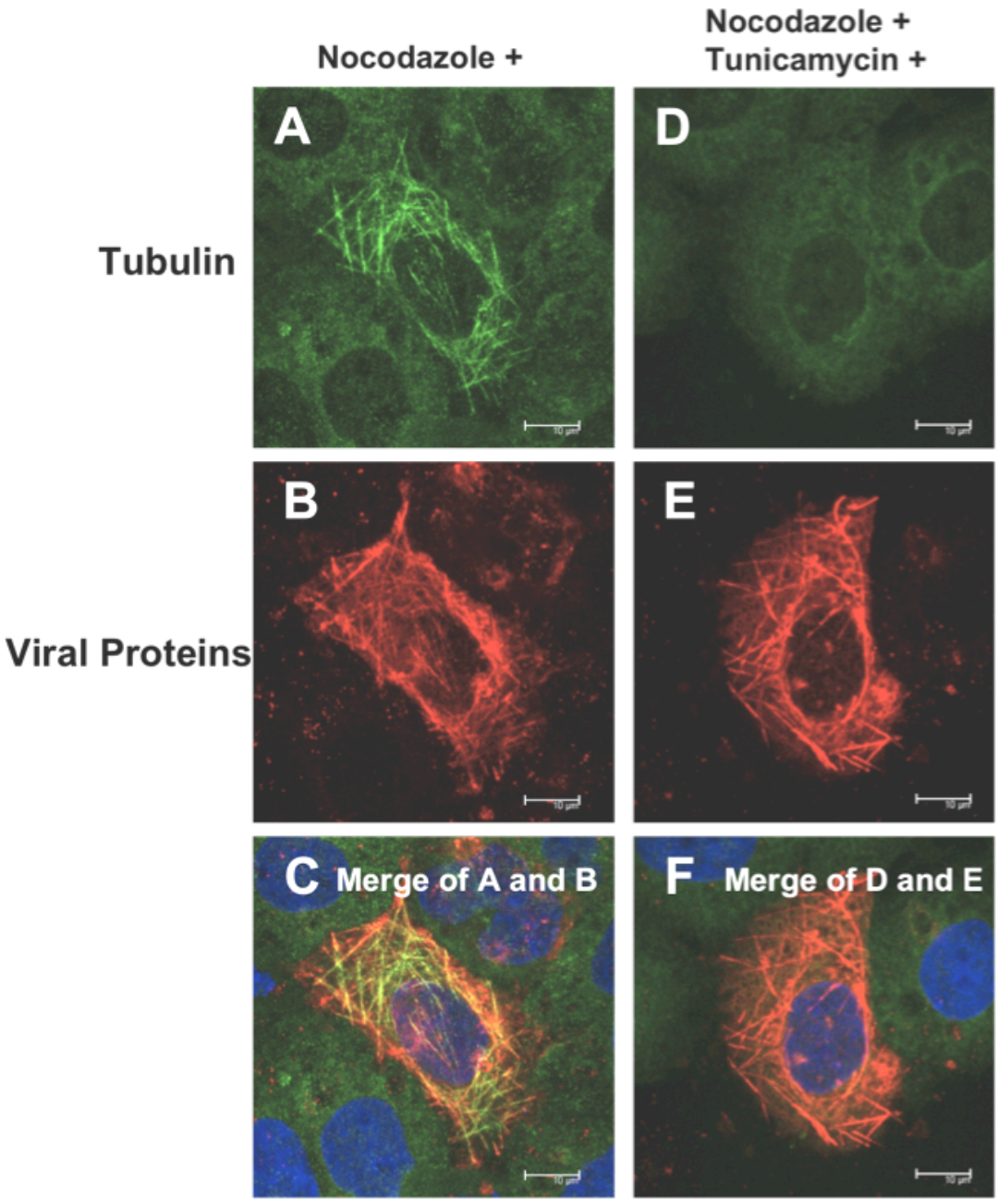
Nocodazole +
Nocodazole +
Tunicamycin +
Tubulin
Viral Proteins
A
D
B
E
C Merge of A and B
F Merge of D and E

6.3 Conclusions

The experiments reported in this chapter focused on analyzing the cellular skeleton (primarily microtubular network) in cells expressing NSP4 in isolation and in virus-infected cells. BSC-1 cells transfected with either glyco+ or glyco- NSP4 displayed disassembly of the microtubular network from the centre of the cytoplasm and its re-polymerization into ring-like structures at the cell periphery. This function of NSP4 was shown to be independent of both glycosylation of the protein and increases of intracellular calcium levels stimulated by expression of NSP4. In contrast other studies using polarized caco-2 cells showed that intracellular calcium levels were important for destruction of the microtubular network in infected cells (Brunet *et al*., 2000b). Our study used a different cell line (i.e. BSC-1 cells) for transfection and infection which might account for the differences seen. Further studies analyzing the role of the centrosome in cells expressing NSP4 following recovery from treatment with the inhibitor of centrosome function, nocodazole, showed that the microtubular network could not reform from a microtubular polymerization centre (i.e. centrosome) suggesting that either the functional disruption of centrosome or that the speed of microtubular polymerization from the centrosome was slower than its de-polymerization caused by the expression of NSP4. A similar pattern of redistribution of the microtubular network has been seen in apoptotic cells (Moss *et al*., 2009; Sanchez-Alcazar *et al*., 2007), however neither apoptosis nor necrosis were detected in 293T cells expressing NSP4 for 48 hours. This implied that expression of NSP4 was sufficient to trigger de-polymerization of the microtubular network and might employ a different mechanism to that found initially in apoptotic cells. A recent study focusing on microtubular disruption by viral infection revealed a role of NSP2 in sequestrating tubulin molecules which lead

to de-polymerization of microtubules throughout the cytoplasm, but this did not start from the centre of cells (Martin *et al*., 2010). The pattern of disrupted microtubular network seen in NSP4 transfected cells was very similar to that seen in virus infected cells i.e. they both initiated microtubular de-polymerization from the centre of cell and induced re-polymerization at cell periphery, suggesting that NSP4 alone might act as the main factor in de-polymerizing the microtubular network whilst NSP2 possibly enhanced the effect of de-polymerization by sequestrating tubulin molecules in infected cells.

In our study the relevance of the NSP4 induced microtubular network destruction seen in transfected cells to the situation in virus infection was also examined. Virus-infected cells consistently showed a pattern of microtubular modification involving both disassembly of microtubules from the centre of the cell and re-polymerization at the cell periphery.

In addition to using antibodies to detect the cytoskeleton in infected cells, attempts were made to detect the cytoskeleton in cytoplasmic extrusions found in both NSP4 transfected and virus-infected cells. Using double antibody staining no convincing evidence of cytoplasmic extrusions were seen in virus-infected cells, but it was suspected that this may have seen due to the fragility of these extrusions. Consistent with this, when single antibody staining of microtubular network and chemical staining of actin filament was used, cytoplasmic extrusions containing microtubules and actin filaments were clearly seen in virus-infected cells. Subsequent inhibitor experiments using either nocodazole or colchicine for β-tubulin or CytoD for F-actin blocked the generation of cytoplasmic extrusion in virus-infected cells. This further supported the hypothesis that the virus employs microtubules and actin filaments to provide trafficking of molecules and physical support of the cytoplasmic extrusions.

Interestingly when tubulin inhibitors were used, de-polymerized microtubules were rearranged to form long tubes in the cytoplasm of virus-infected cells. Colocalization of viral proteins excluding NSP4 with these long microtubular tubes was also demonstrated, indicating their participation in the formation of these tubes. Consistent with this, inhibition of viral protein synthesis using cycloheximide before 8 hpi completely blocked the formation of both viral proteins and microtubules containing tubes. A tunicamycin block was also used in these nocodazole experiments to investigate the role of glycosylation in the formation of these tubes. This treatment of cells inhibited the formation of microtubular tubes but appearance of tubes containing viral proteins was still evident at 10 hpi. The inhibition of microtubular tubes by treatment of tunicamycin suggested the potential involvement of glycosylation of NSP4 in the formation of microtubular tubes.

Taken together our studies on the cytoskeletal network suggested that after viral infection, expression of NSP4 in infected cells leads to the destruction of both the microtubular (in this study) and actin networks (Berkova *et al*., 2007). The destruction of microtubular network by NSP4 is independent of its glycosylation and its ability to raise intracellular calcium levels. This break down process can be greatly enhanced by viral proteins through their promoting aggregation of free tubulin. This microtubular disruption appears to be irreversible and eventually contributes to overall viral pathology.

Chapter 7

Yellow Fluorescent Protein Complementarity Assay For Capturing Intracellular Partners For NSP4

7.1 Introduction

The observation of morphological changes associated with the expression of glycosylated NSP4 in transfected cells matching those seen following virus infection suggested that glycosylated NSP4 was able to interact with cellular metabolic processes. These changes were not seen with non-glycosylated NSP4 and this prompted an investigation of possible interactions between glycosylated NSP4 and cellular proteins. To do this use was made of a two hybrid type assay based on yellow fluorescent protein complementation (YFP-PCA). YFP-PCA involves splitting YFP into two fragments (i.e. N-terminal half and C-terminal half of YFP) that can spontaneously fold to generate functional YFP if the two fragments form a complex. Interaction of two proteins under study each fused to one of the YFP fragments is essential to bring these two YFP fragments together to generate fluorescence (Nyfeler *et al*., 2005). In this study, NSP4 was fused to fragment 1 of YFP (i.e. N-terminal half) as the 'bait' fusion protein and a cDNA library was fused to fragment 2 of YFP as 'prey'. Following transfection of these two plasmids into cells yellow fluorescence positive cells were sorted by FACS analysis. cDNAs that putatively encoded cellular proteins interacting with NSP4 were recovered and analysed in a cyclic panning process (Fig 7.1).

The advantage of the YFP-PCA assay in screening for cellular proteins interacting with full length NSP4 is that it allows the search to be done in live cells following detection of protein-protein interactions in a natural cellular environment. This approach was not practicable in our previous studies because screens based on traditional two-hybrid assays required growth of cell populations showing positive interaction before isolation of the cellular cDNA could be undertaken.

Expression of full length NSP4 is a potent toxin for mammalian, yeast and bacterial

cells. To avoid this problem a truncated NSP4 has usually been employed in this type of experiment (Boshuizen *et al*., 2004). However the YFP PCA assay enables clear detection of interaction indicated by YFP fluorescence in individual cells at only 24-hour post transfection allowing isolation of the cells and extraction of plasmid DNAs that encode interacting proteins. This assay has also been reported to enhance the intensity of fluorescence from positive interactions by trapping and accumulating the YFP complex (Nyfeler *et al*., 2005). This latter property should allow the assay to be used for screening of transient and weak interactions between NSP4 and cellular proteins.

Figure 7.1: Strategy of the YFP-PCA assay system for screening interactions of NSP4 with cellular partners.

Panel A: Schematic representation of the YFP-PCA assay. The interaction of two test proteins brings two non-fluorescent fragments of YFP fused to those proteins into close proximity to reconstitute functional YFP. To study interactions of NSP4 with cellular proteins, YFP1 was fused to NSP4 as bait and YFP2 was fused to a cDNA library constructed from BSC-1 cellular mRNA as prey.

Panel B: The YFP1-NSP4 was constructed using the ampicillin resistant pcDNA3 cloning vector. The YFP2-cDNA was expressed using the kanamycin resistant pEYFP-N1 cloning vector.

Panel C: Optimized flow chart of YFP-PCA based screening of a cDNA library for cellular interaction partners of NSP4.

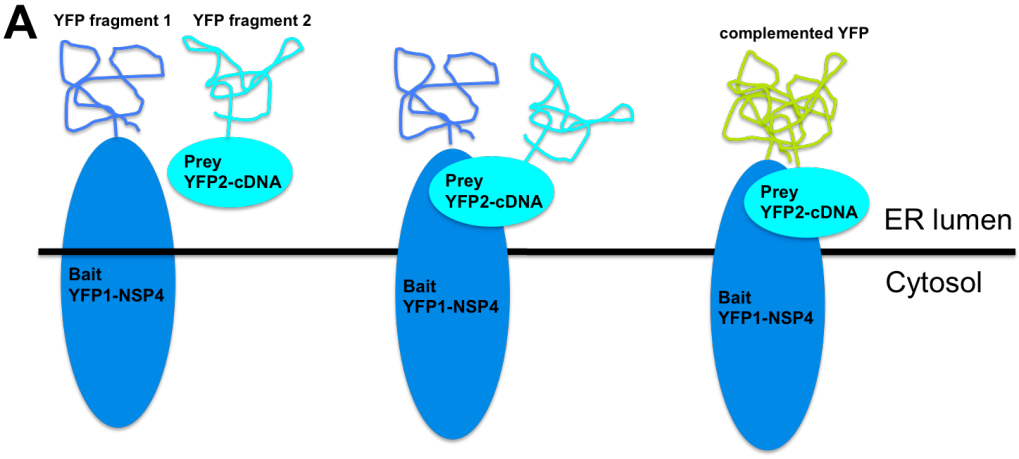

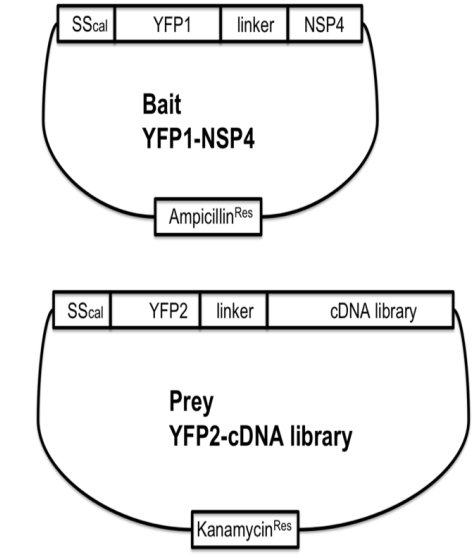

C

Co-expression of YFP1-NSP4 and YFP2-cDNA in 293T cells

↓

FACS-based isolation of yellow fluorescent cells

↓

Extraction of plasmid DNA and electroporation into *E.coli*

↓

Isolation of individual plasmid on kanamycin plates

↓

Co-expression of individual plasmid with either YFP1-NSP4 or YFP1 in 293T cells

↓

Identification of the cDNA insert by sequence analysis

7.2 Results

7.2.1 Construction of YFP-PCA System for Studying Interaction of NSP4

The YFP-PCA system was established using the pcDNA3 cloning vector with YFP fragment 1 (YFP1, amino acids 1–158) and fragment 2 (YFP2; amino acids 159 –239) engineered into two separate plasmid constructs. An ER translocation signal sequence from calreticulin (SS_{cal}) was fused to the N terminus of each YFP fragment. A linker sequence encoding 10 amino acids $(GGGGS)_2$ was also fused to the C terminus of each YFP fragment. Downstream of these linker sequence cDNAs encoding ERGIC-53 (endoplasmic reticulum Golgi intermediate compartment) and MCFD2 (multi-coagulation factor deficiency protein) were inserted to generate positive controls for the assay (Nyfeler *et al*., 2005). Subsequently the YFP2-MCFD2 construct was sub-cloned into the pEYFP-N1 cloning vector replacing the EYFP from the vector to allow exploitation of kanamycin resistance based selection. In this study the ERGIC-53 and MCFD2 sequences were initially replaced by the coding sequences of NSP4, rotavirus VP4 and rotavirus VP6. In addition a cDNA library generated from rotavirus permissive BSC-1 cells was cloned downstream of the C terminus of YFP fragment 2 in three different reading frames to ensure expression of proteins from inserts present in the cDNA library (Fig 7.2).

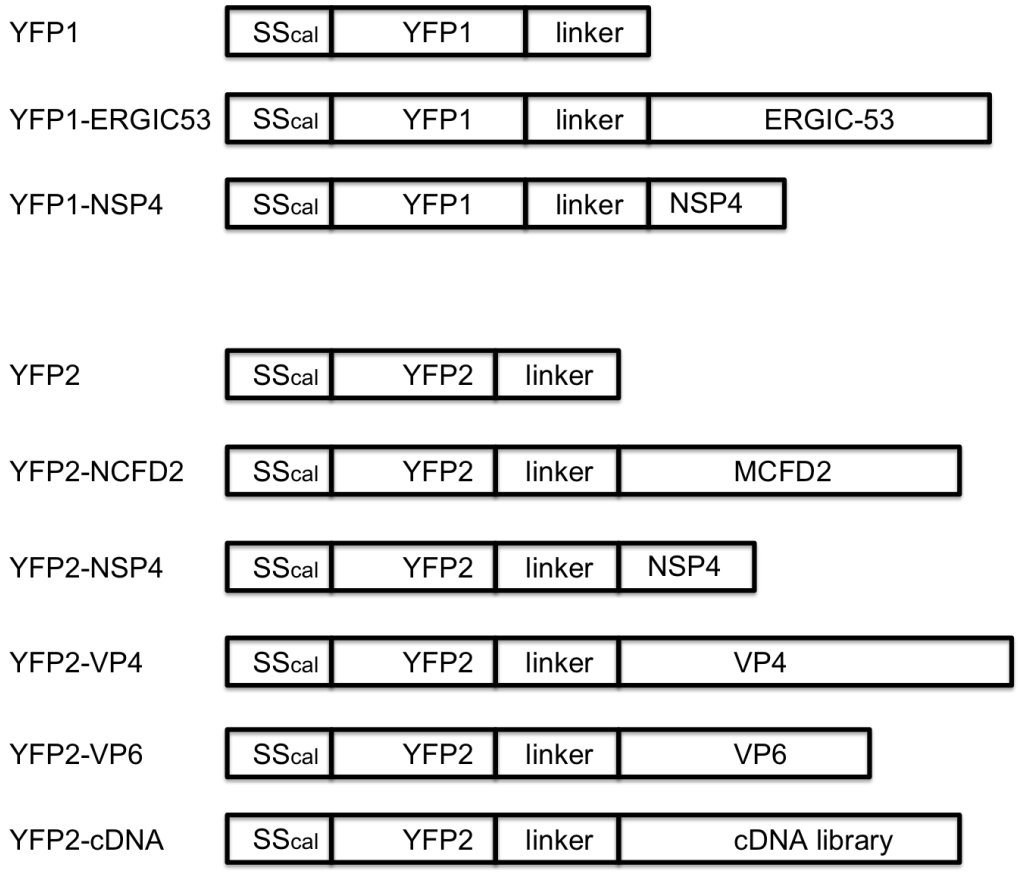

Figure 7.2: Schematic representation of the fusion constructs used in the YFP-PCA assay.

SScal is the signal sequence of calreticulin to ensure more efficient translocation of the fusion protein in the ER. Linker is a 10 amino acid sequence $(GGGGS)_2$. The YFP1 fragment was in the pcDNA3 cloning vector with ampicillin resistance and the YFP2 fragment was in the pEYFP-N1 cloning vector with kanamycin resistance. The cDNA library as cloned into three different reading frames in relation to the YFP2 linker sequences. All the cloning experiments to generate these constructs were carried out as described in Materials and Methods.

7.2.2 Interaction of YFP-PCA Constructs for Studying NSP4

The plasmid constructs described in the previous section were co-transfected into 293T cells. After 24 hours of incubation cells were first examined by UV-light microscopy and then subjected FACS analysis. To test the utility of the assay for examining NSP4's interactions a control experiment in which NSP4 was fused to both YFP1 and YFP2 was examined both by optical observation and FACS analysis. This showed that YFP1-NSP4 was able to interact with YFP2-NSP4 to produce an intense YFP fluorescence in both rotavirus non-permissive cells (293T cells) and permissive cells (BSC-1 cells) (Fig 7.3, 7.4, 7.5 and 7.6). By contrast positive interactions were not seen between YFP1-NSP4 and YFP2-VP4 or YFP2-VP6 (data not shown). The failure to see positive interactions between YFP1-NSP4 and YFP2-VP4 or YFP2-VP6 may reflect the fact that the original interactions reported between these two rotavirus structural proteins and the C terminal half of NSP4 occurred in the cytoplasm and not in the ER lumen where YFP fragment 1 was presented. Having shown that the YFP-PCA assay can be used to study NSP4 interaction with itself the requirement of glycosylation in such interactions was examined. For this the N-linked glycosylation inhibitor tunicamycin was added to the culture medium after co-transfection of YFP1-NSP4 and YFP2-NSP4. Subsequent analysis using UV-light microscopy and FACS analysis showed that this inhibitor dramatically reduced the intensity of fluorescence suggestive of an important role for glycosylation in the NSP4-NSP4 interaction (Fig 7.3E, 7.4E and 7.6). However the use of tunicamycin, a broad-spectrum glycosylation inhibitor, did not in itself provide definitive support for the involvement of glycosylated NSP4 in the interaction. Therefore manipulation of the mutated NSP4 lacking the N-linked glycosylation sites generated for experiments reported in Chapter 3 into the YFP

vectors should be an early future experimental priority to definitively substantiate the results obtained in this study.

Figure 7.3: Interaction between YFP1-NSP4 and YFP2-NSP4 in non-permissive 293T cells.

Cells were transfected with plasmids as described in Materials and Methods. At 24-hour post transfection cells were observed with UV-light microscopy as described in Materials and Methods. (A) Cells transfected with YFP1-NSP4 alone. (B) Cells transfected with YFP2-NSP4 alone in B. (C) Cells transfected with YFP1-NSP4 and YFP2. (D) Cells transfected with YFP1 and YFP2-NSP4. Panel E shows cells transfected with both YFP1-NSP4 and YFP2-NSP4 with the positive fluorescence indicating the interaction of NSP4 with itself. Panel F shows cells transfected with YFP1-NSP4 and YFP2-NSP4 and then treated with tunicamycin (5μg/ml), the reduced fluorescence compared to that seen in the absence of tunicamycin treatment being evident. Images were obtained at magnification of 40×.

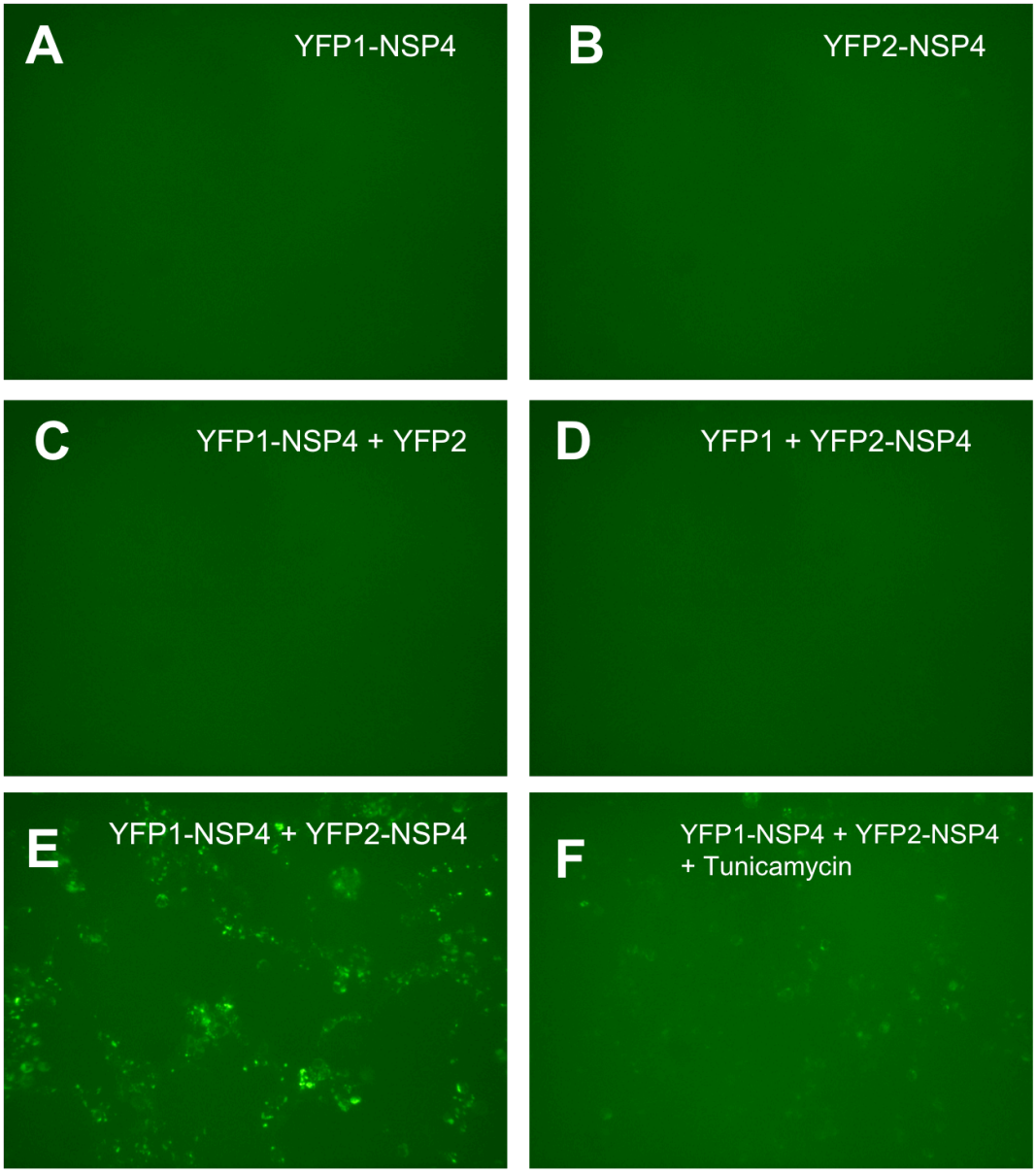
A
YFP1-NSP4
B
YFP2-NSP4
C
YFP1-NSP4 + YFP2
D
YFP1 + YFP2-NSP4
E
YFP1-NSP4 + YFP2-NSP4
F
YFP1-NSP4 + YFP2-NSP4
+ Tunicamycin

Figure 7.4: Interaction between YFP1-NSP4 and YFP2-NSP4 in rotavirus permissive BSC-1 cells.

Cells were transfected with plasmids as described in Materials and Methods. At 24 hours post transfection culture cells were observed with UV-light microscopy as described in Materials and Methods. (A) Cells transfected with YFP1-NSP4 alone. (B) Cells transfected with YFP2-NSP4 alone. (C) Cells transfected with YFP1-NSP4 and YFP2. (D) Cells transfected with YFP1 and YFP2-NSP4. Panel E shows cells transfected with both YFP1-NSP4 and YFP2-NSP4 with the positive fluorescence indicating the interaction of NSP4 with itself. Panel F shows cells transfected with YFP1-NSP4 and YFP2-NSP4 and then treated with tunicamycin (5μg/ml), the reduced fluorescence compared to that seen in the absence of tunicamycin treatment being evident. Images were obtained at magnification of 40×.

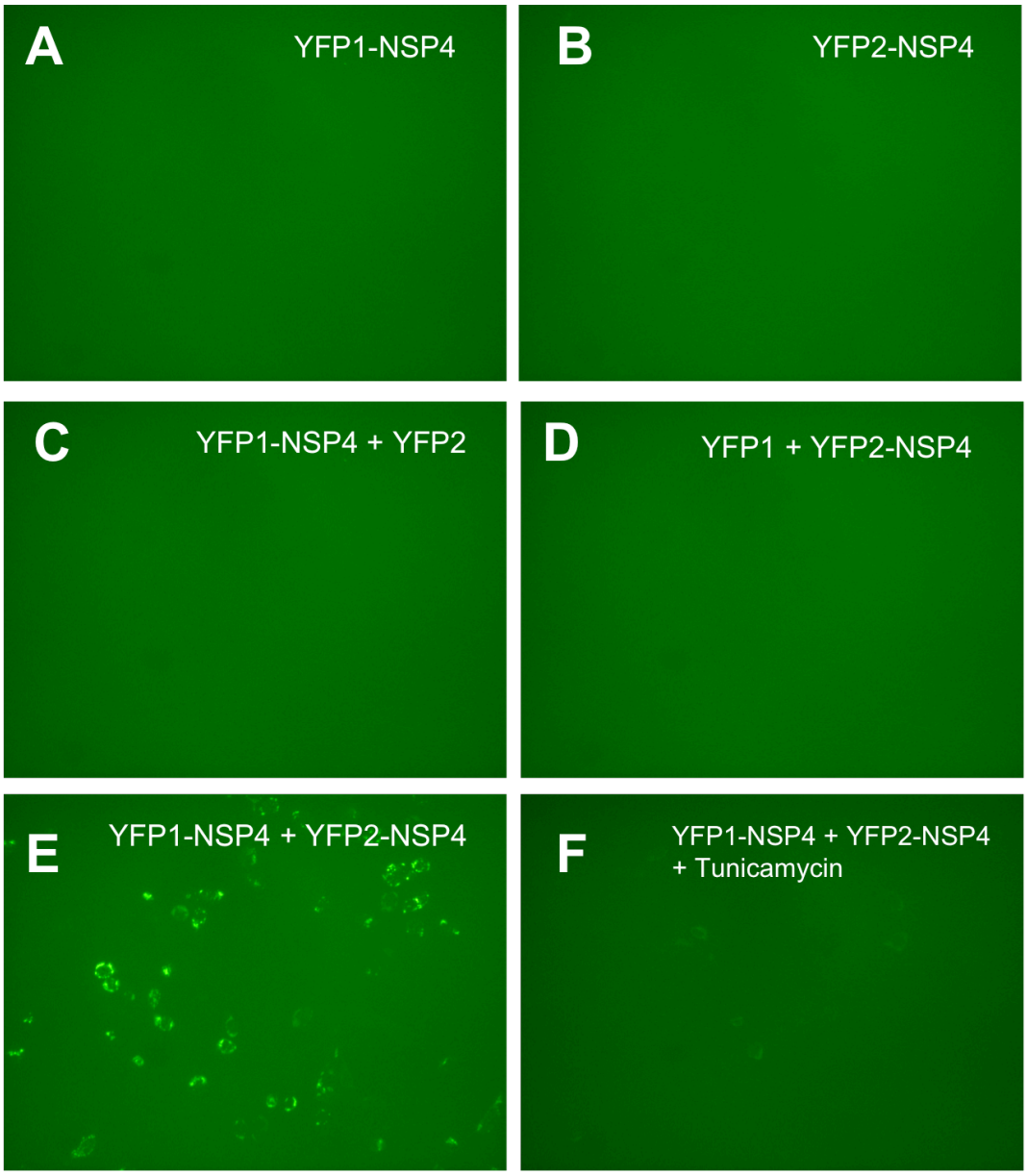
A
YFP1-NSP4
B
YFP2-NSP4
C
YFP1-NSP4 + YFP2
D
YFP1 + YFP2-NSP4
E
YFP1-NSP4 + YFP2-NSP4
F
YFP1-NSP4 + YFP2-NSP4
+ Tunicamycin

Figure 7.5: Confocal examination of the interaction between YFP1-NSP4 and YFP2-NSP4 in BSC-1 cells.

Cells were co-transfected with YFP1-NSP4 and YFP2-NSP4 as described in Materials and Methods. At 24 hours post transfection culture cells were fixed, nuclei stained with DAPI and cells examined by confocal microscopy as described in Materials and Methods. Panel A low magnification of cells expressing YFP1-NSP4 and YFP2-NSP4 showing that the interaction resulted in fluorescence in spots distributing in the cytoplasm. Panel B A higher magnification image of a cell showing the NSP4 self-interaction. A magnification bar of 10 μm is indicated in the bottom right corner of each image.

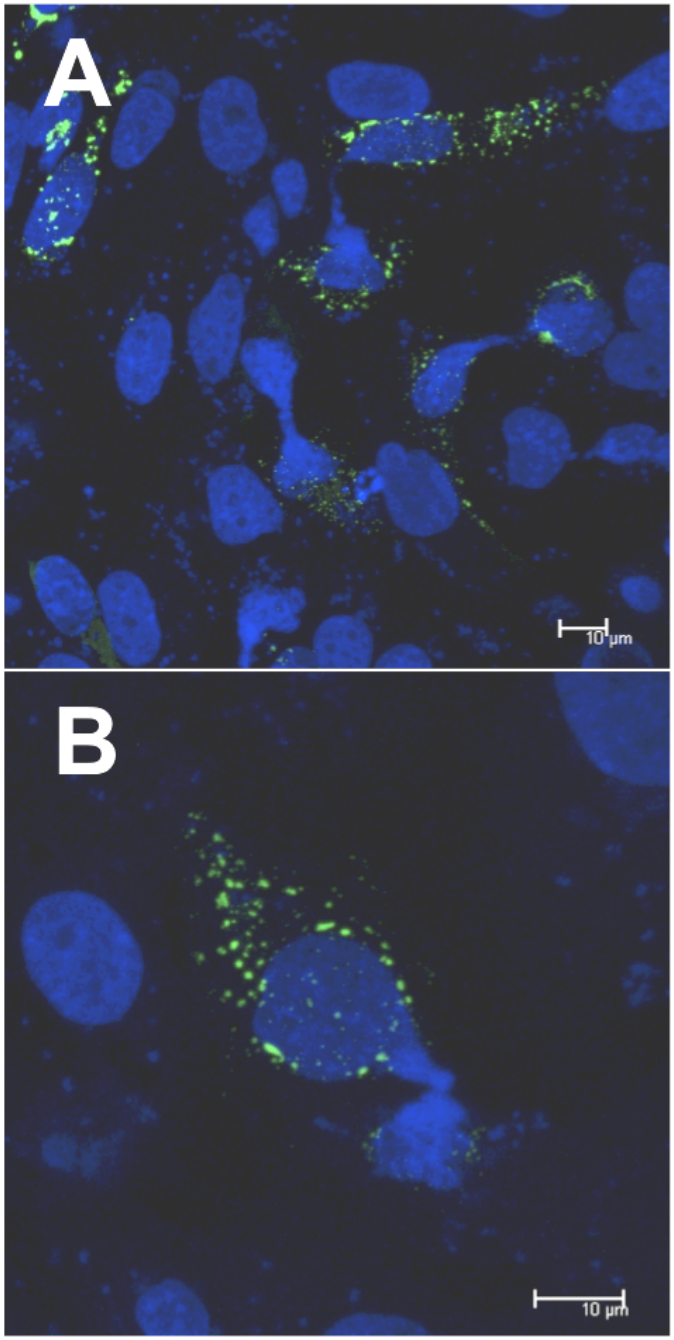
A
10 µm
B
10 µm

Figure 7.6: Disruption of the self-interaction of NSP4 by treatment of 293T cells with tunicamycin.

Cells were transfected with the indicated plasmid constructs and incubated in the presence or absence of tunicamycin as described in Materials and Methods. Subsequent FACS analysis was used to measure the mean value of fluorescence intensity in each sample as described in Materials and Methods. The mean value of fluorescence intensity in cells transfected with YFP1-NSP4+YFP2-NSP4 was set at 100%. Addition of tunicamycin to the culture medium of cells transfected with YFP1-NSP4 and YFP2-NSP4 decreased the mean value of fluorescence intensity by ~80%.

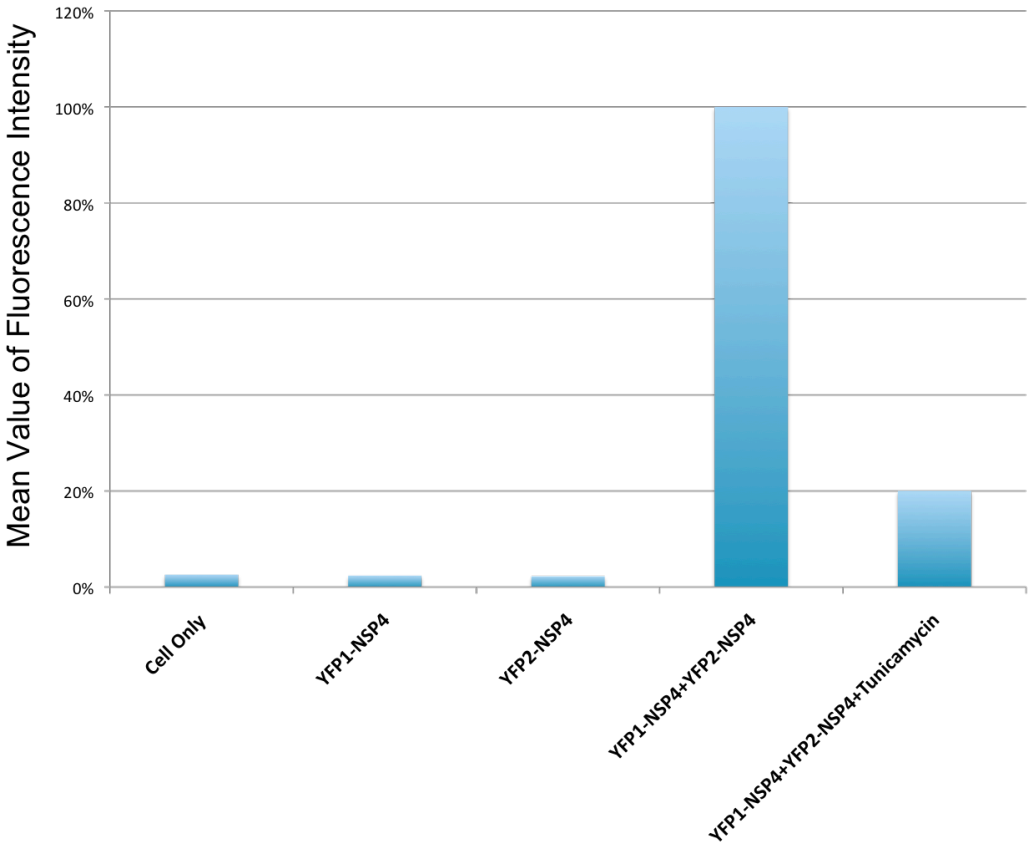
Mean Value of Fluorescence Intensity
120%
100%
80%
60%
40%
20%
0%
Cell Only
YFP1-NSP4
YFP2-NSP4
YFP1-NSP4+YFP2-NSP4
YFP1-NSP4+YFP2-NSP4+Tunicamycin

7.2.3 Optimization of Interactions Between YFP1-NSP4 and YFP2-cDNAs

To test the interaction between NSP4 and the cDNA library, 293T cells were co-transfected with 2 μg of the YFP1-NSP4 construct and 2 μg of the YFP2-cDNA library construct. FACS analysis at 24 hours post transfection showed that 1%-5% of the 20,000 cells analysed were positively fluorescing. By contrast only a few cells were detected in negative controls i.e. cells transfected with either YFP1-NSP4 alone, YFP2-cDNA alone or YFP1-NSP4 and YFP2. This preliminary experiment showed that detection of the fluorescence signal from interactions between YFP1-NSP4 and clones in the YFP2-cDNA library using FACS analysis could be distinguished from background fluorescence noise.

To optimize transfection conditions in the screen different concentrations of YFP2-cDNA (2μg, 1.5μg, 1μg, 0.8μg, 0.5μg, 0.2μg and 0.1μg) were co-transfected with 2 μg of YFP1-NSP4. This optimization was necessary as transfection of large amounts of DNA increased the possibility that each transfected cell receiving a positive cDNA construct would also receive a larger number of irrelevant constructs leading to more rounds of screening being required to isolate/purify a positive cDNA construct. This optimization experiment showed that only 1μg of YFP2-cDNA for each transfection produced equal numbers of fluorescent cells to that of 2μg of YFP2-cDNA. When the amount of YFP2-cDNA used was less than 1 μg, the number of fluorescent cells reduced with the clearest detection of positively fluorescent cells above background fluorescent noise being achieved at 0.2μg of YFP2-cDNA for each transfection. Therefore 0.2μg of YFP2-cDNA plasmid i.e. 1/10 of that for YFP1-NSP4 was used in all future screening assays. This lowered the percentage of fluorescence-positive cells to 0.1%-0.5% and minimized the number of plasmid copies in individual transfected cells to favor subsequent recovery of the plasmids

generating positive interaction (Fig 7.7). Following co-transfection of 2μg of YFP1-NSP4 and 0.2μg of YFP2-cDNA pools with insert of either 1-2kb or over 2kb into 293T cells in a 12-well plate, cells in 4 wells of each pool were used to isolate 1000 positively fluorescing cells using flow cytometry in the actual screen.

Figure 7.7: FACS analysis of 293T cells transfected with YFP1-NSP4 and YFP2-cDNA.

Cells were transfected with indicated bait and prey DNA constructs and analysed using FACS at 24 hours post transfection as described in Materials and Methods. Panel A Control i.e.: non-transfected cells showing only showed 0.035% (i.e. 7 cells) in the gated area. Panel B Cells transfected with YFP1-NSP4 and YFP2 showing 0.05% (i.e. 10 cells) in gated area. Panel C Cells transfected with YFP1-NSP4 and YFP2-cDNA pool with inserts ranging from 1 kb to 2 kb showing 0.22% (i.e. 45 cells) in the gated area. Panel D Cells transfected with YFP1-NSP4 and YFP2-cDNA pool with inserts over 2 kb showing 0.4% (i.e. 80 cells) in the gated area.

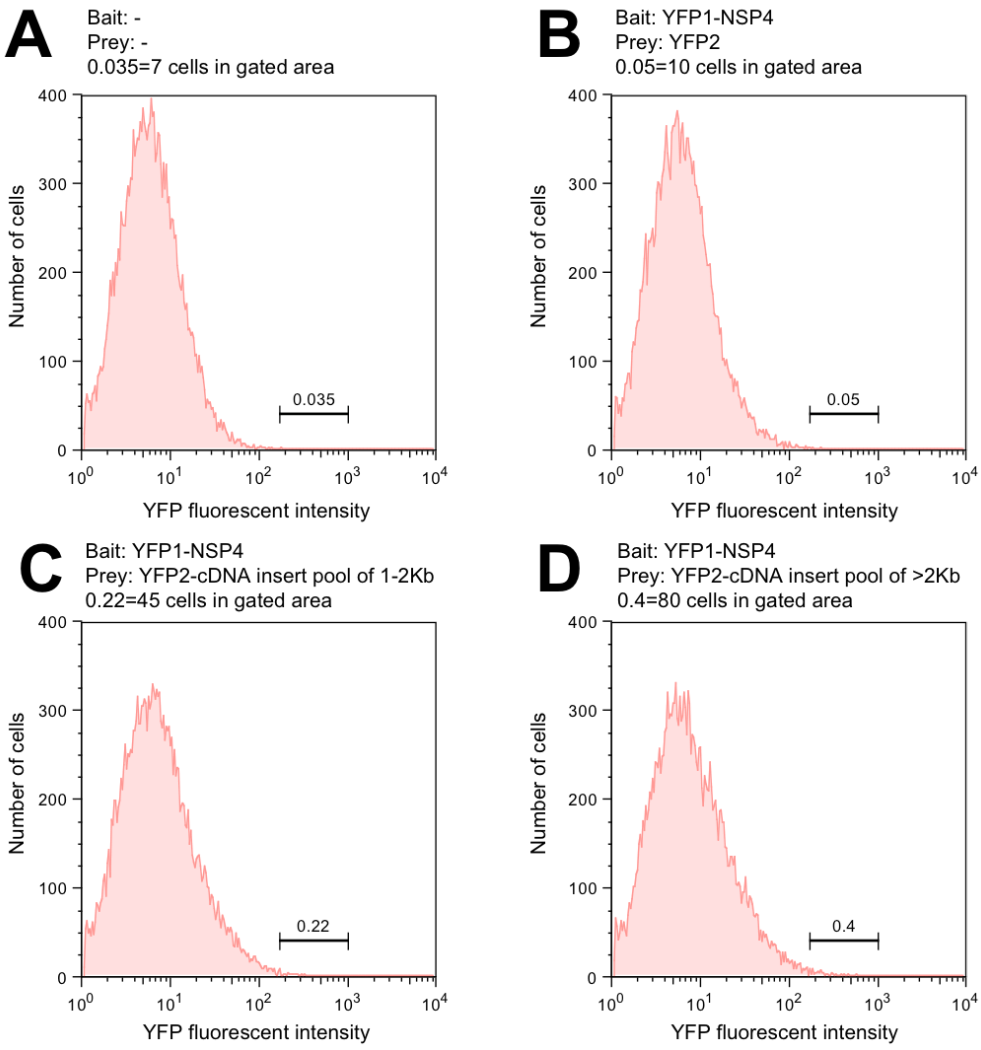
A
Bait: -
Prey: -
0.035=7 cells in gated area
Number of cells
YFP fluorescent intensity
0.035
B
Bait: YFP1-NSP4
Prey: YFP2
0.05=10 cells in gated area
Number of cells
YFP fluorescent intensity
0.05
C
Bait: YFP1-NSP4
Prey: YFP2-cDNA insert pool of 1-2Kb
0.22=45 cells in gated area
Number of cells
YFP fluorescent intensity
0.22
D
Bait: YFP1-NSP4
Prey: YFP2-cDNA insert pool of >2Kb
0.4=80 cells in gated area
Number of cells
YFP fluorescent intensity
0.4

7.2.4 Recovery of c-DNA Containing Plasmids from Screen

1000 sorted fluorescent cells were isolated from each positive transfection sample and the cells lysed, the plasmid DNA extracted and amplified by transformation back into *E. coli*. To maximize the number of bacterial colonies harvested per 1000 cells three different plasmid extraction methods were tested. In the first, heat was used to boil the transfected cells for 5 mins followed by ethanol precipitation of total cellular DNA. This procedure failed to yield any colonies on antibiotic selective plates. The second method used Hirt extraction (Grillner and Blomberg, 1984), which is known to extract low molecular weight DNA from eukaryotic cells. This method produced hundreds of bacterial colonies on selective plates. However it was less efficient than the final method used which was the standard mini-prep kit (Qiagen) normally employed for isolating plasmid DNA from bacterial cells which gave approximately twice as many bacterial colonies from each extraction as the Hirt extraction. Therefore the mini-prep kit and ethanol precipitation were used to extract plasmid DNA from 293T cell in this study. It is also important to note that the YFP-cDNA library was based on the use of pEYFP-N1 as the cloning vector. This was done to favour recovery of YFP2-cDNA from transfected cell extracts as it allowed differentiation from the YFP1-NSP4 that was cloned into the pcDNA3 vector which carries an ampicillin resistance marker. This allowed the recovery of 220 kanamycin resistant bacterial colonies from the plasmid DNA extracted from 1000 fluorescing cells in the actual screen.

7.2.5 Use of YFP2-NSP4 to Examine the Sensitivity of the YFP-PCA Screen

The sensitivity of the YFP-PCA screen was studied following optimization of each step in the screen. For this the YFP2-NSP4 construct was mixed with YFP2 construct in a ratio of $1/10^5$ (i.e. 1 ng of YFP2-NSP4 construct mixed with 100 μg of YFP2 construct). The reason for the use of the dilution was because that ~10^6 bacterial colonies were collected in our construction of the YFP2-cDNA library. If 10 colonies harbored the correct cDNA inserts for positive hits, these positive hits in the library then accounted for $1/10^5$. Co-transfection of 200 ng of the mixed plasmids (i.e. YFP2 and YFP2-NSP4 constructs) with 2 μg of the YFP1-NSP4 in 293T cells resulted in 0.1%-0.5% of fluorescent cells similar to that seen in cells transfected with YFP2-cDNA and YFP1-NSP4. 1000 cells were then collected and extracted for plasmids following isolation of fluorescing cells. After electroporation of the plasmids into bacterial cells, 100 colonies were isolated. Re-transfection of these 100 plasmids with the YFP1-NSP4 in 24-well plates for 24-hour showed two out of 100 gave positive signals. Sequencing of these two clones identified that they were YFP2-NSP4. This control experiment (Fig 7.8) provided some evaluation of the functionality and sensitivity of the YFP-PCA assay established in this study.

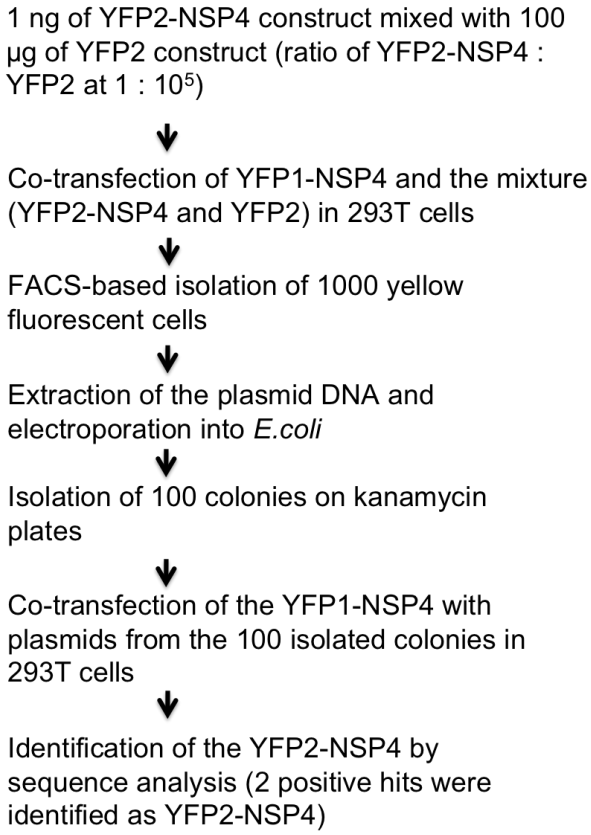

Figure 7.8: Examination of the sensitivity of the YFP-PCA screen.

7.2.6 Re-screening of Positive c-DNA and Final Identification of Cloned Inserts

Purification and re-transfection of the 220 plasmids (see section 7.2.4) into 293T cells with YFP1-NSP4 using a 96-well plate format showed 18 of them gave positive fluorescence and 39 of them gave weak fluorescence. However when re-transfection of the 57 fluorescent positive plasmids with YFP1-NSP4 in 24-well plates was carried out, only the 18 positives showed clearly positive fluorescence. Sequencing of these 18 plasmids showed that two of them encoded proteins (sterol regulatory element (SRE) binding protein and lysine specific demethylase 5C) and the other 16 plasmids only encoded short peptides downstream of YFP fragment 2. To investigate the possibility that the two proteins identified in this screen were actually interacting with the YFP fragment 1 region of the fusion protein rather than the NSP4 region, these two plasmid constructs were re-transfected with YFP1 construct. Figure 7.9 shows that this gave positive fluorescence in both cases showing that the identification of these two proteins represented false positives in the assay.

Figure 7.9: Interactions between YFP1 and two cDNA identified in the YFP-PCA screen.

Cells transfected with the indicated plasmid DNA constructs were examined using UV-light microscopy at 24 hours post transfection as described in Materials and Methods. Panel A Cells transfected with YFP1-NSP4 and YFP2-SRE binding protein showed positive fluorescence indicative of protein-protein interaction. Panel B Co-transfection of YFP1 and YFP2-SRE binding protein also showed positive fluorescence suggesting that the interaction occurred between YFP1 and SRE binding protein rather than NSP4 and SRE binding protein. Panel C Co-expression of YFP1-NSP4 and YFP2-lysine specific demethylase 5C resulted in positive detection of fluorescence. Panel D Co-transfection of YFP1 and YFP2-lysine specific demethylase 5C demonstrated that the interaction also occurred between YFP1 and lysine specific demethylase 5C rather than NSP4 and lysine specific demethylase 5C. Images were taken at magnification of 40×.

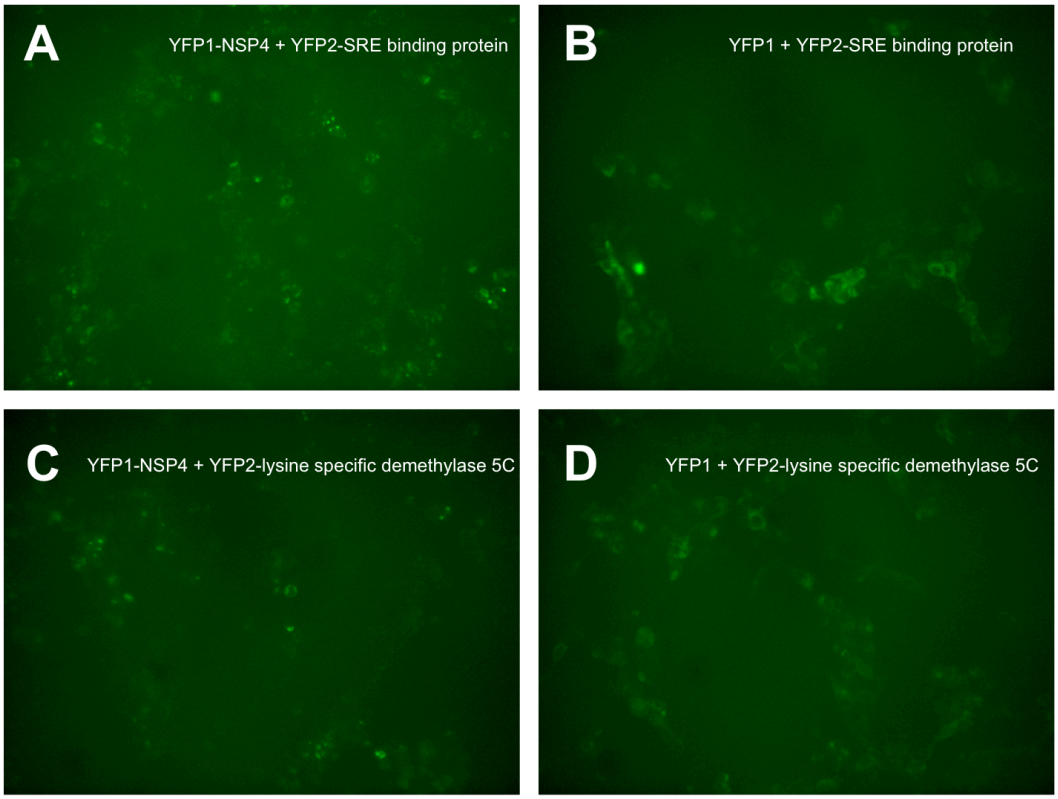
A
YFP1-NSP4 + YFP2-SRE binding protein
B
YFP1 + YFP2-SRE binding protein
C
YFP1-NSP4 + YFP2-lysine specific demethylase 5C
D
YFP1 + YFP2-lysine specific demethylase 5C

7.3 Conclusions

The experiments described in this chapter were aimed at identifying interactions between cellular proteins and rotavirus NSP4. To achieve this an YFP-PCA assay was exploited. This assay had the advantage that it allowed screening of interactions using full length NSP4 in live cells to identify protein-protein interactions. To establish the assay YFP2 in pcDNA3 was cloned into a kanamycin resistant cloning vector pEYFP-N1. And a full-length c-DNA for NSP4 the UKtc strain of rotavirus was fused in frame to the C-terminus of YFP1 and YFP2. Subsequent co-expression of YFP1-NSP4 and YFP2-NSP4 led to detection of positive yellow fluorescence in both 293T and BSC-1 cells.

The capability of the YFP-PCA assay to study involvement of glycosylation in the self-interaction of NSP4 was examined. To do this tunicamycin was added to the culture medium of cells transfected with YFP1-NSP4 and YFP2-NSP4. This treatment dramatically decreased the intensity of fluorescence by ~80%, suggesting that glycosylation is important for self-interaction of NSP4. Confirmation of this suggestion could be achieved through the manipulation of the glyco- mutants constructed in Chapter 3 into the YFP-PCA assay and this should be an important priority as work on NSP4 function moves forward.

To construct the YFP2-cDNA library mRNA from BSC-1 cells was extracted and converted into dsDNA (double-stranded DNA). The dsDNA was fused to YFP fragment 2 in three different reading frames to increase the chance of correct expression of all the c-DNAs present in the c-DNA library. Co-expression of YFP1-NSP4 and YFP2-cDNA was carried out in 293T cells and resulted in the detection of 1%-5% of fluorescent cells. In the screen carried out to identify interaction partners the amount of YFP2-cDNA was reduced to a ratio of 1/10 of that

of YFP1-NSP4 to minimize the number of copies of YFP2-cDNA in each cells. Although this also reduced the detection of fluorescent cells to 0.1%-0.5%, it increased the number of plasmid DNAs harboring truly positive interaction candidates for NSP4 following plasmid recovery on kanamycin plates. Following FACS-based cell isolation of 1000 fluorescence-positive cells, and extraction of plasmid DNA and its electroporation into *E .coli*, 220 kanamycin resistant colonies were obtained. Co-transfection of these 'rescued' YFP2-cDNA plasmids with YFP1-NSP4 showed that 18 out of 220 plasmids demonstrated clear positive fluorescence indicating positive interactions. However following sequence analysis only two out of 18 plasmids encoded proteins. Unfortunately these two proteins were subsequently shown to interact with YFP1 rather than NSP4. Despite isolation of false positive clones in the screen, the control experiment analyzing the sensitivity of the assay indicated the existing possibility to identify cellular partners of NSP4. For further screening, given weak fluorescence could be generated from false-positive clones, a threshold of fluorescent intensity could be set to distinguish real interactions (Nyfeler *et al*., 2008). Because the assay also identified cellular proteins interacting with YFP fragment 1 it is critical to test the interaction of the YFP fragment 1 and the isolated positive candidates.

Chapter 8

Discussion

8.1 Introduction

Rotavirus infection is a common cause of diarrhoea in young infants and children worldwide (Parashar *et al*., 2006). Studies of viral pathogenesis have shown that the virus primarily infects the tips of the villi in the small intestine of the gastrointestinal track. However it has been noted that early in the infection even when only a few epithelial cells are infected, the villi in a large area of the gut have become blunted and damaged prior to wide-spread distribution of the infection (Estes, 2001). An explanation for this observation was forthcoming following the identification of NSP4 as an enterotoxin (Bugarcic and Taylor, 2006; Zhang *et al*., 2000). The currently accepted mode for NSP4 action as an enterotoxin is that following synthesis, it is released from virus-infected cells. This secreted NSP4 is then postulated to bind to cellular receptors on surrounding uninfected cells and induce cytotoxic destruction of these cells (Seo *et al*., 2008).

8.2 Intracellular Expression of Wild Type and Glycosylation Mutants of NSP4

The early studies using pulse-chase analysis revealed that both unglycosylated NSP4 precursor and fully glycosylated NSP4 could be detected in virus-infected cells (McCrae and McCorquodale, 1982). Furthermore following a 2-hour chase of pulse-labeled samples, most of the unglycosylated NSP4 remained unmodified. By contrast the unglycosylated precursor of VP7 could only be detected if N-linked glycosylation was specifically blocked (McCrae and McCorquodale, 1982). The observation of two stable forms of NSP4 in infected cells raises the possibility that these different forms of the protein may differ in terms of their functionality.

A number of investigations have demonstrated that glycosylation is an important modification of NSP4. When expressed intracellularly, fully glycosylated NSP4 is

able to increase intracellular calcium levels (Tian *et al*., 1995; Tian *et al*., 1994). These elevated calcium levels have been shown to participate in a number of important events (formation of viroplasms, disruption of actin and microtubular networks, mediating DLP translocation from viroplasm into the ER lumen, distribution of other viral proteins and increased cytoplasmic membrane permeability) during the viral replication cycle (Berkova *et al*., 2007; Berkova *et al*., 2006; Diaz *et al*., 2008; Estes, 2001; Ruiz *et al*., 2005; Sen *et al*., 2007). Glycosylation has also been implicated as a requirement for secretion because only fully glycosylated NSP4 is detectable in the culture medium of infected polarized caco-2 cells (Bugarcic and Taylor, 2006). Given the importance of glycosylation of NSP4 in viral replication a number of studies have been done regarding its importance for NSP4 function. However they have almost all focused on the use of the broad-spectrum N-linked glycosylation inhibitor tunicamycin. The disadvantage of using tunicamycin is that N-linked glycosylation of cellular proteins is also blocked. This side effect may change the function of these cellular proteins requiring N-linked glycosylation and hence cause misleading results.

To avoid using tunicamycin for studying the functions of different forms of NSP4 we carried out PCR based site-directed mutagenesis to manipulate the coding sequence of NSP4, mutating two asparagines to alanines such that the mutated version of NSP4 would not be glycosylated. Comparison of the native and mutated version of NSP4 was carried out following expression from transfected plasmids in mammalian cells. The results showed that glycosylated NSP4 appeared to alter the cellular morphology of the transfected cells showing cytoplasmic extrusions at as early as 7.5 hours post transfection in BSR-T7 cells. By contrast this alteration in cellular morphology was not seen in cells transfected with a plasmid expressing

unglycosylated NSP4, although observation at later time post-transfection did not show any evidence of these cytoplasmic extrusions in cells expressing either glycosylated or unglycosylated NSP4. In order to examine whether these changes in cellular morphology were a feature of expression of glycosylated NSP4 in a rotavirus permissive cell line, BSC-1 cells were transfected and monitored using confocal microscopy which showed that glycosylated NSP4 stimulated changes in cellular morphology at 24 hours post transfection. Furthermore as with BSR-T7 cells no change in cellular morphology was seen in BSC-1 cells transfected with unglycosylated NSP4. These observations suggested that fully glycosylated NSP4 could modify cellular morphology promoting the formation of long cytoplasmic extrusions. Consistently long cytoplasmic projections have also been reported in fully confluent HEK 293 cells transfected with NSP4 constructs (Berkova *et al*., 2007). Berkova *et al*. also showed that actin participates in the formation of the cytoplasmic projections in a calcium dependent manner, demonstrated by changes in the actin network being inhibited following normalization of calcium levels (Berkova *et al*., 2007). Although this study did not examine the effect of expression of unglycosylated NSP4 in cells (Berkova *et al*., 2007), nevertheless prevention of increases in intracellular calcium levels either by the use of tunicamycin or through the use of RNAi (RNA interference) silencing of NSP4 suggested that increases in the intracellular calcium concentrations required glycosylation of NSP4 in infected cells (Ruiz *et al*., 2005; Zambrano *et al*., 2008). Based on these reported experiments unglycosylated NSP4 can be speculated as not being able to increase intracellular calcium levels. Assuming this to be the case the unglycosylated NSP4 would not be expected to show the alteration in actin network found in cells expressing glycosylated NSP4. The data presented here show that only glycosylated NSP4 could

alter cellular morphology and hence supports the hypothesis that differential glycosylation of NSP4 influences its function. Our study also revealed that the changes in cellular morphology seen in transfected cells expressing glyco+ NSP4 were found in virus-infected cells where cytoplasmic extrusions were seen at 10 hpi. This observation suggested that glyco+ NSP4 is responsible for the alteration in cellular morphology in infected cells.

8.2.1 Future Work

To validate the results obtained to-date, the glycosylation status of the NSP4 used in the study needs to be confirmed using sodium dodecyl sulphate polyacrylamide gel (SDS-PAGE). Furthermore our speculation that unglycosylated NSP4 cannot trigger increases in intracellular calcium levels will require validation. To do this, intracellular calcium indicators need to be employed to monitor calcium levels in cells transfected with an unglycosylated NSP4-GFP fusion protein. If these additional studies confirm the inability of unglycosylated NSP4-GFP to stimulate increases of intracellular calcium levels, then a dichotomy of function for the different forms of NSP4 will be established.

8.3 Analyzing the Formation of Cytoplasmic Extrusions in Virus-Infected Cells

Following the recognition of the cytoplasmic extrusions in 'snapshot' images of fixed samples, real time recording was employed to study the dynamics of their formation. To facilitate this an NSP4-GFP fusion protein was constructed and transfected into both BSR-T7 and BSC-1 cells. In BSR-T7 cells NSP4 specific antibody staining demonstrated that the GFP signal could be used to monitor intracellular localization of NSP4-GFP fusion protein. However cytoplasmic

extrusions were not observed in these experiments probably because visualization of the GFP signal required protein expression for 24 hours which was well beyond the 7.5 hours post transfection time that cytoplasmic extrusions were seen in fixed cells. By contrast, in BSC-1 cells real time observation did confirm the presence of cytoplasmic extrusions at 24 hours post transfection.

To observe cytoplasmic extrusions in virus-infected cells, cells were first transfected with a CMV-YFP construct which expressed YFP to allow the cell morphology of transfected cells to be monitored in real time. Using fluorescent confocal microscopy on these cells following their infection with virus, we were able to show the dynamic process of cytoplasmic extrusions projecting out from the infected cells at 14 hpi. However, photobleaching of the fluorescent protein and photo toxicity prevented YFP fluorescence being used for continuous monitoring of the extrusion process. Therefore transmission light confocal microscopy was employed to record the cytoplasmic extrusions. This minimized photo toxicity caused by the scanning laser and showed a clear dynamic growth of cytoplasmic extrusions with a growth speed of 2 μm/min being estimated. To exclude the possibility that these observations were not rotavirus specific or seen solely in apoptotic cells, control assays employing reovirus and PAC-1 were used. The results showed that cells treated with either reovirus or PAC-1 did not display the cytoplasmic extrusions found in rotavirus-infected cells.

8.3.1 Future Work

An important priority for future experiments is quantitation of the changes observed, that is measurement of the percentage of cells showing cytoplasmic extrusions at different times post infection. To do this, several selected viewing fields containing

20-30 virus-infected BSC-1 cells can be monitored using confocal microscopy. However in addition to doing these studies in BSC-1 cells they should also be performed in differentiated caco-2 cells. The latter are preferable because when fully differentiated they more closely resemble the cells that rotaviruses infect *in vivo*.

8.4 Functioning of the Cytoplasmic Extrusion in Viral Infection

The observation of cytoplasmic extrusions in infected cells led us to speculate that they may function to deliver material from infected cells to uninfected cells. To investigate this possibility, mixtures of virus-infected and uninfected cells separately tagged with Cell Tracker dyes were employed to follow the flow of cellular material from infected cells. No transfer of Cell Tracker dyes among uninfected cells was detected. However, the Cell Tracker dyes from virus-infected cells were found in vesicular structures scattered on the surface of uninfected cells following destruction of the cytoplasmic extrusions and these vesicles were subsequently internalized into uninfected cells. These experiments using Cell Tracker dyes provided support for the possibility that NSP4 was also transferred between cells through the cytoplasmic extrusions. Direct experimental evidence in support of this possibility was obtained using NSP4 specific antibody to stain NSP4 in the scattered vesicle structures on uninfected cells. These results have begun the process of unraveling a new mechanism for the spread of NSP4 cytotoxicity from virus-infected cells to surrounding uninfected cells.

8.4.1 Future Work

Future studies are clearly required to both confirm the observations made thus far and also extend analysis of the process. A start on this could involve using the

recently developed reverse genetic technology for rotaviruses (Troupin *et al*., 2010) to construct a recombinant virus which is able to express fluorescently tagged NSP4. The spread of NSP4 through cytoplasmic extrusions could then be monitored in virus-infected cells using real-time fluorescent confocal microscopy. The efficiency of the cytoplasmic extrusions in spreading NSP4 could also be determined using quantitative imaging (Piston *et al*., 1999).

8.5 Microtubular Network in Cells Expressing NSP4 or Infected with Virus

The cytoplasmic extrusions seen in infected cells implied that the cellular skeleton must be undergoing re-arrangement. The actin network in cells expressing NSP4 has already been studied (Berkova *et al*., 2007) and therefore we focused on analyzing the effect of expression of NSP4 on the microtubular network. Following expression of NSP4 in BSC-1 cells changes to the microtubular network were clearly evident at 24 hours post transfection. The changes seen were glycosylation independent with the glycosylation mutant of NSP4 displaying the same pattern of disassembly of the microtubular network seen in wild type NSP4 transfected cells. Further analysis showed that the disassembly started from the centre of the cell, with a re-polymerization of microtubules occurring to produce a ring like feature at the periphery of the cell. This pattern of disassembly/reassembly was similar to that seen in virus infected cells suggesting that NSP4 functions to alter the microtubular network during the viral replication cycle. It has been reported that NSP2 induces microtubular de-polymerization through sequestration of free tubulin molecules to tubulin granules (Martin *et al*., 2010). However it is possible to speculate that it is actually NSP4 mediates the major changes in microtubular polymerization with NSP2 merely enhancing the effect by its binding to tubulin. Cells undergoing

apoptosis have also been reported to display disassembly of the microtubular network and polymerization of microtubules at the cell periphery (Sanchez-Alcazar *et al*., 2007) similar to that seen in our study. We therefore speculated that NSP4 induced apoptosis might actually be the trigger for the observed changes in the microtubular network. However study of apoptosis and necrosis following expression of NSP4 showed that NSP4 did not trigger either apoptosis or necrosis, suggesting that apoptosis was not the pathway used by NSP4 to mediate changes in the microtubular network.

Detection of β-tubulin and F-actin in the cytoplasmic extrusions suggested that these two proteins were involved in forming these extrusions. In support of this suggestion, the formation of cytoplasmic extrusions was inhibited following addition of chemical inhibitors of either tubulin or actin polymerization. Interestingly when the microtubule network was de-polymerized using nocodazole, the released microtubules were able to form striking long tubes in the cytoplasm of infected cells. Formation of these long microtubular tubes was inhibited by blocking the synthesis of viral proteins suggesting that they caused this phenomenon and thus were potentially capable of accumulating tubulin to enhance the effect of de-polymerization of microtubular network in infected cells.

8.5.1 Future Work

An important next step is to determine whether NSP4 is the only viral protein responsible for microtubular de-polymerization in infected cells. To achieve this, the effect of RNAi specific silencing of NSP4 on the integrity of the microtubular network can be examined.

8.6 Screening for Cellular Interaction Partners of NSP4

The YFP-PCA assay described in the final results chapter established a system for screening cellular partners interacting with full length NSP4. The advantage of this screening assay was that it preserved both of the glycosylation sites in the N-terminal domain of NSP4 and many of the functional domains reported in C-terminal of NSP4. This contrasts with the truncated version of NSP4 with reduced cytotoxicity used in a previous report designed to capture cellular partners of NSP4 (Boshuizen *et al*., 2004). Using a construct in which YFP1 was fused to the N-terminus of NSP4 we attempted to identify cellular proteins involved in the glycosylation of NSP4 or its intracellular trafficking. In the preliminary control experiments NSP4, VP4 and VP6 were all cloned into constructs for use in YFP-PCA assays. Co-transfections of NSP4-NSP4, NSP4-VP4 and NSP4-VP6 demonstrated that only NSP4-NSP4 interaction was seen in the assay. NSP4's ability to interact with itself to form oligomers has been shown previously using SDS-PAGE (Maass and Atkinson, 1990), providing some validation of our use of the YFP-PCA assay approach. Following the screening procedure two proteins (sterol regulatory element (SRE) binding protein and lysine specific demethylase 5C) were isolated as interacting with the YFP1-NSP4 fusion protein. However in the validation step they were identified as false positive clones as they also interacted with YFP1 fragment. Despite the failure to identify cellular partner of NSP4 in the first attempt, the feasibility of the YFP-PCA assay was demonstrated in a control experiment that aimed at examining the sensitivity of the assay. In this control, it was found that the YFP-PCA assay using in our study was sufficient to isolate one target plasmid from a pool containing over 100,000 off-target plasmids.

8.6.1 Future Work

The immediate future work would be to repeat the YFP-PCA screen to further optimize it for identifying cellular partners of NSP4. Furthermore, our YFP1-NSP4 construct was designed to isolate cellular partners interacting with N-terminal tail of NSP4 in the ER. To isolation cellular partners in the cytosol of cells YFP fragment 1 can be fused to the C-terminus of YFP1-NSP4 to construct an YFP1-NSP4-YFP1 fusion protein as bait for screening. Such YFP1-NSP4-YFP1 fusion protein presents YFP fragment 1 both in the ER and the cytosol of cells so that cellular partners fused with YFP fragment 2 and interacting with different domains of NSP4 would be revealed from subsequent screening.

8.7 Future Work on NSP4

8.7.1 Understanding of NSP4 Induced Changes in Calcium Homeostasis and Intracellular Trafficking of NSP4

The Ca^{2+} homeostasis changes in rotavirus-infected cells have been shown to be primarily associated with NSP4 rather than the other viral glycoprotein VP7 using RNAi technology (Diaz *et al*., 2008; Zambrano *et al*., 2008). This disturbance of Ca^{2+} has an important role throughout the viral replication cycle (Ruiz *et al*., 2000; Zambrano *et al*., 2008). However the precise mechanism of this function of NSP4 remains unclear. To gain an understanding of the homeostasis of Ca^{2+} in NSP4 expressing cells, the YFP-PCA assay provides a practicable approach that is able to identify cellular partners of NSP4. By knowing these proteins and their roles in the cellular metabolism, the mechanism used by NSP4 to affect homeostasis of Ca^{2+} can then be proposed. The secretion pathway of NSP4 is also worthy of investigation. One approach would be to focus on possible interactions of NSP4 with cellular

proteins identified by the YFP-PCA assay and known to be involved in the pathway.

8.7.2 Study of NSP4-Caveolin Interaction

Recently NSP4 has been shown to interact with both the N- and C- termini of caveolin (Mir *et al*., 2007; Parr *et al*., 2006). These interactions lead to the observation of an NSP4-caveolae association on the plasma membrane which is believed to be the final cellular destination of secreted NSP4 (Storey *et al*., 2007). The possible involvement of caveolin and caveolae in the putative secretion of NSP4 provides a new approach to study intracellular trafficking of NSP4 probably by studying trafficking pathway of caveolin using confocal microscopy and markers of cellular structures. In addition, the importance of this caveolin-NSP4 interaction in different functionalities of NSP4 can be studied by over-expression of dominant-negative version of caveolin in cells (Sieczkarski and Whittaker, 2002) prior to expression of NSP4. Furthermore, infection on the caveolin knockout mice (Sieczkarski and Whittaker, 2002) with rotavirus would provide an approach to study the relevance of the caveolin-NSP4 interaction to viral pathology.

8.7.3 Entero-toxic Mechanism of Exogenous NSP4

It is known that exogenous addition of NSP4 to cells promotes intracellular calcium increases through a mechanism that is different from that of endogenously expressed NSP4 (Tian *et al*., 1995). To date, studies of exogenous NSP4 have been shown that NSP4 initially binds to cellular receptors (integrins $\alpha1\beta1$ and $\alpha2\beta1$) and stimulates a PLC-IP3 dependent pathway (Dong *et al*., 1997; Seo *et al*., 2008). These actions of NSP4 are currently thought to be responsible for inducing diarrhoea seen in rotaviral

disease (Dong *et al*., 1997; Seo *et al*., 2008). However this conclusion does require additional evidence to substantiate it and the possible involvement of other cellular receptors and pathways have not been excluded. One approach to progress this area could be to exploit the recently developed reverse genetics technology for rotavirus (Troupin *et al*., 2010) using segment 10 (encodes NSP4) mutants carrying introduced point mutations or deletions for the entero-toxic function of NSP4. The pathology of the recombinant virus can be examined and compared to the wild type virus using both tissue culture and experimental animal approaches.

8.8 Remaining questions about NSP4

Many important questions of NSP4 remained to be addressed in the future:

- What is the story of age-dependent diarrhoea induced by NSP4?
- What is/are the cellular signaling pathway(s) that NSP4 participates in?
- Does unglycosylated NSP4 play a role different from glycosylated NSP4 in infected cells?
- Does the secreted NSP4 function similarly both *in vitro* and *in vivo* situation?
- How is the enteric nervous system involved in the pathogenesis of NSP4?
- What are the mechanisms used by endogenously and/or exogenously expressed NSP4 to stimulate cell death?

The occurrence of diarrhoea is a multi-component process involving secretory mediators, water and electrolytes and the responses of different cell types in the intestinal track. The enterotoxin found as being NSP4 shed the light on understanding the basic pathogenesis of rotavirus-induced illness. Knowledge of functionalities of NSP4 is still extending, in the future the story of NSP4 will be better understood by using novel technologies.

9. References

Afrikanova, I., Miozzo, M. C., Giambiagi, S., and Burrone, O. (1996): Phosphorylation generates different forms of rotavirus NSP5. *J Gen Virol* **77**, 2059-2065.

Altenburg, B. C., Graham, D. Y., and Estes, M. K. (1980): Ultrastructural study of rotavirus replication in cultured cells. *J Gen Virol* **46**, 75-85.

Ansari, S. A., Sattar, S. A., Springthorpe, V. S., Wells, G. A., and Tostowaryk, W. (1989): In vivo protocol for testing efficacy of hand-washing agents against viruses and bacteria: experiments with rotavirus and Escherichia coli. *Appl Environ Microbiol* **55**, 3113-3118.

Anthony, I. D., Bullivant, S., Dayal, S., Bellamy, A. R., and Berriman, J. A. (1991): Rotavirus spike structure and polypeptide composition. *J Virol* **65**, 4334-4340.

Arias, C. F., Dector, M. A., Segovia, L., Lopez, T., Camacho, M., Isa, P., Espinosa, R., and Lopez, S. (2004): RNA silencing of rotavirus gene expression. *Virus Res* **102**, 43-51.

Arnoldi, F., Campagna, M., Eichwald, C., Desselberger, U., and Burrone, O. R. (2007): Interaction of rotavirus polymerase VP1 with nonstructural protein NSP5 is stronger than that with NSP2. *J Virol* **81**, 2128-2137.

Au, K. S., Chan, W. K., Burns, J. W., and Estes, M. K. (1989): Receptor activity of rotavirus nonstructural glycoprotein NS28. *J Virol* **63**, 4553-4562.

Au, K. S., Mattion, N. M., and Estes, M. K. (1993): A subviral particle binding domain on the rotavirus nonstructural glycoprotein NS28. *Virology* **194**, 665-673.

Ball, J. M., Tian, P., Zeng, C. Q. Y., Morris, A. P., and Estes, M. K. (1996): Age-dependent diarrhea induced by a rotaviral nonstructural glycoprotein. *Science* **272**, 101-104.

Banyai, K., Papp, H., Dandar, E., Molnar, P., Mihaly, I., Van Ranst, M., Martella, V., and Matthijnssens, J. (2010): Whole genome sequencing and phylogenetic analysis of a zoonotic human G8P[14] rotavirus strain. *Infect Genet Evol* **10**, 1140-1144.

Barardi, C. R., Yip, H., Emsile, K. R., Vesey, G., Shanker, S. R., and Williams, K. L. (1999): Flow cytometry and RT-PCR for rotavirus detection in artificially

seeded oyster meat. *Int J Food Microbiol* **49**, 9-18.

Barro, M., and Patton, J. T. (2005): Rotavirus nonstructural protein 1 subverts innate immune response by inducing degradation of IFN regulatory factor 3. *Proc Natl Acad Sci U S A* **102**, 4114-4119.

Barro, M., and Patton, J. T. (2007): Rotavirus NSP1 inhibits expression of type I interferon by antagonizing the function of interferon regulatory factors IRF3, IRF5, and IRF7. *J Virol* **81**, 4473-4481.

Bass, D. M., Baylor, M., Chen, C., and Upadhyayula, U. (1995): Dansylcadaverine and cytochalasin D enhance rotavirus infection of murine L cells. *Virology* **212**, 429-437.

Baybutt, H. N., and McCrae, M. A. (1984): The molecular biology of rotaviruses. VII. Detailed structural analysis of gene 10 of bovine rotavirus. *Virus Res* **1**, 533-541.

Bergmann, C. C., Maass, D., Poruchynsky, M. S., Atkinson, P. H., and Bellamy, A. R. (1989): Topology of the non-structural rotavirus receptor glycoprotein NS28 in the rough endoplasmic reticulum. *EMBO J* **8**, 1695-1703.

Berkova, Z., Crawford, S. E., Blutt, S. E., Morris, A. P., and Estes, M. K. (2007): Expression of rotavirus NSP4 alters the actin network organization through the actin remodeling protein cofilin. *J Virol* **81**, 3545-3553.

Berkova, Z., Crawford, S. E., Trugnan, G., Yoshimori, T., Morris, A. P., and Estes, M. K. (2006): Rotavirus NSP4 induces a novel vesicular compartment regulated by calcium and associated with viroplasms. *J Virol* **80**, 6061-6071.

Berkova, Z., Morris, A. P., and Estes, M. K. (2003a): Cytoplasmic calcium measurement in rotavirus enterotoxin-enhanced green fluorescent protein (NSP4-EGFP) expressing cells loaded with Fura-2. *Cell Calcium* **34**, 55-68.

Berkova, Z., Morris, A. P., and Estes, M. K. (2003b): PLC-independent elevation of cytoplasmic calcium in mammalian cells inducibly expressing a rotavirus enterotoxin NSP4-EGFP fusion protein. *Gastroenterology* **124**, A313-A313.

Borghan, M. A., Mori, Y., El-Mahmoudy, A. B., Ito, N., Sugiyama, M., Takewaki, T., and Minamoto, N. (2007): Induction of nitric oxide synthase by rotavirus enterotoxin NSP4: implication for rotavirus pathogenicity. *J Gen Virol* **88**, 2064-2072.

Boshuizen, J. A., Rossen, J. W. A., Sitaram, C. K., Kimenai, F. F. P., Simons-Oosterhuis, Y., Laffeber, C., Buller, H. A., and Einerhand, A. W. C. (2004): Rotavirus enterotoxin NSP4 binds to the extracellular matrix proteins laminin-beta 3 and fibronectin. *Journal of Virology* **78**, 10045-10053.

Both, G. W., Siegman, L. J., Bellamy, A. R., and Atkinson, P. H. (1983): Coding assignment and nucleotide sequence of simian rotavirus SA11 gene segment

10: location of glycosylation sites suggests that the signal peptide is not cleaved. *J Virol* **48**, 335-339.

Brandt, C. D., Kim, H. W., Rodriguez, W. J., Arrobio, J. O., Jeffries, B. C., Stallings, E. P., Lewis, C., Miles, A. J., Chanock, R. M., Kapikian, A. Z., and Parrott, R. H. (1983): Pediatric viral gastroenteritis during eight years of study. *J Clin Microbiol* **18**, 71-78.

Bridger, J. C., and Woode, G. N. (1976): Characterization of two particle types of calf rotavirus. *J Gen Virol* **31**, 245-250.

Brunet, J. P., Cotte-Laffitte, J., Linxe, C., Quero, A. M., Geniteau-Legendre, M., and Servin, A. (2000a): Rotavirus infection induces an increase in intracellular calcium concentration in human intestinal epithelial cells: role in microvillar actin alteration. *J Virol* **74**, 2323-2332.

Brunet, J. P., Jourdan, N., Cotte-Laffitte, J., Linxe, C., Geniteau-Legendre, M., Servin, A., and Quero, A. M. (2000b): Rotavirus infection induces cytoskeleton disorganization in human intestinal epithelial cells: implication of an increase in intracellular calcium concentration. *J Virol* **74**, 10801-10806.

Buchholz, U. J., Finke, S., and Conzelmann, K. K. (1999): Generation of bovine respiratory syncytial virus (BRSV) from cDNA: BRSV NS2 is not essential for virus replication in tissue culture, and the human RSV leader region acts as a functional BRSV genome promoter. J Virol 73, 251-259.

Bugarcic, A., and Taylor, J. A. (2006): Rotavirus nonstructural glycoprotein NSP4 is secreted from the apical surfaces of polarized epithelial cells. *J Virol* **80**, 12343-12349.

Burns, J. W., Siadat-Pajouh, M., Krishnaney, A. A., and Greenberg, H. B. (1996): Protective effect of rotavirus VP6-specific IgA monoclonal antibodies that lack neutralizing activity. *Science* **272**, 104-107.

Cabral-Romero, C., and Padilla-Noriega, L. (2006): Association of rotavirus viroplasms with microtubules through NSP2 and NSP5. *Mem Inst Oswaldo Cruz* **101**, 603-611.

Campagna, M., Eichwald, C., Vascotto, F., and Burrone, O. R. (2005): RNA interference of rotavirus segment 11 mRNA reveals the essential role of NSP5 in the virus replicative cycle. *J Gen Virol* **86**, 1481-1487.

Carpio, M., Bellamy, J. E., and Babiuk, L. A. (1981): Comparative virulence of different bovine rotavirus isolates. *Can J Comp Med* **45**, 38-42.

Centers for Disease Control and Prevention (2008): Rotavirus surveillance--worldwide, 2001-2008. *MMWR Morb Mortal Wkly Rep* **57**, 1255-1257.

Centers for Disease Control and Prevention (1999): Withdrawal of rotavirus

vaccine recommendation. *MMWR Morb Mortal Wkly Rep* **48**, 1007.

Chandran, A., and Santosham, M. (2008): RotaTeq: a three-dose oral pentavalent reassortant rotavirus vaccine. *Expert Rev Vaccines* **7**, 1475-1480.

Chen, D., Luongo, C. L., Nibert, M. L., and Patton, J. T. (1999): Rotavirus open cores catalyze 5'-capping and methylation of exogenous RNA: evidence that VP3 is a methyltransferase. *Virology* **265**, 120-130.

Chen, D., and Ramig, R. F. (1993a): Rescue of infectivity by in vitro transcapsidation of rotavirus single-shelled particles. *Virology* **192**, 422-429.

Chen, D., and Ramig, R. F. (1993b): Rescue of infectivity by sequential in vitro transcapsidation of rotavirus core particles with inner capsid and outer capsid proteins. *Virology* **194**, 743-751.

Ciarlet, M., Crawford, S. E., Cheng, E., Blutt, S. E., Rice, D. A., Bergelson, J. M., and Estes, M. K. (2002): VLA-2 (alpha2beta1) integrin promotes rotavirus entry into cells but is not necessary for rotavirus attachment. *J Virol* **76**, 1109-1123.

Cohen, J., Laporte, J., Charpilienne, A., and Scherrer, R. (1979): Activation of rotavirus RNA polymerase by calcium chelation. *Arch Virol* **60**, 177-186.

Collins, J. E., Benfield, D. A., and Duimstra, J. R. (1989): Comparative virulence of two porcine group-A rotavirus isolates in gnotobiotic pigs. *Am J Vet Res* **50**, 827-835.

Colomina, J., Gil, M. T., Codoner, P., and Buesa, J. (1998): Viral proteins VP2, VP6, and NSP2 are strongly precipitated by serum and fecal antibodies from children with rotavirus symptomatic infection. *J Med Virol* **56**, 58-65.

Contin, R., Arnoldi, F., Campagna, M., and Burrone, O. R. (2010): Rotavirus NSP5 orchestrates recruitment of viroplasmic proteins. *J Gen Virol* **91**, 1782-1793.

Cook, S. M., Glass, R. I., LeBaron, C. W., and Ho, M. S. (1990): Global seasonality of rotavirus infections. *Bull World Health Organ* **68**, 171-177.

Crawford, S. E., Labbe, M., Cohen, J., Burroughs, M. H., Zhou, Y. J., and Estes, M. K. (1994): Characterization of virus-like particles produced by the expression of rotavirus capsid proteins in insect cells. *J Virol* **68**, 5945-5952.

Cuadras, M. A., Arias, C. F., and Lopez, S. (1997): Rotaviruses induce an early membrane permeabilization of MA104 cells and do not require a low intracellular Ca2+ concentration to initiate their replication cycle. *J Virol* **71**, 9065-9074.

Dector, M. A., Romero, P., Lopez, S., and Arias, C. F. (2002): Rotavirus gene silencing by small interfering RNAs. *EMBO Rep* **3**, 1175-1180.

Diaz, Y., Chemello, M. E., Pena, F., Aristimuno, O. C., Zambrano, J. L., Rojas, H., Bartoli, F., Salazar, L., Chwetzoff, S., Sapin, C., Trugnan, G., Michelangeli, F., and Ruiz, M. C. (2008): Expression of nonstructural rotavirus protein NSP4 mimics Ca2+ homeostasis changes induced by rotavirus infection in cultured cells. *J Virol* **82**, 11331-11343.

Dong, Y., Zeng, C. Q., Ball, J. M., Estes, M. K., and Morris, A. P. (1997): The rotavirus enterotoxin NSP4 mobilizes intracellular calcium in human intestinal cells by stimulating phospholipase C-mediated inositol 1,4,5-trisphosphate production. *Proc Natl Acad Sci U S A* **94**, 3960-3865.

Eichwald, C., Rodriguez, J. F., and Burrone, O. R. (2004): Characterization of rotavirus NSP2/NSP5 interactions and the dynamics of viroplasm formation. *J Gen Virol* **85**, 625-634.

Eiden, J. J., Wilde, J., Firoozmand, F., and Yolken, R. (1991): Detection of animal and human group B rotaviruses in fecal specimens by polymerase chain reaction. *J Clin Microbiol* **29**, 539-543.

Ellens, D. J., and de Leeuw, P. W. (1977): Detection of infantile gastroenteritis virus (rotavirus) by ELISA. *Lancet* **1**, 1363-1364.

Ericson, B. L., Graham, D. Y., Mason, B. B., Hanssen, H. H., and Estes, M. K. (1983): Two types of glycoprotein precursors are produced by the simian rotavirus SA11. *Virology* **127**, 320-332.

Estes, M. K. (2001): Rotavirus and Their Replication. In e. a. K.M. David (Ed.): *Fields Virology*, pp. 731-741. Philadelphia: Lippincott Williams & Wilkins.

Estes, M. K., Crawford, S. E., Penaranda, M. E., Petrie, B. L., Burns, J. W., Chan, W. K., Ericson, B., Smith, G. E., and Summers, M. D. (1987): Synthesis and immunogenicity of the rotavirus major capsid antigen using a baculovirus expression system. *J Virol* **61**, 1488-1494.

Estes, M. K., Graham, D. Y., Smith, E. M., and Gerba, C. P. (1979): Rotavirus stability and inactivation. *J Gen Virol* **43**, 403-409.

Fabbretti, E., Afrikanova, I., Vascotto, F., and Burrone, O. R. (1999): Two non-structural rotavirus proteins, NSP2 and NSP5, form viroplasm-like structures in vivo. *J Gen Virol* **80 (Pt 2)**, 333-339.

Fleming, F. E., Graham, K. L., Taniguchi, K., Takada, Y., and Coulson, B. S. (2007): Rotavirus-neutralizing antibodies inhibit virus binding to integrins alpha 2 beta 1 and alpha 4 beta 1. *Arch Virol* **152**, 1087-1101.

Flewett, T. H., and G. N. Woode. (1978): Rotaviruses. *Archives of Virology*, 1-25.

Flewett, T. H., Bryden, A. S., Davies, H., Woode, G. N., Bridger, J. C., and Derrick, J. M. (1974): Relation between viruses from acute gastroenteritis of

children and newborn calves. *Lancet* **2**, 61-63.

Fukuhara, N., Yoshie, O., Kitaoka, S., and Konno, T. (1988): Role of VP3 in human rotavirus internalization after target cell attachment via VP7. *J Virol* **62**, 2209-2218.

Fukuhara, N., Yoshie, O., Kitaoka, S., Konno, T., and Ishida, N. (1987): Evidence for endocytosis-independent infection by human rotavirus. *Arch Virol* **97**, 93-99.

Gardet, A., Breton, M., Trugnan, G., and Chwetzoff, S. (2007): Role for actin in the polarized release of rotavirus. *J Virol* **81**, 4892-4894.

Gonzalez, S. A., and Burrone, O. R. (1989): Porcine OSU rotavirus segment II sequence shows common features with the viral gene of human origin. *Nucleic Acids Res* **17**, 6402.

Gorziglia, M., Larrea, C., Liprandi, F., and Esparza, J. (1985): Biochemical evidence for the oligomeric (possibly trimeric) structure of the major inner capsid polypeptide (45K) of rotaviruses. *J Gen Virol* **66 (Pt 9)**, 1889-1900.

Gorziglia, M., Nishikawa, K., and Fukuhara, N. (1989): Evidence of duplication and deletion in super short segment 11 of rabbit rotavirus Alabama strain. *Virology* **170**, 587-590.

Graff, J. W., Ettayebi, K., and Hardy, M. E. (2009): Rotavirus NSP1 inhibits NFkappaB activation by inducing proteasome-dependent degradation of beta-TrCP: a novel mechanism of IFN antagonism. *PLoS Pathog* **5**, e1000280.

Graff, J. W., Mitzel, D. N., Weisend, C. M., Flenniken, M. L., and Hardy, M. E. (2002): Interferon regulatory factor 3 is a cellular partner of rotavirus NSP1. *J Virol* **76**, 9545-9550.

Graham, D. Y., Dufour, G. R., and Estes, M. K. (1987): Minimal infective dose of rotavirus. *Arch Virol* **92**, 261-271.

Graham, K. L., Fleming, F. E., Halasz, P., Hewish, M. J., Nagesha, H. S., Holmes, I. H., Takada, Y., and Coulson, B. S. (2005): Rotaviruses interact with alpha4beta7 and alpha4beta1 integrins by binding the same integrin domains as natural ligands. *J Gen Virol* **86**, 3397-3408.

Graham, K. L., Halasz, P., Tan, Y., Hewish, M. J., Takada, Y., Mackow, E. R., Robinson, M. K., and Coulson, B. S. (2003): Integrin-using rotaviruses bind alpha2beta1 integrin alpha2 I domain via VP4 DGE sequence and recognize alphaXbeta2 and alphaVbeta3 by using VP7 during cell entry. *J Virol* **77**, 9969-9978.

Graham, K. L., Zeng, W., Takada, Y., Jackson, D. C., and Coulson, B. S. (2004): Effects on rotavirus cell binding and infection of monomeric and polymeric

peptides containing alpha2beta1 and alphaxbeta2 integrin ligand sequences. *J Virol* **78**, 11786-11797.

Greenberg, H., McAuliffe, V., Valdesuso, J., Wyatt, R., Flores, J., Kalica, A., Hoshino, Y., and Singh, N. (1983a): Serological analysis of the subgroup protein of rotavirus, using monoclonal antibodies. *Infect Immun* **39**, 91-99.

Greenberg, H. B., Flores, J., Kalica, A. R., Wyatt, R. G., and Jones, R. (1983b): Gene coding assignments for growth restriction, neutralization and subgroup specificities of the W and DS-1 strains of human rotavirus. *J Gen Virol* **64**, 313-320.

Grillner, L., and Blomberg, I. (1984): Restriction enzyme analysis of human cytomegalovirus using DNA extracted from infected cells. *J Med Virol* **14**, 313-322.

Gualtero, D. F., Guzman, F., Acosta, O., and Guerrero, C. A. (2007): Amino acid domains 280-297 of VP6 and 531-554 of VP4 are implicated in heat shock cognate protein hsc70-mediated rotavirus infection. *Arch Virol* **152**, 2183-2196.

Guerrero, C. A., Bouyssounade, D., Zarate, S., Isa, P., Lopez, T., Espinosa, R., Romero, P., Mendez, E., Lopez, S., and Arias, C. F. (2002): Heat shock cognate protein 70 is involved in rotavirus cell entry. *J Virol* **76**, 4096-4102.

Guerrero, C. A., Mendez, E., Zarate, S., Isa, P., Lopez, S., and Arias, C. F. (2000): Integrin alpha(v)beta(3) mediates rotavirus cell entry. *Proc Natl Acad Sci U S A* **97**, 14644-14649.

Gutierrez, M., Isa, P., Sanchez-San Martin, C., Perez-Vargas, J., Espinosa, R., Arias, C. F., and Lopez, S. (2010): Different Rotavirus Strains Enter MA104 Cells through Different Endocytic Pathways: the Role of Clathrin-Mediated Endocytosis. *J Virol* **84**, 9161-9169.

Guzman, E., and McCrae, M. A. (2005): Molecular characterization of the rotavirus NSP4 enterotoxin homologue from group B rotavirus. *Virus Res* **110**, 151-160.

Haffejee, I. E. (1995): The epidemiology of rotavirus infections: a global perspective. *J Pediatr Gastroenterol Nutr* **20**, 275-286.

Harb, M., Becker, M. M., Vitour, D., Baron, C. H., Vende, P., Brown, S. C., Bolte, S., Arold, S. T., and Poncet, D. (2008): Nuclear localization of cytoplasmic poly(A)-binding protein upon rotavirus infection involves the interaction of NSP3 with eIF4G and RoXaN. *J Virol* **82**, 11283-11293.

Haselhorst, T., Fleming, F. E., Dyason, J. C., Hartnell, R. D., Yu, X., Holloway, G., Santegoets, K., Kiefel, M. J., Blanchard, H., Coulson, B. S., and von Itzstein, M. (2009): Sialic acid dependence in rotavirus host cell invasion. *Nat Chem Biol* **5**, 91-93.

Heath, R. R., Stagg, S., Xu, F., and McCrae, M. A. (1997): Mapping of the target antigens of the rotavirus-specific cytotoxic T cell response. *J Gen Virol* **78**, 1065-1075.

Hoffman, R. A., Zhang, G., Nussler, N. C., Gleixner, S. L., Ford, H. R., Simmons, R. L., and Watkins, S. C. (1997): Constitutive expression of inducible nitric oxide synthase in the mouse ileal mucosa. *Am J Physiol* **272**, G383-392.

Holloway, G., Truong, T. T., and Coulson, B. S. (2009): Rotavirus antagonizes cellular antiviral responses by inhibiting the nuclear accumulation of STAT1, STAT2, and NF-kappaB. *J Virol* **83**, 4942-4951.

Honda, K., Yanai, H., Negishi, H., Asagiri, M., Sato, M., Mizutani, T., Shimada, N., Ohba, Y., Takaoka, A., Yoshida, N., and Taniguchi, T. (2005): IRF-7 is the master regulator of type-I interferon-dependent immune responses. *Nature* **434**, 772-777.

Horie, Y., Nakagomi, O., Koshimura, Y., Nakagomi, T., Suzuki, Y., Oka, T., Sasaki, S., Matsuda, Y., and Watanabe, S. (1999): Diarrhea induction by rotavirus NSP4 in the homologous mouse model system. *Virology* **262**, 398-407.

Hoshino, Y., and Kapikian, A. Z. (1996): Classification of rotavirus VP4 and VP7 serotypes. *Arch Virol Suppl* **12**, 99-111.

Hou, Z. L., Huang, T., Huan, Y. M., Pang, W., Meng, M. Y., Wang, P., Yang, M. F., Jiang, L. H., Cao, X. N., and Wu, K. K. (2008): Anti-NSP4 antibody can block rotavirus-induced diarrhea in mice. *Journal of Pediatric Gastroenterology and Nutrition* **46**, 376-385.

Huilan, S., Zhen, L. G., Mathan, M. M., Mathew, M. M., Olarte, J., Espejo, R., Khin Maung, U., Ghafoor, M. A., Khan, M. A., Sami, Z., and *et al.* (1991): Etiology of acute diarrhoea among children in developing countries: a multicentre study in five countries. *Bull World Health Organ* **69**, 549-555.

Imai, M., Akatani, K., Ikegami, N., and Furuichi, Y. (1983): Capped and conserved terminal structures in human rotavirus genome double-stranded RNA segments. *J Virol* **47**, 125-136.

Imataka, H., Gradi, A., and Sonenberg, N. (1998): A newly identified N-terminal amino acid sequence of human eIF4G binds poly(A)-binding protein and functions in poly(A)-dependent translation. *EMBO J* **17**, 7480-7489.

Iosef, C., Chang, K. O., Azevedo, M. S. P., and Saif, L. J. (2002): Systemic and intestinal antibody responses to NSP4 enterotoxin of Wa human rotavirus in a gnotobiotic pig model of human rotavirus disease. *Journal of Medical Virology* **68**, 119-128.

Isa, P., Arias, C. F., and Lopez, S. (2006): Role of sialic acids in rotavirus infection.

Glycoconj J **23**, 27-37.

Isa, P., Sanchez-Aleman, M. A., Lopez, S., and Arias, C. F. (2009): Dissecting the role of integrin subunits alpha 2 and beta 3 in rotavirus cell entry by RNA silencing. *Virus Res* **145**, 251-259.

Izzo, A. A., Mascolo, N., and Capasso, F. (1998): Nitric oxide as a modulator of intestinal water and electrolyte transport. *Dig Dis Sci* **43**, 1605-1620.

Jafri, M., Donnelly, B., Allen, S., Bondoc, A., McNeal, M., Rennert, P. D., Weinreb, P. H., Ward, R., and Tiao, G. (2008): Cholangiocyte expression of alpha2beta1-integrin confers susceptibility to rotavirus-induced experimental biliary atresia. *Am J Physiol Gastrointest Liver Physiol* **295**, G16-G26.

Jagannath, M. R., Kesavulu, M. M., Deepa, R., Sastri, P. N., Kumar, S. S., Suguna, K., and Rao, C. D. (2006): N- and C-terminal cooperation in rotavirus enterotoxin: novel mechanism of modulation of the properties of a multifunctional protein by a structurally and functionally overlapping conformational domain. *J Virol* **80**, 412-425.

Johnson, M. A., and McCrae, M. A. (1989): Molecular biology of rotaviruses. VIII. Quantitative analysis of regulation of gene expression during virus replication. *J Virol* **63**, 2048-2055.

Jourdan, N., Maurice, M., Delautier, D., Quero, A. M., Servin, A. L., and Trugnan, G. (1997): Rotavirus is released from the apical surface of cultured human intestinal cells through nonconventional vesicular transport that bypasses the Golgi apparatus. *J Virol* **71**, 8268-8278.

Kabcenell, A. K., and Atkinson, P. H. (1985): Processing of the rough endoplasmic reticulum membrane glycoproteins of rotavirus SA11. *J Cell Biol* **101**, 1270-1280.

Kalica, A. R., Flores, J., and Greenberg, H. B. (1983): Identification of the rotaviral gene that codes for hemagglutination and protease-enhanced plaque formation. *Virology* **125**, 194-205.

Kaljot, K. T., Shaw, R. D., Rubin, D. H., and Greenberg, H. B. (1988): Infectious rotavirus enters cells by direct cell membrane penetration, not by endocytosis. *J Virol* **62**, 1136-1144.

Kantharidis, P., Dyall-Smith, M. L., and Holmes, I. H. (1983): Completion of the gene coding assignments of SA11 rotavirus: gene products of segments 7, 8, and 9. *J Virol* **48**, 330-334.

Kapikian, H. Y., Chanock RM (2001): Rotaviruses, pp. 1787-1833. In H. P. e. a. Knipe DM (Ed.): *Fields virology*, Lippincott Williams and Wilkins, Philadelphia.

Kojima, K., Taniguchi, K., Urasawa, T., and Urasawa, S. (1996): Sequence analysis of normal and rearranged NSP5 genes from human rotavirus strains isolated in nature: implications for the occurrence of the rearrangement at the step of plus strand synthesis. *Virology* **224**, 446-452.

Korolev, M. B., Khaustov, V. I., and Shekoian, L. A. (1981): Morphogenesis of human rotavirus in a cell culture. *Vopr Virusol* **3**, 309-315.

Kouvelos, K., Petric, M., and Middleton, P. J. (1984a): Comparison of bovine, simian and human rotavirus structural glycoproteins. *J Gen Virol* **65**, 1211-1214.

Kouvelos, K., Petric, M., and Middleton, P. J. (1984b): Oligosaccharide composition of calf rotavirus. *J Gen Virol* **65**, 1159-1164.

Kubes, P. (1992): Nitric oxide modulates epithelial permeability in the feline small intestine. *Am J Physiol* **262**, G1138-1142.

Labbe, M., Baudoux, P., Charpilienne, A., Poncet, D., and Cohen, J. (1994): Identification of the nucleic acid binding domain of the rotavirus VP2 protein. *J Gen Virol* **75**, 3423-3430.

Labbe, M., Charpilienne, A., Crawford, S. E., Estes, M. K., and Cohen, J. (1991): Expression of rotavirus VP2 produces empty corelike particles. *J Virol* **65**, 2946-2952.

Lawton, J. A., Estes, M. K., and Prasad, B. V. (2001): Identification and characterization of a transcription pause site in rotavirus. *J Virol* **75**, 1632-1642.

Lawton, J. A., Zeng, C. Q., Mukherjee, S. K., Cohen, J., Estes, M. K., and Prasad, B. V. (1997): Three-dimensional structural analysis of recombinant rotavirus-like particles with intact and amino-terminal-deleted VP2: implications for the architecture of the VP2 capsid layer. *J Virol* **71**, 7353-7360.

Li, Z., Baker, M. L., Jiang, W., Estes, M. K., and Prasad, B. V. (2009): Rotavirus architecture at subnanometer resolution. *J Virol* **83**, 1754-1766.

Lin, S. L., and Tian, P. (2003): Detailed computational analysis of a comprehensive set of group A rotavirus NSP4 proteins. *Virus Genes* **26**, 271-282.

Liu, M., Mattion, N. M., and Estes, M. K. (1992): Rotavirus VP3 expressed in insect cells possesses guanylyltransferase activity. *Virology* **188**, 77-84.

Lopez, S., and Arias, C. F. (2004): Multistep entry of rotavirus into cells: a Versaillesque dance. *Trends Microbiol* **12**, 271-278.

Lopez, T., Camacho, M., Zayas, M., Najera, R., Sanchez, R., Arias, C. F., and Lopez, S. (2005a): Silencing the morphogenesis of rotavirus. *J Virol* **79**,

184-192.

Lopez, T., Rojas, M., Ayala-Breton, C., Lopez, S., and Arias, C. F. (2005b): Reduced expression of the rotavirus NSP5 gene has a pleiotropic effect on virus replication. *J Gen Virol* **86**, 1609-1617.

Ludert, J. E., Michelangeli, F., Gil, F., Liprandi, F., and Esparza, J. (1987): Penetration and uncoating of rotaviruses in cultured cells. *Intervirology* **27**, 95-101.

Lundgren, O., Peregrin, A. T., Persson, K., Kordasti, S., Uhnoo, I., and Svensson, L. (2000): Role of the enteric nervous system in the fluid and electrolyte secretion of rotavirus diarrhea. *Science* **287**, 491-495.

Lundgren, O., and Svensson, L. (2001): Pathogenesis of rotavirus diarrhea. *Microbes Infect* **3**, 1145-1156.

Maass, D. R., and Atkinson, P. H. (1990): Rotavirus proteins VP7, NS28, and VP4 form oligomeric structures. *J Virol* **64**, 2632-2641.

Malik, J., Gupta, S. K., Bhatnagar, S., Bhan, M. K., and Ray, P. (2008): Evaluation of IFN-gamma response to rotavirus and non-structural protein NSP4 of rotavirus in children following severe rotavirus diarrhea. *J Clin Virol* **43**, 202-206.

Martin, D., Duarte, M., Lepault, J., and Poncet, D. (2010): Sequestration of free tubulin molecules by the viral protein NSP2 induces microtubule depolymerization during rotavirus infection. *J Virol* **84**, 2522-2532.

Martin-Latil, S., Mousson, L., Autret, A., Colbere-Garapin, F., and Blondel, B. (2007): Bax is activated during rotavirus-induced apoptosis through the mitochondrial pathway. *J Virol* **81**, 4457-4464.

Mason, B. B., Graham, D. Y., and Estes, M. K. (1980): In vitro transcription and translation of simian rotavirus SA11 gene products. *J Virol* **33**, 1111-1121.

Mason, B. B., Graham, D. Y., and Estes, M. K. (1983): Biochemical mapping of the simian rotavirus SA11 genome. *J Virol* **46**, 413-423.

Mattion, N. M., Mitchell, D. B., Both, G. W., and Estes, M. K. (1991): Expression of rotavirus proteins encoded by alternative open reading frames of genome segment 11. *Virology* **181**, 295-304.

McAdaragh, J. P., Bergeland, M. E., Meyer, R. C., Johnshoy, M. W., Stotz, I. J., Benfield, D. A., and Hammer, R. (1980): Pathogenesis of rotaviral enteritis in gnotobiotic pigs: a microscopic study. *Am J Vet Res* **41**, 1572-1581.

McCormack, P. L., and Keam, S. J. (2009): Rotavirus vaccine RIX4414 (Rotarix): a review of its use in the prevention of rotavirus gastroenteritis. *Paediatr Drugs* **11**, 75-88.

McCrae, M. A., and Faulkner-Valle, G. P. (1981): Molecular biology of rotaviruses. I. Characterization of basic growth parameters and pattern of macromolecular synthesis. *J Virol* **39**, 490-496.

McCrae, M. A., and McCorquodale, J. G. (1982): The molecular biology of rotaviruses. II. Identification of the protein-coding assignments of calf rotavirus genome RNA species. *Virology* **117**, 435-443.

McCrae, M. A., and McCorquodale, J. G. (1983): Molecular biology of rotaviruses. V. Terminal structure of viral RNA species. *Virology* **126**, 204-212.

McCrae, M. A., and McCorquodale, J. G. (1987): Expression of a major bovine rotavirus neutralisation antigen (VP7c) in Escherichia coli. *Gene* **55**, 9-18.

Michelangeli, F., Ruiz, M. C., del Castillo, J. R., Ludert, J. E., and Liprandi, F. (1991): Effect of rotavirus infection on intracellular calcium homeostasis in cultured cells. *Virology* **181**, 520-527.

Mir, K. D., Parr, R. D., Schroeder, F., and Ball, J. A. (2007): Rotavirus NSP4 interacts with both the amino- and carboxyl-termini of caveolin-1. *Virus Research* **126**, 106-115.

Mitchell, D. B., and Both, G. W. (1990a): Completion of the genomic sequence of the simian rotavirus SA11: nucleotide sequences of segments 1, 2, and 3. *Virology* **177**, 324-331.

Mitchell, D. B., and Both, G. W. (1990b): Conservation of a potential metal binding motif despite extensive sequence diversity in the rotavirus nonstructural protein NS53. *Virology* **174**, 618-621.

Montero, H., Arias, C. F., and Lopez, S. (2006): Rotavirus Nonstructural Protein NSP3 is not required for viral protein synthesis. *J Virol* **80**, 9031-9038.

Moss, D. K., Wilde, A., and Lane, J. D. (2009): Dynamic release of nuclear RanGTP triggers TPX2-dependent microtubule assembly during the apoptotic execution phase. *J Cell Sci* **122**, 644-655.

Musalem, C., and Espejo, R. T. (1985): Release of progeny virus from cells infected with simian rotavirus SA11. *J Gen Virol* **66**, 2715-2724.

Narang, H. K., and Codd, A. A. (1983): Action of commonly used disinfectants against enteroviruses. *J Hosp Infect* **4**, 209-212.

Nelson, E. A., Widdowson, M. A., Kilgore, P. E., Steele, D., and Parashar, U. D. (2009): A decade of the Asian Rotavirus Surveillance Network: achievements and future directions. *Vaccine* **27**, F1-3.

Newton, K., Meyer, J. C., Bellamy, A. R., and Taylor, J. A. (1997): Rotavirus

nonstructural glycoprotein NSP4 alters plasma membrane permeability in mammalian cells. *J Virol* **71**, 9458-9465.

Nyfeler, B., Michnick, S. W., and Hauri, H. P. (2005): Capturing protein interactions in the secretory pathway of living cells. *Proc Natl Acad Sci U S A* **102**, 6350-6355.

Nyfeler, B., Reiterer, V., Wendeler, M. W., Stefan, E., Zhang, B., Michnick, S. W., and Hauri, H. P. (2008): Identification of ERGIC-53 as an intracellular transport receptor of alpha1-antitrypsin. *J Cell Biol* **180**, 705-712.

O'Ryan, M. L., Hermosilla, G., and Osorio, G. (2009): Rotavirus vaccines for the developing world. *Curr Opin Infect Dis* **22**, 483-489.

Offit, P. A., Blavat, G., Greenberg, H. B., and Clark, H. F. (1986): Molecular basis of rotavirus virulence: role of gene segment 4. *J Virol* **57**, 46-49.

Offit, P. A., Coupar, B. E., Svoboda, Y. M., Jenkins, R. J., McCrae, M. A., Abraham, A., Hill, N. L., Boyle, D. B., Andrew, M. E., and Both, G. W. (1994): Induction of rotavirus-specific cytotoxic T lymphocytes by vaccinia virus recombinants expressing individual rotavirus genes. *Virology* **198**, 10-16.

Padilla-Noriega, L., Paniagua, O., and Guzman-Leon, S. (2002): Rotavirus protein NSP3 shuts off host cell protein synthesis. *Virology* **298**, 1-7.

Parashar, U. D., Gibson, C. J., Bresse, J. S., and Glass, R. I. (2006): Rotavirus and severe childhood diarrhea. *Emerg Infect Dis* **12**, 304-306.

Parr, R. D., Storey, S. M., Mitchell, D. M., McIntosh, A. L., Zhou, M. L., Mir, K. D., and Ball, J. M. (2006): The rotavirus enterotoxin NSP4 directly interacts with the caveolar structural protein caveolin-1. *Journal of Virology* **80**, 2842-2854.

Patton, J. T. (1996): Rotavirus VP1 alone specifically binds to the 3' end of viral mRNA, but the interaction is not sufficient to initiate minus-strand synthesis. *J Virol* **70**, 7940-7947.

Patton, J. T., Jones, M. T., Kalbach, A. N., He, Y. W., and Xiaobo, J. (1997): Rotavirus RNA polymerase requires the core shell protein to synthesize the double-stranded RNA genome. *J Virol* **71**, 9618-9626.

Patton, J. T., Silvestri, L. S., Tortorici, M. A., Vasquez-Del Carpio, R., and Taraporewala, Z. F. (2006): Rotavirus genome replication and morphogenesis: role of the viroplasm. *Curr Top Microbiol Immunol* **309**, 169-187.

Pedley, S., Bridger, J. C., Brown, J. F., and McCrae, M. A. (1983): Molecular characterization of rotaviruses with distinct group antigens. *J Gen Virol* **64**, 2093-2101.

Pedley, S., Bridger, J. C., Chasey, D., and McCrae, M. A. (1986): Definition of two new groups of atypical rotaviruses. *J Gen Virol* **67**, 131-137.

Perez, J. F., Chemello, M. E., Liprandi, F., Ruiz, M. C., and Michelangeli, F. (1998): Oncosis in MA104 cells is induced by rotavirus infection through an increase in intracellular Ca2+ concentration. *Virology* **252**, 17-27.

Perez-Vargas, J., Romero, P., Lopez, S., and Arias, C. F. (2006): The peptide-binding and ATPase domains of recombinant hsc70 are required to interact with rotavirus and reduce its infectivity. *J Virol* **80**, 3322-3331.

Petrie, B. L., Estes, M. K., and Graham, D. Y. (1983): Effects of tunicamycin on rotavirus morphogenesis and infectivity. *J Virol* **46**, 270-274.

Petrie, B. L., Greenberg, H. B., Graham, D. Y., and Estes, M. K. (1984): Ultrastructural localization of rotavirus antigens using colloidal gold. *Virus Res* **1**, 133-152.

Piron, M., Delaunay, T., Grosclaude, J., and Poncet, D. (1999): Identification of the RNA-binding, dimerization, and eIF4GI-binding domains of rotavirus nonstructural protein NSP3. *J Virol* **73**, 5411-5421.

Piron, M., Vende, P., Cohen, J., and Poncet, D. (1998): Rotavirus RNA-binding protein NSP3 interacts with eIF4GI and evicts the poly(A) binding protein from eIF4F. *EMBO J* **17**, 5811-5821.

Piston, D. W., Patterson, G. H., and Knobel, S. M. (1999): Quantitative imaging of the green fluorescent protein (GFP). *Methods Cell Biol* **58**, 31-48.

Pizarro, J. L., Sandino, A. M., Pizarro, J. M., Fernandez, J., and Spencer, E. (1991): Characterization of rotavirus guanylyltransferase activity associated with polypeptide VP3. *J Gen Virol* **72**, 325-332.

Plascencia-Villa, G., Saniger, J. M., Ascencio, J. A., Palomares, L. A., and Ramirez, O. T. (2009): Use of recombinant rotavirus VP6 nanotubes as a multifunctional template for the synthesis of nanobiomaterials functionalized with metals. *Biotechnol Bioeng* **104**, 871-881.

Poncet, D., Laurent, S., and Cohen, J. (1994): Four nucleotides are the minimal requirement for RNA recognition by rotavirus non-structural protein NSP3. *EMBO J* **13**, 4165-4173.

Prasad, B. V., Rothnagel, R., Zeng, C. Q., Jakana, J., Lawton, J. A., Chiu, W., and Estes, M. K. (1996): Visualization of ordered genomic RNA and localization of transcriptional complexes in rotavirus. *Nature* **382**, 471-473.

Prasad, B. V., Wang, G. J., Clerx, J. P., and Chiu, W. (1988): Three-dimensional structure of rotavirus. J Mol Biol 199, 269-275.

Preiss, T., and Hentze, M. W. (1998): Dual function of the messenger RNA cap structure in poly(A)-tail-promoted translation in yeast. *Nature* **392**, 516-520.

Quan, C. M., and Doane, F. W. (1983): Ultrastructural evidence for the cellular uptake of rotavirus by endocytosis. *Intervirology* **20**, 223-231.

Rainsford, E. W., and McCrae, M. A. (2007): Characterization of the NSP6 protein product of rotavirus gene 11. *Virus Res* **130**, 193-201.

Ray, P., Malik, J., Singh, R. K., Bhatnagar, S., Bahl, R., Kumar, R., and Bhan, M. K. (2003): Rotavirus nonstructural protein NSP4 induces heterotypic antibody responses during natural infection in children. *J Infect Dis* **187**, 1786-1793.

Resta-Lenert, S., and Barrett, K. E. (2002): Enteroinvasive bacteria alter barrier and transport properties of human intestinal epithelium: role of iNOS and COX-2. *Gastroenterology* **122**, 1070-1087.

Richardson, S., Grimwood, K., Gorrell, R., Palombo, E., Barnes, G., and Bishop, R. (1998): Extended excretion of rotavirus after severe diarrhoea in young children. *Lancet* **351**, 1844-1848.

Ruiz, M. C., Cohen, J., and Michelangeli, F. (2000): Role of Ca2+in the replication and pathogenesis of rotavirus and other viral infections. *Cell Calcium* **28**, 137-149.

Ruiz, M. C., Diaz, Y., Pena, F., Aristimuno, O. C., Chemello, M. E., and Michelangeli, F. (2005): Ca2+ permeability of the plasma membrane induced by rotavirus infection in cultured cells is inhibited by tunicamycin and brefeldin A. *Virology* **333**, 54-65.

Sabara, M., Babiuk, L. A., Gilchrist, J., and Misra, V. (1982): Effect of tunicamycin on rotavirus assembly and infectivity. *J Virol* **43**, 1082-1090.

Sanchez-Alcazar, J. A., Rodriguez-Hernandez, A., Cordero, M. D., Fernandez-Ayala, D. J., Brea-Calvo, G., Garcia, K., and Navas, P. (2007): The apoptotic microtubule network preserves plasma membrane integrity during the execution phase of apoptosis. *Apoptosis* **12**, 1195-1208.

Sanchez-San Martin, C., Lopez, T., Arias, C. F., and Lopez, S. (2004): Characterization of rotavirus cell entry. *J Virol* **78**, 2310-2318.

Sapin, C., Colard, O., Delmas, O., Tessier, C., Breton, M., Enouf, V., Chwetzoff, S., Ouanich, J., Cohen, J., Wolf, C., and Trugnan, G. (2002): Rafts promote assembly and atypical targeting of a nonenveloped virus, rotavirus, in Caco-2 cells. *J Virol* **76**, 4591-4602.

Sen, A., Agresti, D., and Mackow, E. R. (2006): Hyperphosphorylation of the rotavirus NSP5 protein is independent of serine 67, [corrected] NSP2, or [corrected] the intrinsic insolubility of NSP5 is regulated by cellular

phosphatases. *J Virol* **80**, 1807-1016.

Sen, A., Feng, N., Ettayebi, K., Hardy, M. E., and Greenberg, H. B. (2009): IRF3 inhibition by rotavirus NSP1 is host cell and virus strain dependent but independent of NSP1 proteasomal degradation. *J Virol* **83**, 10322-10335.

Sen, A., Sen, N., and Mackow, E. R. (2007): The formation of viroplasm-like structures by the rotavirus NSP5 protein is calcium regulated and directed by a C-terminal helical domain. *J Virol* **81**, 11758-11767.

Seo, N. S., Zeng, C. Q., Hyser, J. M., Utama, B., Crawford, S. E., Kim, K. J., Hook, M., and Estes, M. K. (2008): Inaugural article: integrins alpha1beta1 and alpha2beta1 are receptors for the rotavirus enterotoxin. *Proc Natl Acad Sci U S A* **105**, 8811-8818.

Sieczkarski, S. B., and Whittaker, G. R. (2002): Dissecting virus entry via endocytosis. *J Gen Virol* **83**, 1535-1545.

Silvestri, L. S., Taraporewala, Z. F., and Patton, J. T. (2004): Rotavirus replication: plus-sense templates for double-stranded RNA synthesis are made in viroplasms. *J Virol* **78**, 7763-7774.

Silvestri, L. S., Tortorici, A. A., Vasquez-Del Carpio, R., and Patton, J. T. (2005): Rotavirus glycoprotein NSP4 is a modulator of viral transcription in the infected cell. *Journal of Virology* **79**, 15165-15174.

Song, X. F., and Hao, Y. (2009): Adaptive evolution of rotavirus VP7 and NSP4 genes in different species. *Comput Biol Chem* **33**, 344-349.

Sotelo, P. H., Schumann, M., Krause, E., and Chnaiderman, J. (2010): Analysis of rotavirus non-structural protein NSP5 by mass spectrometry reveals a complex phosphorylation pattern. *Virus Res* **149**, 104-108.

Storey, S. M., Gibbons, T. F., Williams, C. V., Parr, R. D., Schroeder, F., and Ball, J. M. (2007): Full-length, glycosylated NSP4 is localized to plasma membrane caveolae by a novel raft isolation technique. *J Virol* **81**, 5472-5483.

Suzuki, H., Kitaoka, S., Konno, T., Sato, T., and Ishida, N. (1985): Two modes of human rotavirus entry into MA 104 cells. *Arch Virol* **85**, 25-34.

Suzuki, H., Kutsuzawa, T., Konno, T., Ebina, T., and Ishida, N. (1981): Morphogenesis of human rotavirus type 2 Wa strain in MA 104 cells. *Arch Virol* **70**, 33-41.

Tafazoli, F., Zeng, C. Q., Estes, M. K., Magnusson, K. E., and Svensson, L. (2001): NSP4 enterotoxin of rotavirus induces paracellular leakage in polarized epithelial cells. *J Virol* **75**, 1540-1546.

Taraporewala, Z., Chen, D., and Patton, J. T. (1999): Multimers formed by the

rotavirus nonstructural protein NSP2 bind to RNA and have nucleoside triphosphatase activity. *J Virol* **73**, 9934-9943.

Taraporewala, Z. F., and Patton, J. T. (2001): Identification and characterization of the helix-destabilizing activity of rotavirus nonstructural protein NSP2. *J Virol* **75**, 4519-4527.

Tarun, S. Z., Jr., and Sachs, A. B. (1995): A common function for mRNA 5' and 3' ends in translation initiation in yeast. *Genes Dev* **9**, 2997-3007.

Taylor, J. A., J. C. Meyer, M. A. Legge, J. A. O'Brien, J. E. Street, V. J. Lord, C. C.Bergmann, and A. R. Bellamy. (1992): Transient expression and mutational analysis of therotavirus intracellular receptor: the C-terminal methionine residue is essential for ligandbinding. *J Virol* **66**, 3566-3572.

Taylor, J. A., O'Brien, J. A., Lord, V. J., Meyer, J. C., and Bellamy, A. R. (1993): The RER-localized rotavirus intracellular receptor: a truncated purified soluble form is multivalent and binds virus particles. *Virology* **194**, 807-814.

Tian, P., Estes, M. K., Hu, Y., Ball, J. M., Zeng, C. Q., and Schilling, W. P. (1995): The rotavirus nonstructural glycoprotein NSP4 mobilizes Ca2+ from the endoplasmic reticulum. *J Virol* **69**, 5763-5772.

Tian, P., Hu, Y., Schilling, W. P., Lindsay, D. A., Eiden, J., and Estes, M. K. (1994): The nonstructural glycoprotein of rotavirus affects intracellular calcium levels. *J Virol* **68**, 251-257.

Torres-Vega, M. A., Gonzalez, R. A., Duarte, M., Poncet, D., Lopez, S., and Arias, C. F. (2000): The C-terminal domain of rotavirus NSP5 is essential for its multimerization, hyperphosphorylation and interaction with NSP6. *J Gen Virol* **81**, 821-830.

Troupin, C., Dehee, A., Schnuriger, A., Vende, P., Poncet, D., and Garbarg-Chenon, A. (2010): Rearranged genomic RNA segments offer a new approach to the reverse genetics of rotaviruses. *J Virol* **84**, 6711-6719.

Vasquez-Del Carpio, R., Gonzalez-Nilo, F. D., Riadi, G., Taraporewala, Z. F., and Patton, J. T. (2006): Histidine triad-like motif of the rotavirus NSP2 octamer mediates both RTPase and NTPase activities. *J Mol Biol* **362**, 539-554.

Vende, P., Piron, M., Castagne, N., and Poncet, D. (2000): Efficient translation of rotavirus mRNA requires simultaneous interaction of NSP3 with the eukaryotic translation initiation factor eIF4G and the mRNA 3' end. *J Virol* **74**, 7064-7071.

Vesikari, T. (2008): Rotavirus vaccines. *Scand J Infect Dis* **40**, 691-695.

Vitour, D., Lindenbaum, P., Vende, P., Becker, M. M., and Poncet, D. (2004): RoXaN, a novel cellular protein containing TPR, LD, and zinc finger motifs,

forms a ternary complex with eukaryotic initiation factor 4G and rotavirus NSP3. *J Virol* **78**, 3851-3862.

Vizzi, E., Calvino, E., Gonzalez, R., Perez-Schael, I., Ciarlet, M., Kang, G., Estes, M. K., Liprandi, F., and Ludert, J. E. (2005): Evaluation of serum antibody responses against the rotavirus nonstructural protein NSP4 in children after rhesus rotavirus tetravalent vaccination or natural infection. *Clin Diagn Lab Immunol* **12**, 1157-1163.

Ward, R. L., Bernstein, D. I., Young, E. C., Sherwood, J. R., Knowlton, D. R., and Schiff, G. M. (1986): Human rotavirus studies in volunteers: determination of infectious dose and serological response to infection. *J Infect Dis* **154**, 871-880.

Weclewicz, K., Kristensson, K., and Svensson, L. (1994): Rotavirus causes selective vimentin reorganization in monkey kidney CV-1 cells. *J Gen Virol* **75**, 3267-3271.

Weiss, C., and Clark, H. F. (1985): Rapid inactivation of rotaviruses by exposure to acid buffer or acidic gastric juice. *J Gen Virol* **66**, 2725-2730.

Wentz, M. J., Patton, J. T., and Ramig, R. F. (1996): The 3'-terminal consensus sequence of rotavirus mRNA is the minimal promoter of negative-strand RNA synthesis. *J Virol* **70**, 7833-7841.

Weycker, D., Sofrygin, O., Kemner, J. E., Pelton, S. I., and Oster, G. (2009): Cost of routine immunization of young children against rotavirus infection with Rotarix versus RotaTeq. *Vaccine* **27**, 4930-4937.

Wu, H. X., Taniguchi, K., Urasawa, T., and Urasawa, S. (1998): Serological and genomic characterization of human rotaviruses detected in China. *Journal of Medical Virology* **55**, 168-176.

Wyatt, R. G., James, W. D., Bohl, E. H., Theil, K. W., Saif, L. J., Kalica, A. R., Greenberg, H. B., Kapikian, A. Z., and Chanock, R. M. (1980): Human rotavirus type 2: cultivation in vitro. *Science* **207**, 189-191.

Xu, A. M., Bellamy, A. R., and Taylor, J. A. (2000): Immobilization of the early secretory pathway by a virus glycoprotein that binds to microtubules. *Embo Journal* **19**, 6465-6474.

Xu, L., Harbour, D., and McCrae, M. A. (1990): The application of polymerase chain reaction to the detection of rotaviruses in faeces. *J Virol Methods* **27**, 29-37.

Yeager, M., Dryden, K. A., Olson, N. H., Greenberg, H. B., and Baker, T. S. (1990): Three-dimensional structure of rhesus rotavirus by cryoelectron microscopy and image reconstruction. J Cell Biol 110, 2133-2144.

Zambrano, J. L., Diaz, Y., Pena, F., Vizzi, E., Ruiz, M. C., Michelangeli, F.,

Liprandi, F., and Ludert, J. E. (2008): Silencing of rotavirus NSP4 or VP7 expression reduces alterations in Ca2+ homeostasis induced by infection of cultured cells. *J Virol* **82**, 5815-5824.

Zarate, S., Cuadras, M. A., Espinosa, R., Romero, P., Juarez, K. O., Camacho-Nuez, M., Arias, C. F., and Lopez, S. (2003): Interaction of rotaviruses with Hsc70 during cell entry is mediated by VP5. *J Virol* **77**, 7254-7260.

Zarate, S., Romero, P., Espinosa, R., Arias, C. F., and Lopez, S. (2004): VP7 mediates the interaction of rotaviruses with integrin alphavbeta3 through a novel integrin-binding site. *J Virol* **78**, 10839-10847.

Zeng, C. Q., Estes, M. K., Charpilienne, A., and Cohen, J. (1998): The N terminus of rotavirus VP2 is necessary for encapsidation of VP1 and VP3. *J Virol* **72**, 201-208.

Zeng, C. Q., Wentz, M. J., Cohen, J., Estes, M. K., and Ramig, R. F. (1996): Characterization and replicase activity of double-layered and single-layered rotavirus-like particles expressed from baculovirus recombinants. *J Virol* **70**, 2736-2742.

Zhang, M. D., Zeng, C. Q. Y., Dong, Y. J., Ball, J. M., Saif, L. J., Morris, A. P., and Estes, M. K. (1998): Mutations in rotavirus nonstructural glycoprotein NSP4 are associated with altered virus virulence. *Journal of Virology* **72**, 3666-3672.

Zhang, M. D., Zeng, C. Q. Y., Morris, A. P., and Estes, M. K. (2000): A functional NSP4 enterotoxin peptide secreted from rotavirus-infected cells. *Journal of Virology* **74**, 11663-11670.